9-5-2017 4:45 PM

A Biomechanical Investigation of Load Sharing at the Distal Forearm

Martine E. McGregor
The University of Western Ontario

Supervisor
Johnson, James A
The University of Western Ontario
King, Graham JW
The University of Western Ontario

Graduate Program in Biomedical Engineering
A thesis submitted in partial fulfillment of the requirements for the degree in Master of Engineering Science

Abstract

Loading at the distal forearm has been previously examined under static loads, however there remains no consensus on how loading is affected by active wrist and forearm motion. This work examines load magnitudes and load sharing at the distal radius and ulna during of active wrist and forearm motion. Two instrumented implants were designed to measure *in vitro* loading in cadaveric specimen. The implants were evaluated and found reliable for use in further biomechanical studies. An *in vitro* study investigated the effect of joint angle and direction of joint motion on loads in the distal radius and ulna during active flexion-extension, radioulnar deviation and dart throw motion. Loads through the distal radius and ulna were significantly greater in extension and reverse dart throw motion than in flexion and forward dart throw motion. A subsequent study examined the effect of radial length changes, joint angle and direction of motion on distal radius and ulna loading during active forearm rotation. Load magnitudes through the distal radius were greater in supination than in pronation. Radial lengthening found to increase radial loading and decrease ulnar loading and radial shortening decreased distal radius loading and increased distal ulna loading throughout forearm rotation, in a quasilinear fashion. This work improves the understanding of forearm bone loading and will assist clinicians in the development of rehabilitation techniques, surgical protocols and implant designs.

Keywords: distal radius, distal ulna, bone loading, wrist, forearm, biomechanics, dynamic wrist/forearm motion, Kienbock's disease

Co-Authorship Statement

CHAPTER 1 ***Sole Author –*** *Martine McGregor*

CHAPTER 2 ***Study Design –*** *Martine McGregor, Diana Isa, Jim Johnson, Graham King*
Data Collection – *Martine McGregor, Diana Isa, Mark Welsh, Dan Langohr*
Data Analysis – *Martine McGregor, Dan Langohr*
Statistical Analysis – *Martine McGregor*
Manuscript Preparations – *Martine McGregor*
Manuscript Revisions – *Jim Johnson, Graham King*

CHAPTER 3 ***Study Design –*** *Martine McGregor, Diana Isa, Jim Johnson, Graham King*
Data Collection – *Martine McGregor, Diana Isa, Mark Welsh, Clare Padmore, Dan Langohr*
Data Analysis – *Martine McGregor, Dan Langohr*
Statistical Analysis – *Martine McGregor*
Manuscript Preparations – *Martine McGregor*
Manuscript Revisions – *Jim Johnson, Graham King*

CHAPTER 4 ***Study Design –*** *Martine McGregor, Diana Isa, Jim Johnson, Graham King*
Data Collection – *Martine McGregor, Diana Isa, Mark Welsh, Clare Padmore, Dan Langohr*
Data Analysis – *Martine McGregor, Dan Langohr*
Statistical Analysis – *Martine McGregor*
Manuscript Preparations – *Martine McGregor*
Manuscript Revisions – *Jim Johnson, Graham King*

CHAPTER 5 ***Sole Author –*** *Martine McGregor*

APPENDIX A ***Sole Author –*** *Martine McGregor*

APPENDIX B ***Sole Author –*** *Martine McGregor*

APPENDIX C ***Sole Author –*** *Martine McGregor*

Acknowledgments

The work completed for this thesis was possible only through the contributions of many individuals. First and foremost, I would like to thank my advisors Dr. Johnson and Dr. King for their guidance, expertise, and commitment to excellence in research. Dr. Johnson, thank you for your curiosity, patience and kindness. It has been a very special honor to work under such an accomplished academic researcher and professional engineer. Dr. King, thank you for your medical expertise, sense of humor and dedication to the scientific process. I am incredibly grateful for the opportunity you have given me to participate and contribute to the world renowned research you conduct.

I would like to thank Diana for being my research partner throughout this project. Thank you for your commitment to this project and holding to your convictions when there was something standing between us and our goals. This work would have taken an insurmountable amount of time if it weren't for you pushing us through.

I would like to thank Dan and Dr. Suh for their contributions as members of my advisory committee. Dan, thank you for both your physical and intellectual contributions to this work. Without you data collection and analysis would not have been possible. Dr. Suh, thank you for your guidance to both Diana and I and thank you for the never-ending supply of motivation, positive energy and of course, Timbits.

Thank you to all of my colleagues at the HULC for their mentorship and friendship. Mark and Duncan, thank you for coming out of retirement to assist with this work. A special thank you to Mark who took it upon himself to become an expert on the wrist simulator to assist testing days. Clare and Helen, thank you for pioneering the "Wrist Team" and handing down your knowledge and expertise on the wrist simulator and testing day protocols. Jordan, thank you for your sunny disposition and your willingness to assist with any software or hardware issues that arose throughout testing.

Lastly, I would like to thank my family and friends in both Manitoba and Ontario. To my parents, thank you for your unyielding support and always encouraging me to achieve my never ending list of goals. To Josh, thank you for everything and all that you do for me.

Table of Contents

List of Figures

List of Tables

List of Appendices

List of Abbreviations

DOF	Degrees of Freedom
DRUJ	Distal Radioulnar Joint
ECRB	Extensor Carpi Radialis Brevis
DTM	Dart Throwers Motion
ECRL	Extensor Carpi Radialis Longus
ECU	Extensor Carpi Ulnaris
FCR	Flexor Carpi Radialis
FCU	Flexor Carpi Ulnaris
FEM	Flexion-Extension Motion
PQ	Pronator Quadratus
PSM	Pronation-Supination Motion
PT	Pronator Teres
RUD	Radial-Ulnar Deviation

Chapter 1

1 *Introduction*

Overview

The purpose of this thesis is to examine load magnitude and sharing in the distal forearm. Forearm loading during active wrist and forearm motion and the effect of radial length change during active forearm pronation-supination motion. This introductory chapter provides an overview of anatomy, kinematics, forearm bone loading and existing experimental apparatuses and joint motion simulators. In conclusion, rationale and outline will be presented and thesis objectives hypotheses will be clearly stated.

1.1 Anatomy of the Wrist and Forearm

1.1.1 *Bony Anatomy*

Bone is a tough, elastic and dynamic tissue that gives mechanical structure to the human body (Figure 1.1). Different bones are made up of different combinations of the same two tissue types: cortical and cancellous bone. Cortical, or compact, bone is the stiff outer layer while cancellous, or trabecular, bone is the porous inner layer. There are distinctive types of bones that perform different structural and mechanical tasks. There are the long and short bones of the extremities, flat bones of the skull and pelvis and irregular bones like the mandible.

Long bones make up most the skeletal structure of our upper extremities including the humerus, radius, ulna, metacarpals and phalanges. Long bones have a shaft, the diaphysis, and two distinct ends called the metaphyses.[1] The diaphysis is roughly cylindrical and with a central medullary canal. It is made up of thick cortical bone that thins towards the metaphysis. The metaphysis, or ends, are expanded so as to provide space for muscle attachment and to increase the surface of joint articulations.[1] They are primarily cancellous bone with a thin layer of encasing cortical bone.[1] Short bones boast strength and compactness. They are composed predominantly of cancellous bone and covered by a thin layer of cortical bone.[2] Examples of short bones in the upper extremity are the eight carpal bones of the wrist.

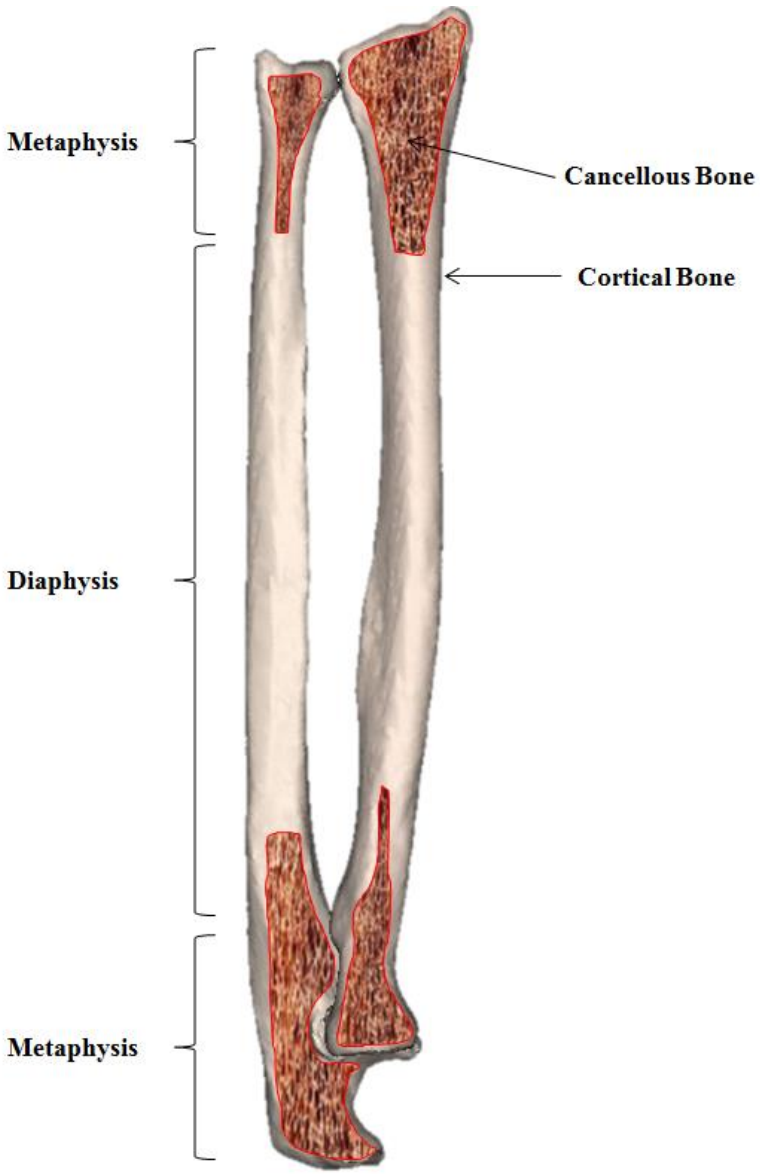

Figure 1.1: Anatomy of Long Bone. *Long bones are comprised of two metaphyses at the distal and proximal ends and one central diaphysis. The metaphyses have a thin layer of cortical bone concealing cancellous bone. The diaphysis is comprised of a thick layer of cortical bone with a central medullary canal.*

1.1.1.1 *Radius*

The forearm contains two long bones, the radius and the ulna (Figure 1.1). Of the two long bones of the forearm, the radius is longer and larger than the ulna found on the lateral side of the forearm (Figure 1.2).[1] It is a long bone while a slight longitudinal curve. Like all long bones, it has two metaphyses at either end of a long body. The proximal end is small and cylindrical to assist with elbow movement, while the distal end is large and the prime component of the wrist joint. The proximal metaphysis consists of a head, neck and tuberosity. The head is relatively cylindrical and with a fovea on the top to allow for articulation with both the proximal ulna and distal humerus during elbow flexion and forearm rotation.[1]

The body of the radius is prism shaped and has three major surfaces. The volar surface is concave and is the site of pronator quadratus insertion. The dorsal surface is convex towards the metaphyses and concave through the diaphysis. The proximal dorsal surface is covered by the supinator. The distal dorsal surface features three prominent grooves that act to maintain the tendon lines of action. The lateral surface is convex throughout, with the pronator teres inserting along the rough centre ridge.[1]

The distal radial metaphysis is quadrilateral in shape with two major articular surfaces. The distal articular surface articulates with the scaphoid and lunate carpal bones forming the radiocarpal joint. The medial articular surface, or the sigmoid notch, articulates with the ulnar head to form the distal radioulnar joint (DRUJ). There is a small ridge separating the radiocarpal joint and the DRUJ which doubles as the radial attachment of the triangular fibrocartilage (TFC).[1]

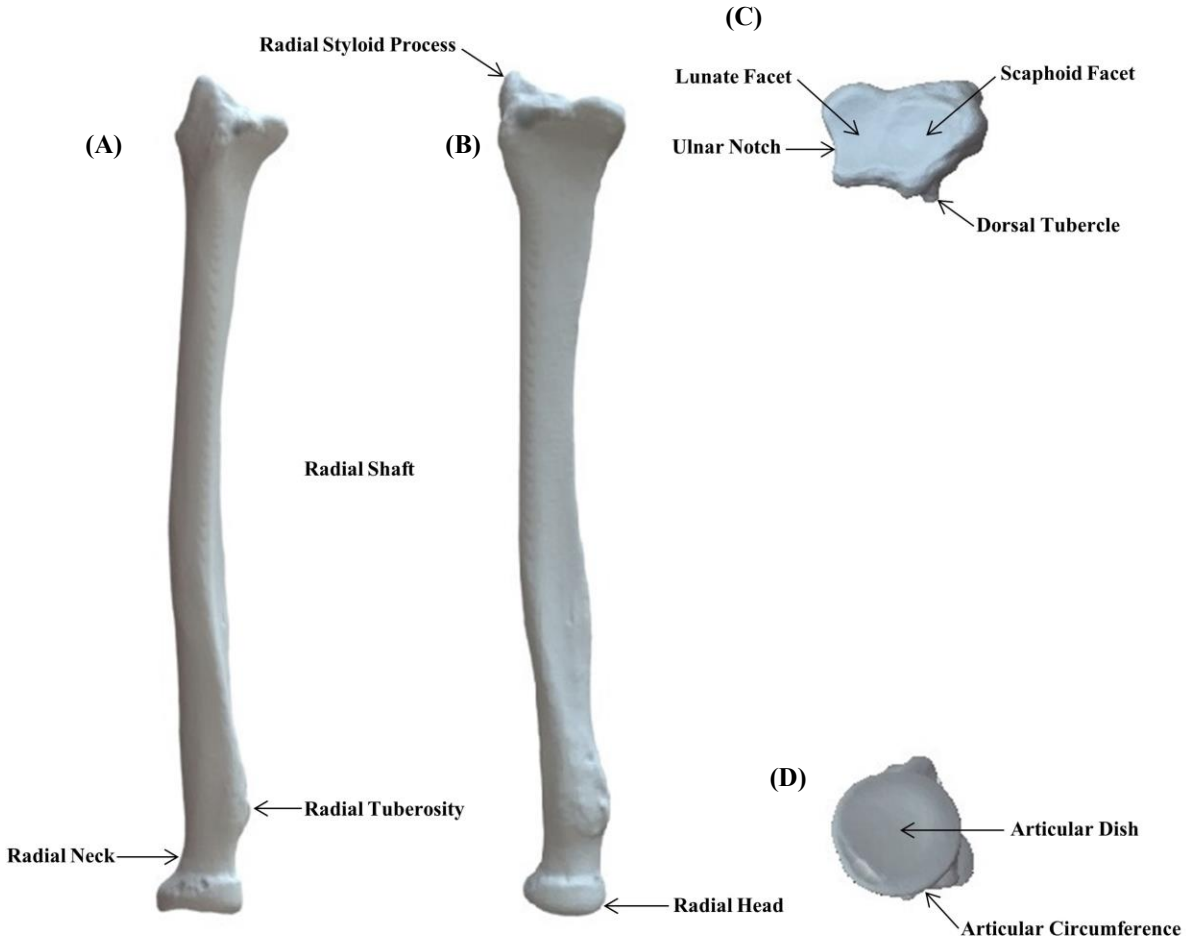

Figure 1.2: Bony Anatomy of the Radius. *Bony anatomy of the left radius with important features and landmarks highlighted. (A) Lateral view, (B) anterior view, (C) distal articular surface, and (D) proximal articular surface.*

1.1.1.2 *Ulna*

The ulna is a long bone located in the medial forearm, parallel to the radius (Figure 1.3). The proximal end is thick and strong and is the primary forearm bone of the elbow joint. It has two curved processes, the olecranon and coronoid process, and two concave articular notches, the greater sigmoid and the radial. The olecranon process articulates with the humerus and its medial border acts as the origin site for the flexor carpi ulnaris (FCU). The coronoid process is a triangular protrusion on the front of the ulna, it articulates with the radius laterally, and it the origin site of the anterior capsule and one of two pronator teres heads. The greater sigmoid notch is a curved depression formed by the olecranon and coronoid processes which articulates with the trochlea of the humerus to provide elbow flexion and extension. The radial notch is a narrow articular surface located on the lateral side of the coronoid process that articulates with the rotating radius during forearm pronation and supination.[1]

The body of the ulna tapers in the proximal to distal direction, with three borders and three surfaces. The proximal body is slightly curved laterally; the central section is straight and the lower body curves laterally again.[1]

The distal metaphysis has two important features, the ulnar head and the ulnar styloid process. The ulnar head is a rounded surface that articulates with the radius at the sigmoid notch and the triangular articular disc at its distal surface. The styloid process projects from the ulnar head on the medial-dorsal side of the ulna and extends distally past the head. The ulnar head and styloid are separated by the triangular fibrocartilage (TFC) attachment site and a shallow groove for the extensor carpi ulnaris tendon.[1]

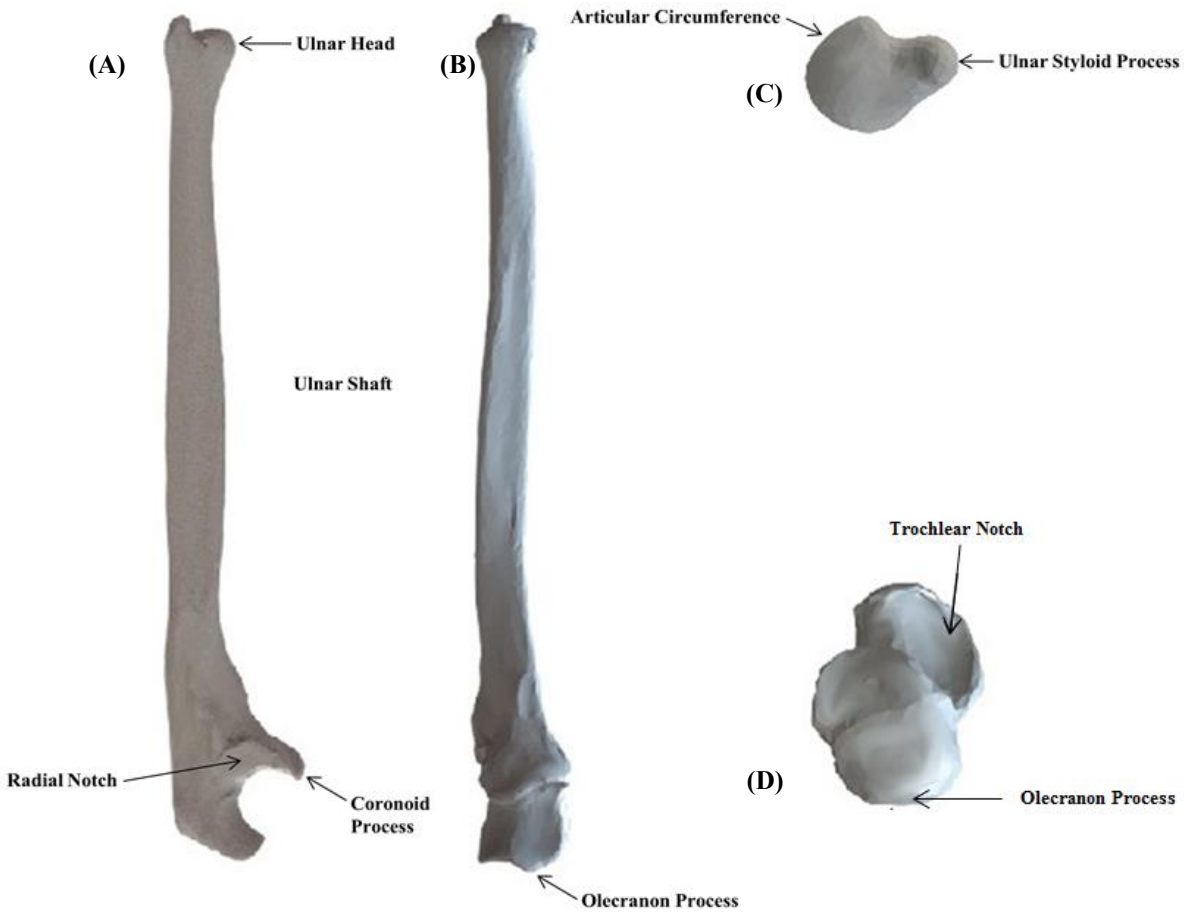

Figure 1.3: Bony Anatomy of the Ulna. *Bony anatomy of the left radius with important features and landmarks highlighted. (A) Lateral view, (B) anterior view, (C) distal articular surface, and (D) proximal articular surface.*

1.1.1.3 *Carpal Bones*

The carpus consists of eight short bones located in the wrist joint (Figure 1.4). The shape of each carpal bone varies but the structure remains the same, cancellous bone enclosed by a thin layer of cortical bone.[1] The carpal bones are arranged into two rows: a proximal carpal row and a distal carpal row. The proximal carpal row contains the scaphoid, lunate and triquetrum, while the distal carpal row contains the pisiform trapezium, trapezoid, capitate and hamate bones. Each of the carpal bones, with the exception of the pisiform, has six surfaces for articulation and soft tissue attachment.[1]

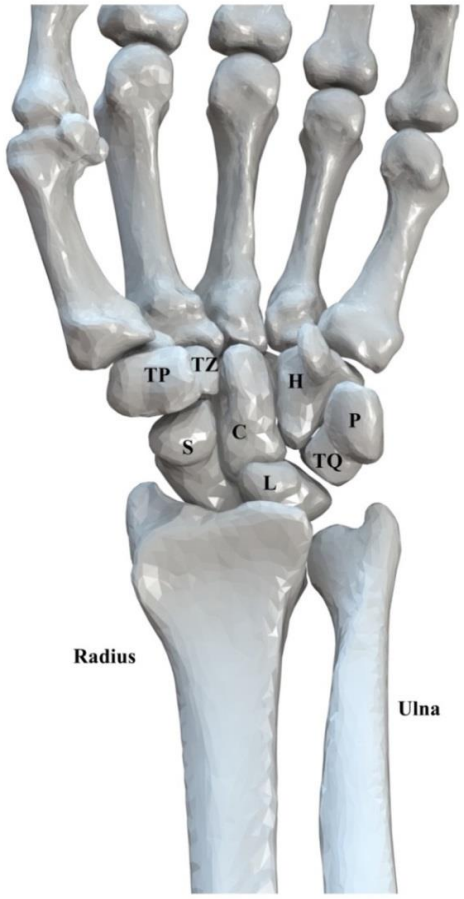

Figure 1.4: Carpal Bones. *Volar view of the bony anatomy of the left wrist showing the eight carpal bones, distal radius and distal ulna individually labeled. The proximal carpal row consists of the scaphoid (S), lunate (L), and triquetrum (TQ). The distal row consists of the pisiform (P), trapezium (TP), trapezoid (TZ), and hamate (H).*

The scaphoid is the largest bone is the proximal carpal row and is the stabilizing link between the distal and proximal carpal rows (Figure 1.5).[1] The scaphoid has four articular surfaces, accounting for 80 percent of its total surface area, including the medial facet and the lateroproximal, distal medial and distal surfaces. The medial articular facet is semilunar in shape and articulates with the lateral lunate. The lateroproximal articular surface is convex and articulates with scaphoid fossa on the distal radius. The distal medial articular surface is a concave oval facet and articulates with the lateral capitate. The distal articular surface is convex and articulates with the proximal trapezium and trapezoid.[2] The scaphoid tuberosity is a non-articular surface located between the lateroproximal and the distal articular surfaces. The scaphoid tuberosity is the site of ligamentous attachment for the radioscaphocapitate and scaphotrapezial-trapezoid ligaments, further explained below (Section 1.13, Figures 1.10, 1.11). In neutral wrist position, the long axis of the scaphoid is oriented obliquely in the sagittal and coronal plates. [2]

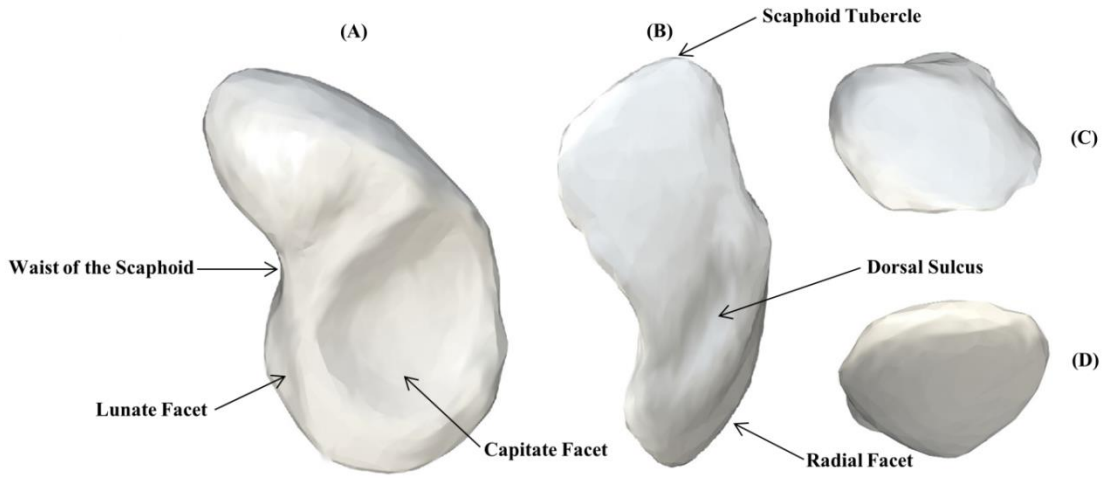

Figure 1.5: Bony Anatomy of the Scaphoid. *Bony anatomy of the left scaphoid with important landmarks and articulations labeled. (A) Medial view, (B) dorsolateral view, (C) distal articular surface, and (D) proximal articular surface.*

The lunate is considered to be the keystone carpal bone (Figure 1.6).[2] The lunate is moon shaped and larger volarly than it is dorsally. Like the scaphoid, the lunate also has four articular surfaces. The proximal articular surface is biconvex, with two thirds articulating with the distal radius and one third with the triangular fibrocartilage. The distal articular surface is biconcave and articulates with the head of the capitate and the proximal hamate. The lateral and medial articular surfaces are flat semilunar surfaces that articulate with the scaphoid and triquetrum, respectively.[2] The lunate also has two non-articular surfaces on its volar and dorsal aspects. The palmar surface is the site of ligamentous attachment for the long radiolunate, short radiolunate, radioscapholunate and scapholunate ligaments, further explained below (Section 1.13, Figures 1.10, 1.11). The dorsal surface is the site of stabilizing ligament attachment and vascular supply.[2] The anatomic characteristics of the lunate are important for the diagnosis and pathogenesis of Keinbock's disease. [2]

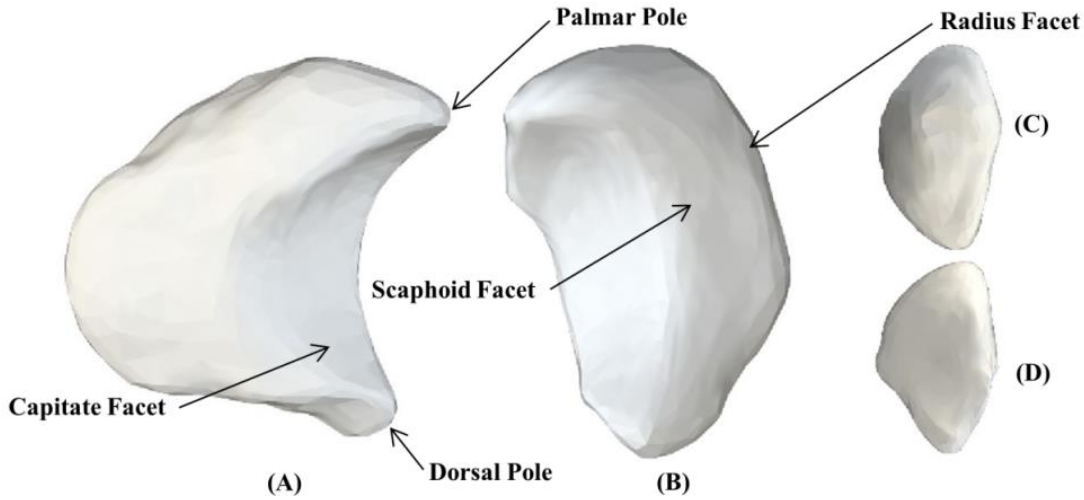

Figure 1.6: Bony Anatomy of the Lunate. *Bony anatomy of the left lunate with important landmarks and articulations labeled. (A) Distal articular surfaces, (B) proximal articular surfaces, (C) medial view, and (D) lateral view.*

1.1.1.4 *Metacarpals*

There are five long cylindrical metacarpals that make up the structure of the palm, as seen in (Figure 1.7, 1.8).[1] The naming convention of the metacarpals starts with the thumb as the first metacarpal medially towards the small finger as the fifth metacarpal. Like other long bones, metacarpals consist of a proximal metaphysis, a diaphysis and a distal metaphysis. The concave proximal metaphysis of each metacarpal articulates with a corresponding carpal(s) of the distal carpal row. The proximal metacarpal also articulates with the adjoining metacarpal bones via flat mediolateral surfaces. The body of the metacarpals have a medial, lateral and dorsal surface. The medial and lateral surfaces are concave and separated by a distinct anterior ridge.[1] The dorsal surface is broad and flat and supports the insertion of the extensor tendons of the wrist, and the volar surface is grooved in the middle for the smooth passage of the flexor tendons.[1] The distal portion articulates with individual corresponding phalanges (I-V).

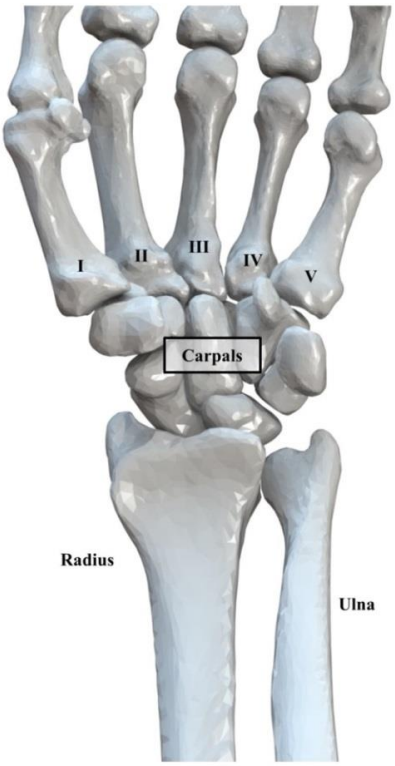

Figure 1.7: Bony Anatomy of the Metacarpals. *Volar view of the bony anatomy of the left wrist showing the distal radius, distal ulnar, carpal bones and five metacarpals individually labeled. The thumb, or most radial metacarpal, is termed the first metacarpal (I) and the most ulnar metacarpal is termed the fifth metacarpal (V).*

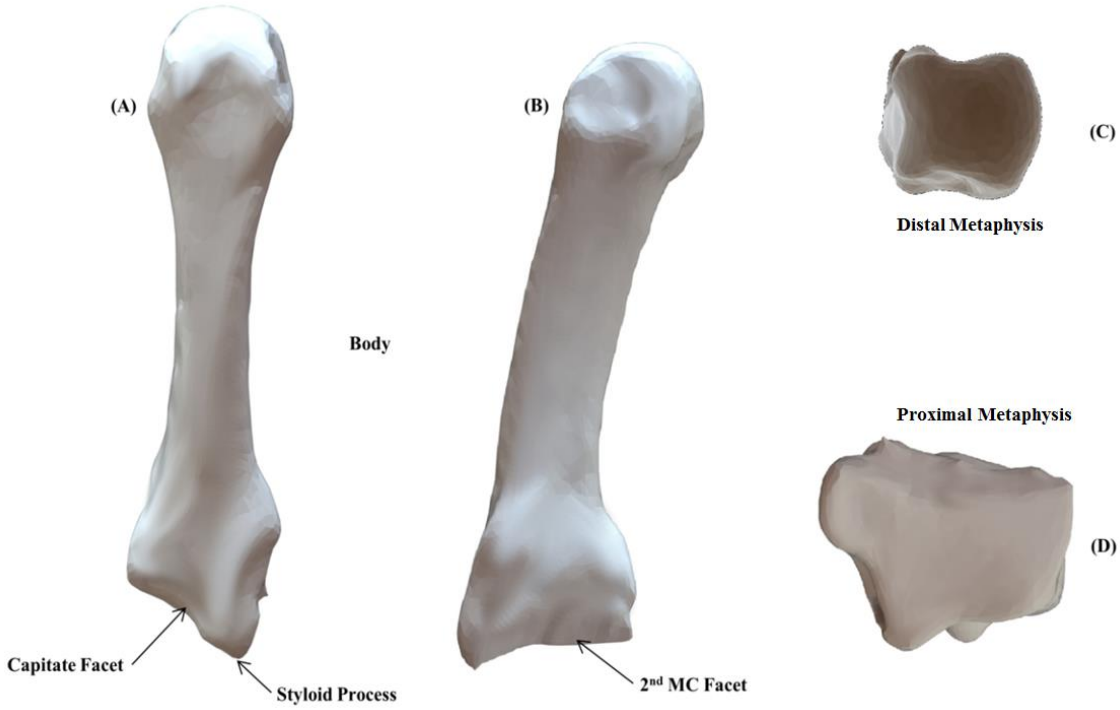

Figure 1.8: Bony anatomy of the Third Metacarpal. *Bony anatomy of the left third (III) metacarpal with important landmarks and articulations labeled. (A) Dorsal view, (B) lateral view, (C) distal articular surface, (D) proximal articular surface.*

1.1.2 *Joints*

The wrist and forearm bones articulate with one another at distinct joints, each with individual biomechanical and kinematic characteristics.[2] The three major synovial joints of the wrist are the distal radioulnar joint (DRUJ), the radiocarpal joint, and the midcarpal joint (Figure 1.9). The distal radius, ulna and eight carpal bones are covered in articular cartilage at their articular surfaces. Articular cartilage provides flexibility, cushion, and smooth surfaces for joints to articulate and track efficiently. [1]

1.1.2.1 *Distal Radioulnar Joint*

The DRUJ is a complex pivot joint comprised of two separate articulations: vertically, between the ulnar head and the sigmoid notch of the distal radius and horizontally, between the ulnar dome and the proximal aspect of the TFC (Figure 1.9).[2] The movement at these two articulations allow forearm pronation and supination to occur. During pronation and supination, the radius rotates around an axis originating at the centre of the radial head and extending to the foveal sulcus at the base of the ulnar styloid. [1] The radiocarpal unit rotates freely around the fixed ulna. Forward rotation of the radius or backwards rotation of the palm is termed pronation. The backwards rotation of the radius or forward rotation of the palm is termed supination. There are individual variations in the range of forearm motion from 150°-180° at the DRUJ, with 30° occurring at the radio- and mid-carpal joints.[2] Bony articulations account for a small amount of joint constraint, however, the joint it primarily constrained by static constraints and dynamic muscle stabilizers. The static constraints of the DRUJ include the triangular fibrocartilage complex, dorsal and volar radioulnar ligament, and the ulnar collateral ligament. The dynamic muscle stabilizers of the DRUJ are the extensor carpi ulnaris and the pronator quadratus.[2]

1.1.2.2 *Radiocarpal (Wrist) Joint*

The radiocarpal joint is the condyloid articulation formed between the distal surfaces of the radius and TFC and the proximal carpal row, consisting of the scaphoid, lunate and triquetrum (Figure 1.9).[2] The distal surface of the radius has two distinct facets for the articulation of the proximal scaphoid and lunate. The triquetrum does not articulate with a bone, but rather with the distal surface of the triangular fibrocartilage complex.[2] The radiocarpal joint is surrounded by a joint capsule and strengthened by the dorsal and volar radiocarpal ligaments and the ulnar and radial collateral ligaments.[2] The radiocarpal joint contributes primarily to flexion-extension motion and radioulnar deviation, or wrist abduction and adduction.[2]

1.1.2.3 *Midcarpal Joint*

The midcarpal joint is the term used to describe the articulation between the proximal and distal carpal rows. The midcarpal joint is comprised of three distinct components (Figure 1.9).[2] Laterally, the convex surface of the scaphoid articulates with the concave surfaces of the trapezium and trapezoid. Centrally, the concave surfaces of the scaphoid and the lunate make a near ball and socket joint with the convex surfaces of the capitate and hamate. Medially, the hamate forms a gliding joint with the triquetrum.[2] Stabilizing soft tissues include the dorsal and volar radioulnar ligaments and the ulnar and radial collateral ligaments.[2]

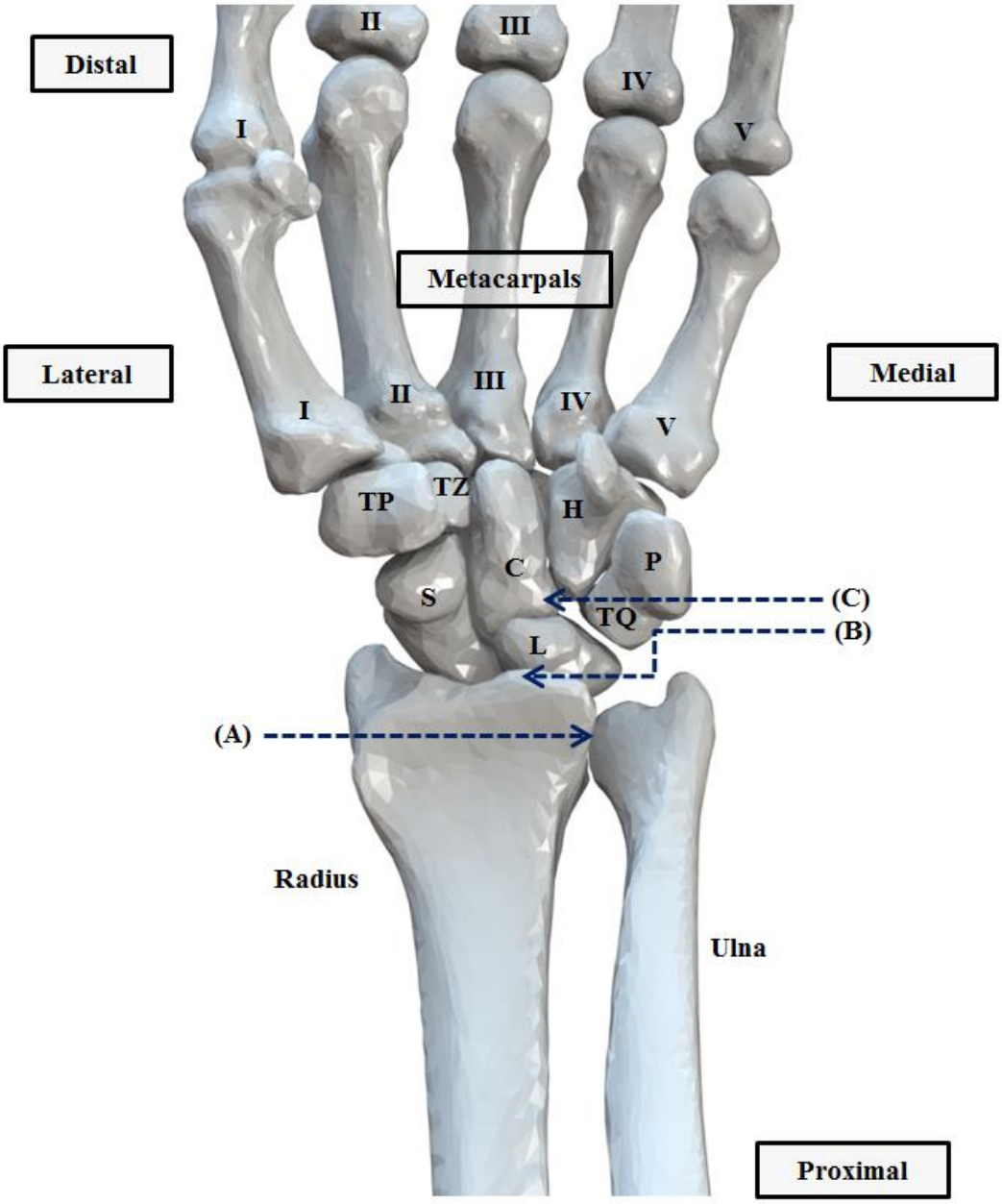

Figure 1.9: Joints of the Wrist. *Volar view of the bony anatomy of the left wrist illustrating the three major articulations between the carpal bones, radius and ulna. The wrist is comprised of three major joints: (A) distal radioulnar joint, (B) radiocarpal joint, and (C) midcarpal joint.*

1.1.3 *Ligamentous Anatomy*

Ligaments are fibrous bundles of connective tissue that connect bone to bone and provide joint stability. The wrist is constrained by ligaments on the dorsal and volar sides (Figures 1.10 & 1.11).[2] The accepted naming convention followed has the bone of origin indicated as the prefix and the bone of insertion as the suffix. The ligaments of the wrist can be grouped by their location within the joint capsule of the wrist.[2] The sub-categories of wrist ligaments include: radiocarpal, ulnocarpal, distal radioulnar, intercarpal and carpometacarpal.

The radioscaphocapitate (RSC) ligament is the most radial of the palmar ligaments. The RSC ligament originates on the radius, proximal to the radial styloid and directly on the radio-volar aspect of the distal radial ridge (Figure 1.10). [2] The RSC ligament has multiple insertions, the first of which is located on the lateral waist of the scaphoid. The second scaphoid insertion of the RSC ligament is on the radial aspect of the waist and volarly on the proximal margin. [2] The remaining RSC ligament continues ulnarly and distally, crossing over the volar proximal aspect of the scaphocapitate joint and inserts on the capitate head.[2]

The long radiolunate (LRL) ligament, sometimes referred to as the radioulnotriquetrial ligament, originates on the volar rim of the distal radius spanning the length of the scaphoid fossa (Figures 1.10, 1.11).[2] The superficial ulnar fibers of the LRL overlap with the superficial radial fibers of the RSC. The LRL moves ulnarly past the volar surface and proximal pole of the scaphoid and inserts on the radial margin of the volar lunate surface.[2]

The short radiolunate (SRL) ligament is thick and forms the floor of the radiolunate space (Figures 1.10, 1.11).[2] The SRL originates on the volar rim of the radius, proximal to the lunate fossa. The SRL then directs distally and inserts on the proximal articular surface and volar ridge of the lunate [2]

The ulnocarpal ligaments, consisting of the *ulnolunate, ulnotriquetrial and ulnocapitate ligaments,* form the ulnar and volar walls of the ulnar half of the radiocarpal joint, providing medial support during joint extension (Figure 1.10, 1.11).[2] The group of

ulnocarpal ligaments largely originate from the volar radioulnar ligament, not directly from the ulna, which allows for consistent tension.[2] It is hard to distinguish the ulnocarpal ligaments from one another by anything other than their individual insertions. The ulnolunate ligament is directly continuous with the SRL and it also inserts on the radial margin of the volar lunate surface.[2] The ulnotriquetrial inserts on the proximal volar aspect of the triquetrum.[2]

The distal radioulnar ligaments act to stabilize the distal radioulnar joint throughout forearm rotation and maintain joint congruity between the ulnar head and the sigmoid notch of the radius (Figures 1.10, 1.11).[2] The distal-volar radioulnar ligament forms the volar portion of the triangular fibrocartilage complex (TFCC). The distal-volar radioulnar ligament originates on the anterior surface of the sigmoid notch on the radius and inserts on the anterior head of the ulnar.[2] The distal-dorsal radioulnar ligament originates on the dorsal surface of the ulnar notch and inserts on the dorsal margin of the ulnar head.[2]

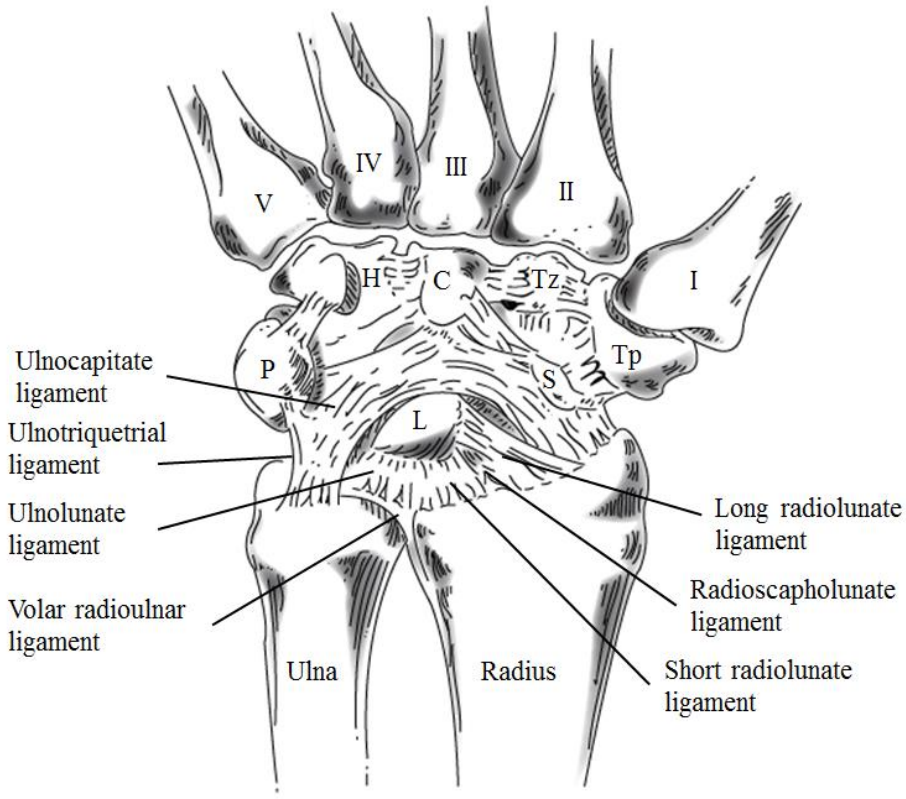

Figure 1.10: Volar Ligaments of the Wrist. *A schematic of the volar ligaments constraining the wrist joints of the right hand. Radiocarpal, ulnocarpal and distal radioulnar ligaments are individually labeled.*

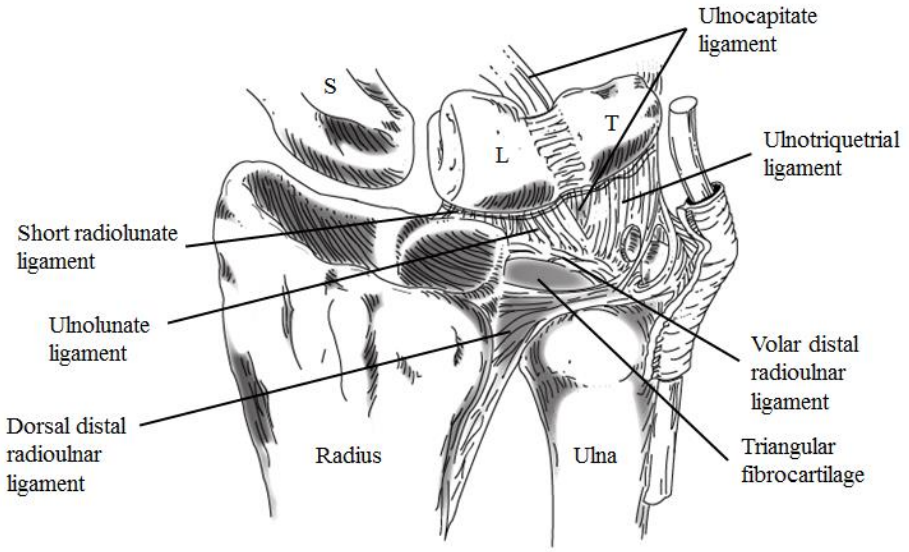

Figure 1.11: Dorsal Ligaments of the Wrist. *A schematic of the dorsal ligaments constraining the wrist joints of the right hand. Radiocarpal, ulnocarpal and distal radioulnar ligaments are individually labeled.*

1.1.4 *Musculature*

There are three types of muscles in the human body: smooth, cardiac and skeletal. Skeletal muscles are fibrous bundles or bands of soft tissue whose essential function is to contract, or shorten, to stabilize joints and control joint motion.[3] Muscles are connected to bones at both their origin and insertion through viscoelastic, collagenous tissues called tendons.[4] Muscle contraction occurs through the sliding interactions of microfilaments, actin and myosin, and generates joint tension. This tension creates a moment with respect to the joint center by which muscles act to manipulate joint position.[4] The force exerted by each muscle is dependent on size, type and the distance from the muscle insertion to the joint centre. During joint motion, the bone from which the muscle originates stays stationary and the insertion bone moves.[4] Muscles rarely work alone; instead they work in synergistic groups with the muscle exerting the most force the most being dubbed the prime mover.[4] The muscles acting in the direction of motion at any given time are termed the agonists. Each muscle group typically has an opposing muscle or muscles, called antagonist(s), acting to move the joint in the opposite direction.[4]

Wrist motion is primarily controlled through six forearm muscles: the flexor carpi ulnaris (FCU), flexor carpi radialis (FCR), abductor pollicis longus (APL), extensor carpi ulnaris (ECU), extensor carpi radialis longus (ECRL), and extensor carpi radialis brevis (ECRB), (Figure 1.12).[2] The flexor muscles are located in the volar compartment and extensors in the dorsal compartment. Forearm motion is primarily controlled through four separate muscles: the biceps brachii, supinator, pronator teres (PT), and pronator quadratus (PQ).[4]

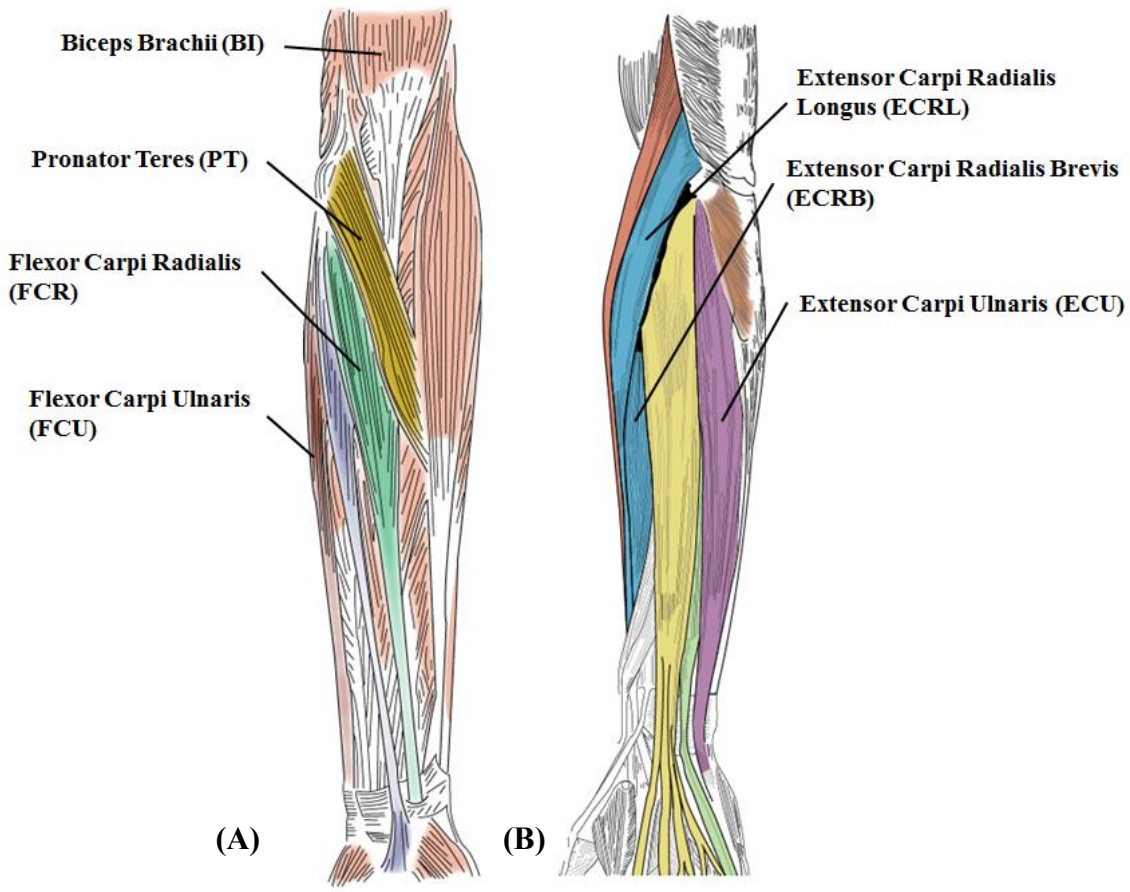

Figure 1.12: Muscles of the Wrist and Forearm. *Forearm muscles of the anterior or volar compartment (A) and posterior or dorsal compartment (B) of the right wrist and forearm. The muscles necessary for wrist flexion, extension, radioulnar deviation and forearm pronation and supination are individually labeled.*

1.1.4.1 ***Volar Compartment***

The volar compartment contains the FCU, FCR and APL muscles (Figure 1.12). These muscles act together to generate wrist flexion and radioulnar deviation. The muscles of the volar compartment are listed below.

1.1.4.1.1 *Flexor Carpi Ulnaris*

The FCU is the prime wrist flexor muscle and acts with the ECU to contribute to ulnar wrist deviation, or adduction. The FCU lies on the ulnar side of the forearm and ends in a tendon that occupies the lower half of the muscle. Its two heads originate on the medial epicondyle of the humerus and the medial olecranon of the ulna and insert on the hamate, dorsal pisiform and proximal 5th metacarpal.[1]

1.1.4.1.2 *Flexor Carpi Radials*

The FCR contributes to wrist flexion and acts with the ECRL and ECRB to generate radial wrist deviation, or abduction. The FCR originates on the medial epicondyle of the humerus and inserts into the base of the 2nd metacarpal.[1]

1.1.4.1.1 *Abductor Pollicis Longus*

The APL primarily acts to abduct the first metacarpal and it also assists in wrist flexion and radial deviation. The APL originates at the dorsolateral ulnar body, from the interosseous membrane, and the central portion of the dorsal radius and inserts lateral side of the 1st metacarpal.[1]

1.1.4.2 ***Dorsal Compartment***

The dorsal component contains the ECRL, ECRB and ECU muscles (Figure 1.12). These muscles act together to generate wrist extension and contribute to radioulnar wrist movements. The muscles of the dorsal compartment are listed below

1.1.4.2.1 *Extensor Carpi Radialis Brevis*

The ECRB contributes to wrist extension and radial wrist deviation in addition to acting as a wrist stabilizer during finger flexion. The ECRB is shorter and thicker than the ECRL. The ECRB originates on the later epicondyle of the humerus and inserts on the dorsolateral surface of the 3rd metacarpal.[1] The ECRB ends in a flat tendon and lies in a groove on the dorsal radius adjacent to the ERCL.

1.1.4.2.2 *Extensor Carpi Radialis Longus*

The ECRL contributes to both wrist extension and radial deviation, or abduction. The ECRL originates on the lower, lateral supracondylar ridge of the humerus and inserts on the dorsolateral side of the 2nd metacarpal.[1] The ECRL ends in a flat tendon that lies in the grooves present on the dorsal radius along with the ECRB.

1.1.4.2.3 *Extensor Carpi Ulnaris*

The ECU is the primary wrist extensor and contributes to ulnar deviation. The ECU originates on the lateral epicondyle of the humerus and the dorsal border of the ulna and inserts on the dorsomedial side of the 5th metacarpal. [1] The ECU ends in a flat tendon that sits in the foveal sulcus created by the ulnar head and ulnar styloid process.

1.1.4.3 ***Forearm Rotators***

Forearm rotation is generated and controlled by four major muscles: the biceps brachii, supinator, pronator teres (PT) and pronator quadratus (PQ) (Figure 1.12)

1.1.4.3.1 *Biceps Brachii*

The biceps brachii is the prime mover involved in forearm supination and contributes to elbow flexion. The biceps brachii is a long fusiform muscle that has two heads that originate from the coronoid process of the ulna and the supraglenoid tuberosity at the upper margin of the glenoid cavity. The biceps brachii inserts on the radial tuberosity.[1]

1.1.4.3.2 *Supinator*

The supinator assists the biceps brachii in forearm supination. The supinator is a broad muscle that originates on the lateral epicondyle of the humerus and the proximal ulna and inserts on the proximal, anterolateral radius.[1]

1.1.4.3.3 *Pronator Teres*

The PT passes obliquely across the forearm and acts as the primary forearm pronator. The PT has two heads of origin, the: humeral and ulnar head. The humeral head originates on the medial epicondyle, while the ulnar head originates on the medial side of the coronoid process. The PT inserts on the rough impression of the medial side of the radius halfway down the diaphysis.[1]

1.1.4.3.4 *Pronator Quadratus*

The PQ assists the PT in forearm pronation. The PQ is a small, flat muscle extending across the distal radius and ulna. The PQ originates on the distal anteromedial ulna and inserts on the distal anterolateral surface of the radius.[1]

1.2 Wrist Kinematics

1.2.1 *Range of Motion*

1.2.1.1 *Flexion-Extension Motion*

Planar wrist flexion-extension motion (FEM) occurs at the radiocarpal and midcarpal joints in coronal plane around the sagittal plane (Figure 1.13).[5] Ranges of FEM motion vary between individuals and average 60-90° of wrist flexion and 55-75° of wrist extension. The radiocarpal joint contributes more in wrist flexion (66%) and the midcarpal joint more in extension (66%).[6] Wrist FEM occurs at the radiocarpal and midcarpal joints under the control of the FCR, FCU, ECRL, ECRB and ECRL muscles. Wrist FEM is constrained by the dorsal radiocarpal ligaments during wrist extension and the volar radiocarpal ligaments during wrist flexion.[2]

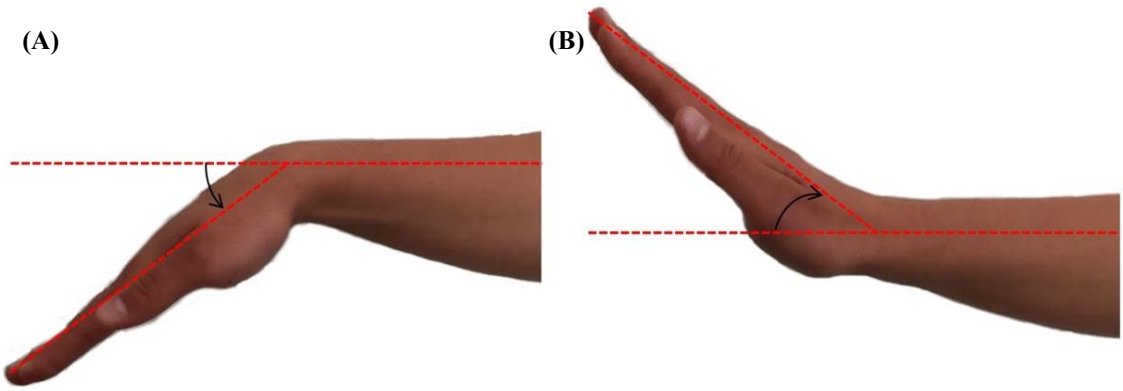

Figure 1.13 Range of Wrist Motion: Flexion-Extension. *Wrist joint motion in planar flexion (A) and in planar extension (B).*

1.2.1.2 *Radioulnar Deviation*

Planar wrist radioulnar deviation (RUD) refers to wrist abduction and adduction and occurs at the radiocarpal and midcarpal joints around the sagittal plane of the hand (Figure 1.14).[5] There are individual differences in RUD range of motion with the average being 15-25° of radial deviation and 30-45° of ulnar deviation. Radial deviation occurs primarily at the midcarpal joint, while ulnar deviation occurs primarily at the radiocarpal joint.[2,5] Radial deviation is controlled by the FCR, ECRB and ECRL muscles and ulnar deviation by the FCU and ECU muscles. RUD is constrained by the radial and ulnar collateral ligaments and limited by the prominent radial styloid.[2]

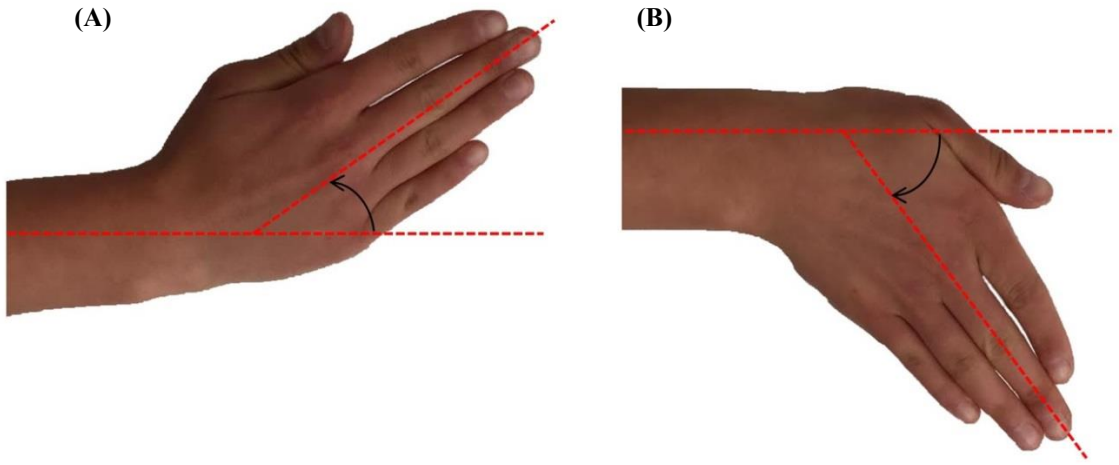

Figure 1.14: Range of Wrist Motion: Radial-Ulnar Deviation. *Wrist joint motion in planar radial deviation (A) and in planar ulnar deviation (B).*

1.2.1.3 ***Dart Throw Motion***

Dart throw motion (DTM) has been adapted experimentally to better represent the range of motion of daily activities (Figure 1.15).[7,8,9] During extension the wrist radial deviates and during flexion the wrist ulnar deviates. Dart throw motion is a combination wrist flexion-extension motion (FEM) and wrist radioulnar deviation (RUD) and occurs at the radiocarpal and midcarpal joints around the sagittal plane of the hand. There are varying opinions on which range of motion best represents a dart throw motion. The maximum proposed FEM range of motion is 30° of extension to 50° of flexion and the minimum is 20° of extension and 20° of flexion.[9,10,1] While there is discrepancy as to how much FEM to include, 10° of radial and 10° of ulnar deviation has been widely agreed on. Wrist FEM occurs under the control of the FCR, FCU, ECRL, ECRB and ECRL muscles, radial deviation is controlled by the FCR, ECRB and ECRL muscles and ulnar deviation by the FCU and ECU muscles.[2] For this study, the forward DTM is defined as 30° of wrist extension with 10° of radial deviation to 30° of flexion with 10° of ulnar deviation and reverse DTM defined as to 30° of flexion with 10° of ulnar deviation and 30° of wrist extension with 10° of radial deviation. This range of motion is thought to best reflect the range of motion of daily activities.[9]

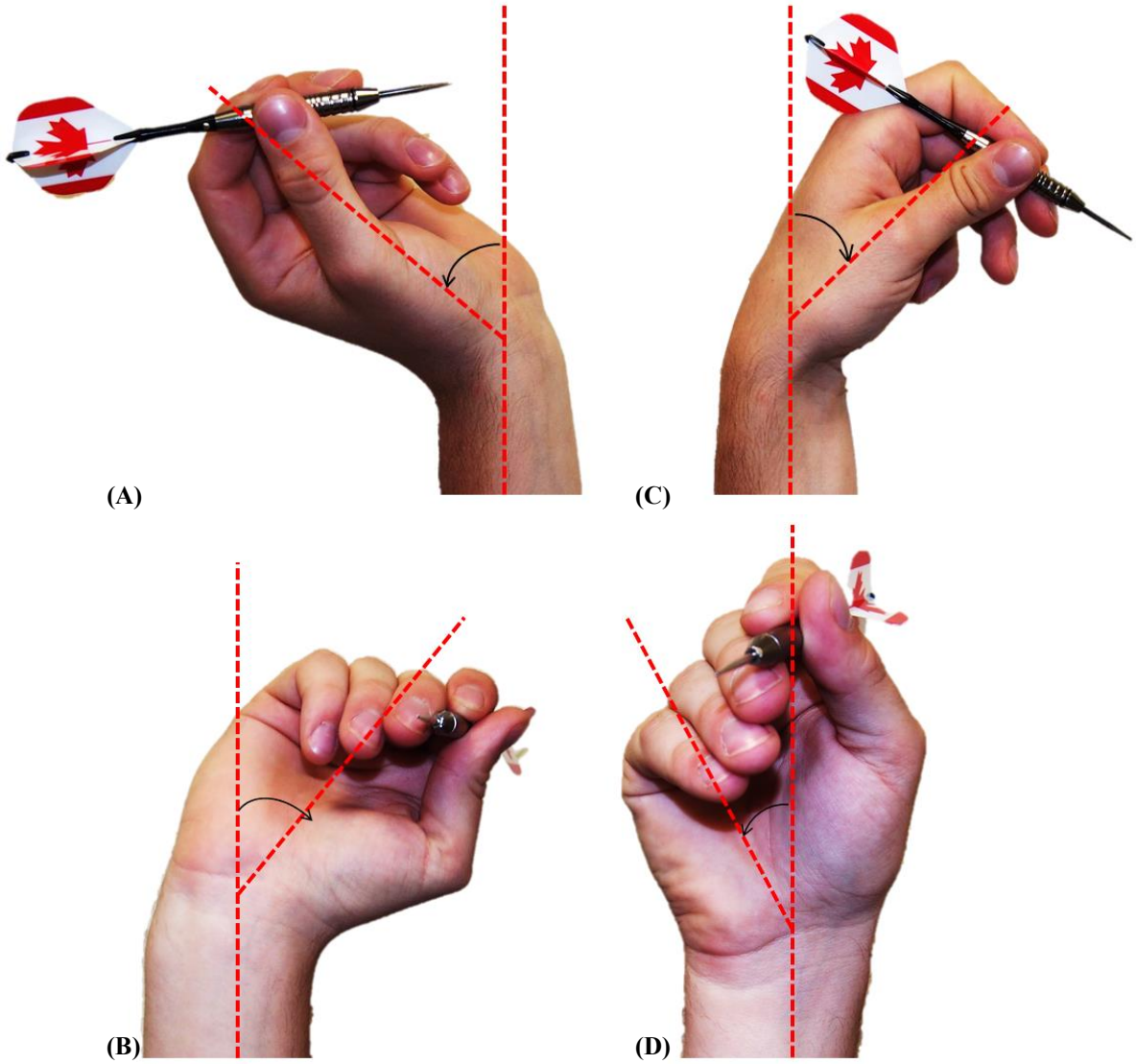

Figure 1.15: Range of Wrist Motion: Dart Throw. *Wrist joint motion in combined wrist extension (A) and radial deviation (B) and wrist flexion (C) and ulnar deviation (D).*

1.2.1.4 ***Pronation-Supination Motion***

Forearm pronation-supination motion (PSM) occurs at the distal radioulnar joints (DRUJ) and the proximal radioulnar joint (PRUJ) around a forearm axis stemming from the center of the radial head and extending to the ulnar sulcus between the ulnar head and styloid (Figure 1.16).[2] Average range-of-motion for forearm rotations is 60-80° of pronation and 60-85° or supination. PSM motion is controlled by the biceps brachii, supinator, PT and PQ.[2] Wrist supination is constrained by the dorsal and volar radioulnar ligaments, while wrist pronation is constrained by the crossing of the radius over the ulna.[12]

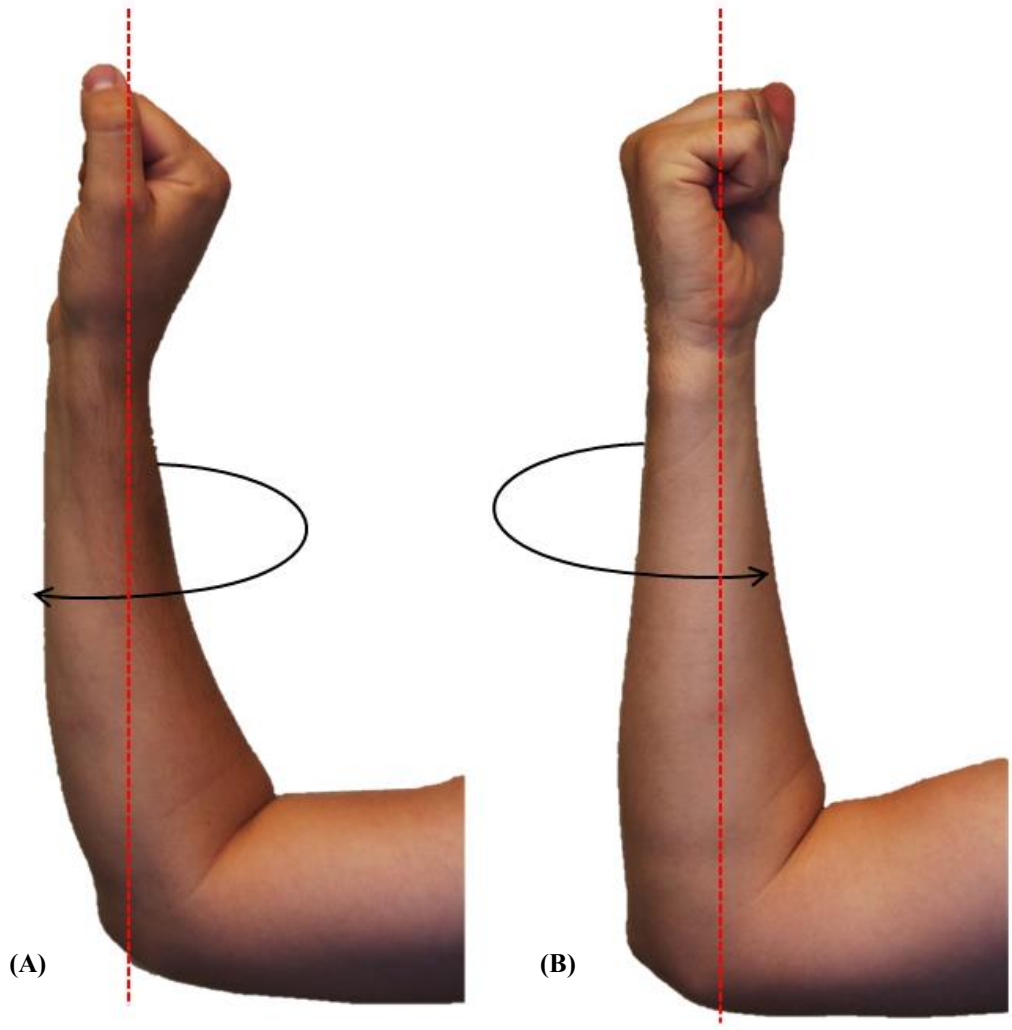

Figure 1.16 Range of Wrist Motion: Pronation-Supination. *Forearm pronation (A) and supination (B) occurs the distal radioulnar joint in the wrist. Pronation motion results in a palm down forearm position while supination motion results in a palm up position.*

1.3 Clinical Disorders of the Wrist and Forearm

1.3.1 *Wrist Fractures*

Wrist fractures are the most commonly occurring injury of the skeletal system with a cumulative life time incidence of 15% in women and 3% in men (Figure 1.17).[13,14] There are different types of wrist fractures determined by their fracture mechanism and associated malunions and misalignments. Distal radius fractures are the most common wrist fractures, and account for and one sixth of all skeletal fractures.[15-20] The most common fracture mechanism is a fall on a dorsiflexed hand, often leading to a Colles' fracture with dorsal angulation of the distal radius. The malunions and misalignments associated with distal radius fractures include changes in radial inclination, radial length or height, ulnar variance and dorsal-volar angulation.[21] Malunions and misalignments that occur following wrist fractures frequently lead to ulnar sided wrist pain, weakness, stiffness and degenerative diseases such as arthritis.[22-28] There is no single treatment for a wrist fracture; there is a range of treatments dependent on the type and severity of fracture, patient age and activity level. Common wrist fracture treatments include: splinting, casting, pin-fixation, external fixation and open reduction and internal fixation.[2]

Figure 1.17: Wrist Fracture. *Corresponding radiographic images of a distal radial fracture before (A) and after (B) an open reduction and internal fixation procedure to reduce and realign the wrist joint.*

1.3.2 *Kienbock's Disease*

Kienbock's disease is a wrist condition caused by the avascular necrosis and degradation of the lunate carpal bone with associated negative ulnar variance (Figure 1.18).[2, 29] Kienbock's disables the wrists of young active individuals with the onset ages most commonly between 20-25 years old. Patients present with chronic wrist pain, dorsal swelling, and decreased range of motion and are usually unable to recall a distinct traumatic event as a cause. There is literature to suggest that Kienbock's disease is caused by multiple minor traumatic events causing stress fractures of the lunate.[2] However, there is no known cause for Kienbock's disease; there is a list of risk factors that may be predicative, including: ulnar variance, lunate geometry, lunate vascularity, triangular fibrocartilage complex compliance and various congenital and developmental disorders.[2, 30-32] Many possible treatment options are prescribed to reduce wrist pain and delay inevitable joint degradation and arthritis, including: radial shortening, ulnar lengthening, wrist denervation, intercarpal fusions, proximal row carpectomy lunate revascularization, core decompression, or lunate excision with or without prosthetic replacement.[2, 33-35]

Figure 1.18: Keinbock's Disease. *Corresponding radiographic images of a patient presenting with negative ulnar variance due to Kienbock's disease before (A) and after (B) a radial shortening osteotomy to theoretically reduce the loading on the lunate.*

1.3.3 *Ulnar Impaction Syndrome*

Ulnar impaction syndrome, also known as ulnar carpal abutment, is the impaction of the distal ulnar head against the ulnar carpal bones and the triangular fibrocartilage (TFC) and is often associated with positive ulnar variance (Figure 1.20).[2, 36, 37] Ulnar impaction causes increased loading through the ulna at the ulnocarpal joint. Ulnar impaction also causes increased wear of the TFC.[36] Ulnar impaction syndrome can be acquired through traumatic wrist injury, overuse, or it may be congenital caused by Madelung's syndrome.[2, 38] Patients present with ulnar sided wrist pain, clicking at the wrist joint, and activity related swelling. Ulnar impaction syndrome can be treated either surgically or non-surgically. Examples of non-surgical intervention include altering daily activities, rest, splinting, therapy and/or non-steroidal anti-inflammatories.[2] Surgical inventions used to treat severe cases and include: ulna shortening, DRUJ fusion, ulnar resection or Wafer's procedure, and arthroscopic resection of the distal ulnar surface of the ulna beneath the triangular fibrocartilage.[2, 39-42]

Figure 1.19: Ulnar Impaction Syndrome. *A patient radiographic depicting ulnar impaction syndrome and corresponding positive ulnar variance (A) and following surgical intervention with an ulnar shortening osteotomy*

1.3.4 *Arthritis*

Arthritis is a degenerative joint disease characterized by the erosion of articular cartilage leading to painful bone on bone contact (Figure 1.20). Arthritis may be caused by a combination of aging, autoimmune disease, or previous traumatic skeletal or soft tissue injury. There are different types of arthritis depending on the mechanism of disease progression including: osteoarthritis, rheumatoid arthritis, and post-traumatic arthritis.[2,43] Osteoarthritis most frequently occurs in elderly populations due to age related cartilage deterioration resulting in joint degeneration, pain and stiffness. Rheumatoid arthritis is an autoimmune disease causing chronic joint inflammation, pain and stiffness in multiple joints at once.[43] Post-traumatic arthritis is either an immediate or delayed result of a previous traumatic skeletal or soft tissue injury. In post-traumatic arthritis, joint damage may occur at the time of injury or may be due to cartilage degeneration caused by poor joint alignment or direct cartilage damage.[43] While there is no cure for arthritis, there are many of non-surgical and surgical treatment options designed to reduce pain and delay disease progression. Non-surgical treatments include steroid injections in the joint capsule, splinting and oral anti-inflammatory medications. Surgical treatments for wrist arthritis include: proximal row carpectomy, carpal fusion, and partial to total wrist arthroplasty.[2, 43]

Figure 1.20: Distal Radioulnar Joint Arthritis. *A radiographic of a patient presenting with osteoarthritis before (A) and after (B) a total wrist arthroplasty.*

1.4 Load Measurement Techniques

An understanding of load transfer through the distal forearm is an important biomechanical measurement. The aforementioned traumatic injuries and degenerative diseases (Section 1.3) may cause changes in axial load transfer through the distal radius and ulna. Improving the understanding of forearm load transfer in native wrists is critical for improving existing biomechanical models, optimizing rehabilitation protocols and influencing surgical techniques. Various load measurement techniques and electrical sensors have been used to measure the changes in load transfer through the distal forearm. Two different electrical devices frequently used in biomechanical studies to measure *in vitro* forces are briefly outlined below.

1.4.1 *Strain Gauges*

Strain gauges are a type of electrical sensor that converts applied force, or strain, into electrical resistance. Strain is the displacement or deformation caused by either external or internal forces. Strain gauges convert the changes in mechanical deformation to electrical resistance which can then be calibrated to measure applied force.

1.4.2 *Load Cells*

Load cells are electrical transducers that generate electrical signal from applied force. There are a variety of load cell constructs including: hydraulic, piezoelectric, pneumatic, and strain gauge. Strain gauge load cells are the most common and are manufactured in different sizes with different load capacities. Load cells are stiff and have good resonance, making them excellent tools for measuring applied loads. The Subminiature Model 11 load cells from Honeywell were used for the entirety of this thesis (Figure 1.21) (Morristown, NJ, USA). The concept of a load cell implanted into bone is illustrated in the inset of Figure 1.21.

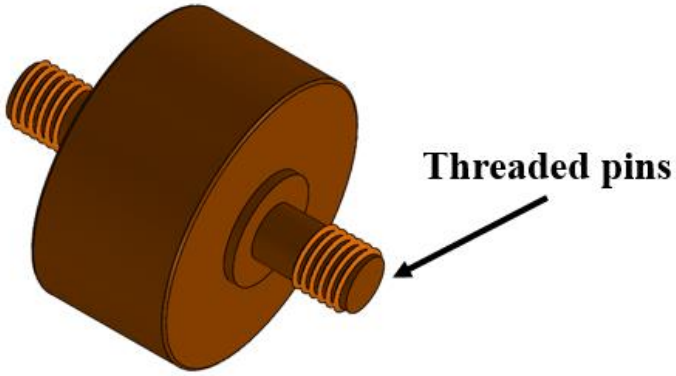

Figure 1.21: Subminiature Model 11 Load Cell (Honeywell Model 11, Golden Valley, MN, 2008). *The body component of a uniaxial load cell used for biomechanical testing.*

1.5 **Distal Forearm Load Sharing**

The wrist is a complex joint with multiple articulations making it difficult to actively simulate motion and measure bone loads. Changes in axial bone loads may be due to degenerative diseases, traumatic skeletal injuries or compromised soft tissue integrity. Improving knowledge of bone and joint loading is imperative for improving existing biomechanical models, influencing implant design and optimizing rehabilitation protocols. Previous studies have examined forearm bone load sharing under static loading scenarios and have concluded that the radius carries a greater percentage of load than the ulna at the distal forearm.

An early biomechanical study implanted uniaxial load cells mid-diaphysis in the radius and ulna and determined that load sharing between the radius and ulna occurs in an 82/18 ratio.[44] This study has led to the wide adoption of the 80/20 forearm load-sharing ratio by clinical communities. Additional studies have both confirmed and challenged the widely accepted 80/20 during static and dynamic loading.[42, 44-48] The ulnar contribution in forearm load-sharing has been shown to decrease to 13-14% under dynamic loading scenarios.[47, 48] Dynamic loading scenarios are of more clinical interest as they more realistically represent what is observed *in vivo*.

Wrist and forearm position influence the forearm load-sharing ratio. The percentage of load supported by the ulna is thought to peak with wrist extension, ulnar deviation and forearm pronation.[44, 45, 47, 49] This information is critical for planning rehabilitation protocols and postoperative recommendations. There is a lack of literature on the role direction of motion and active forearm pronation-supination has on forearm bone loading.

Joint reaction forces can be measured via *in vitro* instrumented experimental implants, telemetrized orthopedic implants and finite element modeling. Instrumented implants have been employed extensively in the shoulder, hip and knee. *Palmer et al.* completed the first influential study to use *in vitro* experimental measurement devices at the wrist.[44] They implanted uniaxial load cells in cadaveric specimen and subjected them to static axial tendon loads. They reported an 80/20 forearm load-sharing relationship between the radius and ulna respectively. This ratio has been widely accepted clinically and is still

considered the gold standard today. Additional studies have employed both uniaxial load cells in the radius and ulna to examine the effects of soft tissue sectioning on forearm bone loading under static applied loads.[45, 50-52] These implants vary from in-line with the axis of the bones to offset from the axis to the medial or lateral side of the bone.

Harley et al. completed the first forearm load sharing study to employ an *in vitro* experimental measurement device during active motion wrist simulation.[47] They used a basic device design with two six degree of freedom load cells offset from the long axis of the radius and ulna with external screw fixation. The bone between the two fixation points was sectioned to ensure that all loads were transmitted through the load cell. The loads recorded were not indicative of native loads transmitted axially through the bone because the load cells were not located in an anatomically correct position.[47] Instead, loads had to be reported as percentages of total bone load or transformed to the estimated loads at the anatomically correct positions.

Knowles et al. designed an instrumented experimental implant to examine axial loads through the proximal radius in-line with the bone at the radial head .[53] They used intramedullary fixation to fix the implant in place at its distal and proximal junctions and a Model 11 Honeywell subminiature load cell to collect axial loads. *Knowles et al.* completed a validation study of their implant that demonstrated the Model 11 Honeywell load cell to be highly reliable and accurate in measuring axial bone loads.[53]

The lengths of the radius and ulna also effect bone loading in the distal forearm. Ulnar load have been shown to significantly increase with as little as 2mm of radial shortening and ulnar lengthening.[44] Research groups have suggested that this implies natural positive ulnar variance would therefore increase ulnar bone loads.[52, 54] However, very little correlation has been found between natural ulnar variance and ulnar loads.[46, 47] This is thought to be due to the inversely proportional relationship between TFCC thickness and ulnar variance.[47] The biomechanical implications of ulnar bone length on ulnar loading have been translated to various clinical applications, including ulnar osteotomies as a treatment of ulnar impaction syndrome.[42, 44, 46, 48, 51, 52, 54]

Small changes in soft tissue integrity can contribute to significant changes in bone loading. The TFC plays an imperative role in distal forearm bone loads and changes in its thickness and integrity affect the loads transmitted through the distal radius and ulna.[44,47] Sectioning the TFC decreases distal ulna loading by decreasing the constraining effect at the DRUJ.[44, 55, 56]

1.6 In-Vitro Testing Simulators

In vitro experimental measurement devices and active joint motion simulators are imperative to improve the understanding human biomechanics. These technologies are usually tested using *in vitro* cadaveric models. Previous studies have been conducted using implantable experimental measurement devices and active wrist motion simulators.

Experimental simulators have been developed to recreate both active and passive joint motion. Active joint motion simulation aims to recreate *in* vivo loading scenarios. During active wrist motion simulation, forces are applied directly to the tendons of each muscle to achieve desired joint motion. Joint motion is controlled through force-position algorithms. Muscles that generate joint motion work under an agonist - antagonist relationship, where the agonist, or prime mover, muscles act in the direction of motion and the antagonists in the opposite direction. In joint motion simulation, the agonists control the angular velocity of the motion and the antagonists maintain only a basic tone load to maintain joint constraint. When the direction of motion is reversed the agonist muscles become the antagonists.

Dunning et al. developed an active wrist and hand motion simulator that employed pneumatic actuators to generate joint motion. This simulator actuates nine muscles to recreate various finger and wrist movements in cadaveric specimens. [57] Motion is tracked using a passive electromagnetic tracking system; however no real-time positional feedback is provided. Specimens are mounted with the elbow in 90° of flexion and the humerus perpendicular to the ground, with finger tips directed forward. The *Dunning* simulator uses an open loop control system and required extensive tuning to achieve desired motions for each specimen. [57] The simulators inability to adjust for interspecimen variability made for poor repeatability.

The first active, repeatable planar wrist motion simulator was developed by *Werner et al*.[58] The six major muscles responsible for wrist flexion and extension are actuated through a multichannel servo hydraulic system. Electromagnetic trackers are fixed to the ulna, third metacarpal and lunate and real-time joint position feedback is used to control the motion path. [58] Specimen are amputated mid-humerus, mounted with the elbow in 90°

of flexion and the humerus parallel to the ground, with finger tips directed upwards. The major limitation of this simulator is that all surrounding soft tissues, excluding tendons and ligaments, must be sectioned and resected.

Iglesias et al. have developed an *in vitro* active wrist motion simulator that performs in multiple, gravity loaded positions (Figure 1.22).[59] Joint motion is simulated by a servomotor manifold that actuates the ECU, ECRL, ECRB, FCU, FCR, PT and biceps brachii. Each servomotor is instrumented with a strain gauge to allow real-time feedback of tendon loads throughout motion.[59] *Iglesias'* simulator effectively maintains target tendon loads and achieves repeatable active wrist motion. This simulator can achieve both active wrist flexion-extension and radioulnar deviation, similar to the simulators outlined above. It is also capable of performing multiplanar motions such as dart throw motion and wrist circumduction. By actuating the PT and biceps brachii the *Iglesias* simulator generated active forearm pronation-supination. Optical trackers are attached to the third metacarpal, radius and ulna and real-time joint position feedback is relayed to force-position algorithms allowing for precise simulator control.[59] All muscles were loaded with a 8.9N tone load to maintain joint stability during active motion.

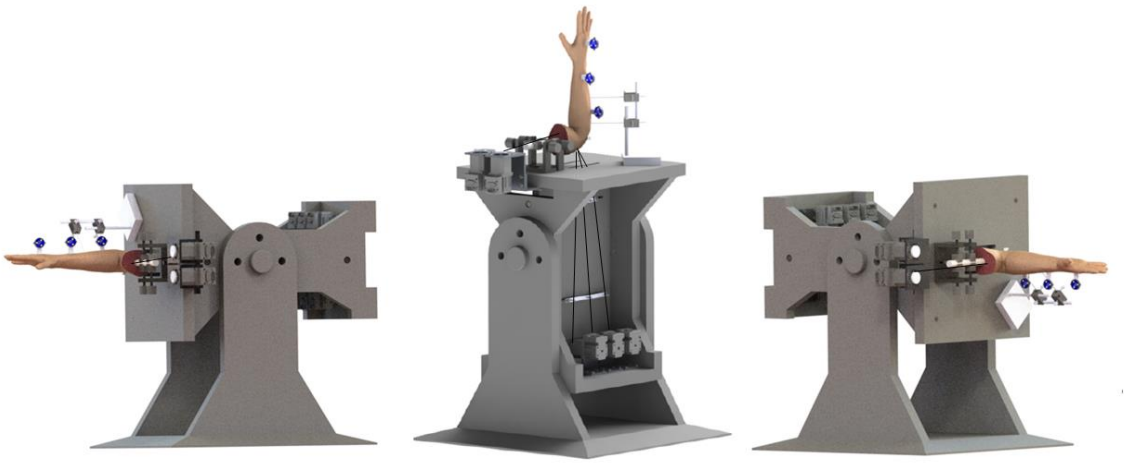

Figure 1.22: Iglesias' Active Motion Wrist Simulator. *Active wrist motion simulator developed by* Iglesias et al. *in three variable gravity load positions.*

1.7 Thesis Rationale

A comprehensive understanding of wrist loading is important for improving existing biomechanical models, influencing surgical techniques and optimizing rehabilitation protocols. In order to understand the consequences of distal radial fractures, ulnar impaction and DRUJ instability, clinicians must first have an extensive understanding of healthy joint biomechanics and native forearm bone loads. An improved knowledge of native and pathological forearm bone loads will assist clinicians in developing rehabilitation techniques, surgical procedures and implant designs.

Measuring and recording *in vivo* bone loads is extremely invasive and infringes on ethical boundaries. Therefore, *in vitro* measurements from cadaveric specimen remain the gold standard for biomechanical researchers. While *in vitro* models address ethical conflicts, basic human anatomy and adjacent soft tissues continue to pose challenges to data collection. As discussed, instrumented experimental devices have long been used to measure and calculate joint reaction forces and axial bone loads. Simple implant designs containing both commercial and custom load cells have been employed to measure *in vitro* distal radius and ulna loads under applied static loads.[45, 50, 52, 55] Existing experimental implants designs are invasive, anatomically inaccurate and disruptive to surrounding soft tissues. The limitations of existing experimental implants prevent them from reliably and accurately collecting forearm bones loads. Therefore, an implant to collect *in vitro* radial and ulnar load measurements with minimal soft tissue disruption and anatomic load cell placement is necessary for improved experimental data collection.

Forearm load sharing, as documented above, has been extensively examined under static loading scenarios. The radius is known to be subjected to larger loads than the ulna at the distal forearm. Static forearm bone load sharing is widely accepted as an 80/20 ratio between the radius and ulna, respectively. [42, 44, 45, 46, 47, 48] While static distal forearm bone loading has been successfully defined and clinically accepted, radial and ulnar loads remain poorly understood during dynamic loading scenarios. Dynamic loading of the wrist joint implies actuating forearm tendons to produce the full range of wrist motions. Researchers have only recently begun to examine the effects of active joint motion on forearm bone loading. Preliminary work indicates that forearm bone loads change

significantly with changes in wrist flexion-extension and radioulnar deviation.[47] The forearm bone load sharing ratio for dynamic loading differs from that of static loading scenarios with an 87/13 radius to ulna ratio reported at neutral wrist position.[47] Triangular fibrocartilage (TFC) integrity plays an important role in forearm bone load sharing in static loading scenarios and should therefore be examined under dynamic tendon loading.[44] The effects of active motion, wrist and forearm position and TFC integrity on forearm bone loading are still poorly understood. Further research is required to address the voids in the literature and improve existing biomechanical models.

Native biomechanics of the wrist and forearm may be altered by wrist fractures, Kienbock's disease, and ulnar impaction. Such traumatic injuries and degenerative diseases are often associated with joint malunions and malignments causing changes in bone length.[21] Changes in radial and ulnar lengths effect bone loading in the distal forearm. Significant changes in ulnar loading occur with as little as 2mm of ulnar lengthening. [44] The biomechanical implications of forearm bone length on radius and ulna loads have been directly applied to clinical interventions, such as ulnar osteotomies for the treatment of ulnar impaction.[42, 44, 46, 48, 50, 51, 52] Therefore, additional examination of radial and ulnar length changes and their effect on distal forearm loading should be conducted using active motion simulation.

1.8 Objectives and Hypotheses

1.8.1 *Specific Objectives*

The objectives of this thesis are as follows:

1. To design and evaluate an experimental apparatus for examining *in vitro* axial distal forearm bone loads during active wrist flexion-extension, radial-ulnar deviation and dart throw motion;
2. To determine the effect of joint position and motion direction on forearm bone loading throughout active wrist flexion-extension, radial-ulnar deviation, and dart throw motion;
3. To determine the effect of radial length change, joint position and direction of motion on distal forearm load magnitude and forearm bone load sharing during active forearm pronation-supination.

1.8.2 *Specific Hypotheses*

1. The experimental load measurement will be capable of measuring radial and ulnar loads with reliability greater than 95%.
2. Distal radius and ulna loading loads will change with wrist and forearm motion and direction of motion.
3. Radial length and forearm rotation angle will affect distal radius and ulna loading as well as load sharing between the bones. Increased radial length will increase axial loads through the radius and increase the percentage of total forearm bone load through the radius.

1.9 Thesis Overview

Chapter 2: Describes the design and development of two instruments modular implants capable of measuring *in vitro* bone loads and simulating bone length changes. Additionally, investigates the repeatability of both the radial and ulnar sided implants.

Chapter 3: Investigates *in vitro* axial bone loads in the distal radius and ulnar and the effect of joint angle and direction of motion during active simulated wrist motion.

Chapter 4: Investigates the effect of radial length change, joint rotation angle and direction of motion during active simulated forearm rotation.

Chapter 5: Gives a general summary, discussion and conclusion of the work presented and the potential areas of future work.

1.10 References

1. Gray H. *Anatomy of the Human Body*. 20th ed. (Philadelphia: Lea & Febiger, ed.). New York, NY; 1918.

2. Cooney WP. *The Wrist: Diagnosis and Operative Treatment*. Vol 8. 2nd ed. (Kluwer W, ed.). Philadelphia, Balitmore, New York, Lodon, Buenos Aires, Hong Kong, Sydney, Tokyo; 2011.

3. Litchtman DM, Schneider JR, Swafford AR, Mack GR. Staging and its use in the determination of treatment modalities for Kienbock's disease. *Hand Clin.* 1993; 9(3), 409-416.

4. Wu G, van der Helm FCT, Veeger HEJD, et al. ISB recommendation on definitions of joint coordinate systems of various joints for the reporting of human joint motion--Part II: shoulder, elbow, wrist and hand. *J Biomech*. 2005; 38(5):981-992.

5. Lippert L. Clinical Kinesiology and Anatomy of the Upper Extremities. In: *Clinical Kinesiology and Anatomy*. 5th ed. F.A. Davis; 2011.

6. Ruby LK, An KN, Linscheid RL, Cooney WP, Chao EY. The effect of scapholunate ligament section on scapholunate motion. *J Hand Surg Am*. 1987; 12(5 Pt 1):767-771.

7. Crisco JJ, Coburn JC, Moore DC, Akelman E, Weiss AP, Wolfe SW. In vitro radiocarpal kinematics and the dart thrower's motion. *J Bone Joint Surg Am.* 2005; 87(12), 2729-2740.

8. Palmer AK, Werner FW, Murphy D, Glisson R. Functional wrist motion: a biomechanical study. *J Hand Surg Am.* 1985; 10(1), 39-46.

9. Werner FW, Green JK, Short WH, Masaoka S. Scaphoid and lunate motion during a wrist dart throw motion. *J Hand Surg Am.* 2004; 29(3), 418-422.

10. Waters MS, Wener FW, Haddad SF, McGrattan ML, Short WH. Biomechanical Evaluation of Schaphois and Lunate Kinematics FOllowing Selective Sectioning of Protions of the Scapholunate Interosseous Ligament. *J Hand Surg Am.* 2006; 41(2), 208-2013.

11. Dimitris C, Werner FW, Joyce DA, Harley BJ. Force in the Scapholunate Interosseous Ligament During Active Wrist Motion. *J Hand Surg Am*. 2015; 40(8):1525-1533.

12. Acosta R, Hnat W, Scheker LR. Distal radio-ulnar ligament motion during supination and pronation. *J Hand Surg Br*. 1993; 18(4):502-505.

13. S, Graf. Fractures of the distal end of the distal radius: Classification of treatment and indications for external fixation. *Injury.* 1994; 25(1), 14-25.

14. Levine, MA. Fractures of the Distal Radius. Orthop Knowl Update, Trauma. (pp. 67-82). Published 1996.

15. Souer JS, Lozano-Calderon SA, Ring D. Predictors of wrist function and health status after operative treatment of fractures of the distal radius. *J Hand Surg Am.* 2008; 33(2), 157-163.

16. Cooney WP. Fractures of the distal radius. A modern treatment-based classification. *Orthop Clin North Am. 1993; 24*(2), 211-216.

17. Maschke SD, Evans PJ, Schub D, Drake R, Lawton JN. Radiographic evaluation of dorsal screw penetration after volar fixed-angle plating of the distal radius: a cadaveric study. *Hand. 2007;2*(3), 144-150.

18. Lill CA, Goldhahn J, Albrecht A, Eckstein F, Gatzka C, Schneider E. Impact of bone density on distal radius fracture patterns and comparison between five different fracture classifications. *J Orthop Trauma.* 2003; 17(4), 271-278.

19. Belloti JC, Tamaoki MJ, Franciozi CE, *et al.* Are distal radius classifications reproducible? Intra and interobserver aggreement. *Sao Paulo Med J.* 2008; 126(3), 180-185.

20. Nesbitt KS, Failla JM, Les C. Assessment of instability factors in adult distal radius fractures. *J Hand Surg Am.* 2004; 29(6), 1128-1138.

21. Graham T. Surrgical correction of malunited fractures of the disal radius. *J Am Acan Orthop Surg.* 1997; 5, 270-281.

22. Adams BD. Effects of radial deformity on distal radioulnar joint mechanics. *J Hand Surg Am.* 1993; 18(3), 492-498.

23. Fernandez DL. Correction of post-traumatic wrist deformity in sdults by osteotomy, bone-grafting and internal fixation. *J Bone Joint Surg Am.* 1982; 64(8), 1164-1178.

24. Fernandez DL. Radial osteotomy and Bowers arthroplasty for malunited fractures of the distal end of the radius. *J Bone Joitn Surg Am.* 1988; 70(10), 1538-1551.

25. Jupiter JB, Ring D. A comparison of early and late reconstruction of malunited fractures of the distal end of the radius. *J Bone Joint Surg Am.* 1996; 78(5), 739-748.

26. Cooney WP, Dobyns JH, Linscheid RL. Complications of Colles' fractures. *J Bone Joint Surg Am.* 1980; 33(4), 895-907.

27. Gartland JJ Jr, Werley CW. Evaluation of healed Colles' fractures. *J Bone Joint Surg Am.* 1951; 33(4), 895-907.

28. Gliatis JD, Plessas SJ, Davis TR. Outcome of distal radial fractures in young adults. *J Hand Surg Br.* 2000; 25(6), 535-543.

29. Beckenbaugh RD, Shives TC, Dobyns JH, Linscheid RL. Kienbock's disease: the natural history of Kienbock's disease and consideration of lunate fractures. *Clin Orthop Relat Res.* 1980; 149, 98-106.

30. Jensen CH. Intraosseous pressure in Kienbock's disease. *J Hand Surg Am.* 1993; 18(2), 355-359.

31. Gelberman RH, Salamon P, Jurist JM, Posch JL. Ulnar variance in Kienbock's disease. *J Bone J Surg Am.* 1975; 57(5), 674-676.

32. Litchtman DM, Schneider JR, Swafford AR, Mack GR. (1981). Ulnar midcarpal instability - clinical and laboratory analysis. *J Hand Surg Am.* 1981; 6(5), 515-523.

33. Armistead RB, Linscheid RL, Dobyns JH, Beckenbaugh RD. Ulnar lengthening as a treatment for Kienbock's disease. *J Bone J Surg Am.* 1982; 64(2), 170-178.

34. Weiss AP, Weiland AJ, Moore JR, Wilgis EF. Radial shortening for Kienbock disease. *J Bone Joint Surg Am.* 1991; 73(3), 384-391.

35. Nakamura R, Horii E, Watanabe K, Nakao E, Kato H, Tsunoda K. Proximal row carpectomy versus limited wrist arthrodesis for advanced Kienbock's disease. *J Hand Surg Br.* 1998; 23(6), 741-745.

36. Friedman AL, Palmer AK. The ulnar impaction syndrome. *Hand Clin.* 1991; 7(2), 295-310.

37. Cerezal L, Pinal F, Abascal F, Garcia-Valtuille R, Pereda T, Canga A. Imaging findings in ulnar-sided wrist impaction syndromes. *Radiographics.* 2002; 22(1), 105-121.

38. Huguet S, Leheup B, Aslan M, Muller F, Dautel G, Journeau P. Radiological and clinical analysis of Madelung's deformity in children. *Orthop Traumatol Surg Res.* 2014; 100(6), 349-352.

39. Nishiwaki M, Nakamura T, Nagura T, Toyama Y, Ikegami H. Ulnar-shortening effect on distal radioulnar joint pressure: a biomechanical study. *J Hand Surj Am.* 2008; 33(2), 198-205.

40. Minami A, Kato H. Ulnar shortening for triangular fibrocartilage complex tears associated with ulnar positive variance. *J Hand Surg Am.* 1998; 23(5), 904-908.

41. Feldon P, Terrono AL, Belsky MR. Wafer distal ulna resection for triangular fibrocartilage tears and/or ulna impaction syndrome. *J Hand Surg Am.* 1992; 17, 731-737.

42. Markolf KL, Tejwani SG, Benhaim P. Effects of wafter resection and hemirection from the distal ulnar on load-sharing at the wrist: a cadaveric study. *J Hand Surg Am.* 2005; 30(2), 351-358.

43. Brubacher J, Fischer S. American Academy of Orthopaedic Surgeons - Arthritis of the Wrist. Published 2016.

44. Palmer AK, Werner FW. Biomechanics of the distal radioulnar joint. *Clinical Orthop.* 1984; (187), 26-35.

45. Trumble T, Glisson RR, Seaber AV, Urbaniak JR. Forearm force transmisison after surgical treatment of distal radioulnar joint disorders. *J Hand Surg Am.* 1987; 12(2), 196-202.

46. Werner FW, Palmer AK, Fortino MD, Short WH. Force transmission through the distal ulna: effect of ulnar variance, lunate fossa angulation, and radial and palmar tilt of the distal radius. *J Hand Surg Am*. 1992; 17(3)

47. Harley B, Pereria M, Werner F, Kinney D, Sutton L. Force Variations in the Distal Radius and Ulna: Effect of Ulnar Variance and Forearm Motion. *J Hand Surg Am.* 2015; 40(2), 211-216.

48. Greenberg JA, Werner FW, Smith JM. Biomechanical analysis of distal metaphyseal ulnar shortening osteotomy. *J Hand Surg Am.* 2013; 38(1), 1914-1919.

49. Ekenstam FW, Palmer AK, Glisson RR. The load on the radius and ulna in different positions of the wrist and forearm. A cadaver study. *Acta Orthop Scand.* 1984; 55(3), 363-365.

50. Rabinowitz RS, Light TR, Havey RM, Gourineni P, Patwardhad AG, Satori MJ, Vrbos L. The role of the interosseous membrane and triangular fibrocartilage. *J Hand Surg Am.* 1994; 19(3), 385-393.

51. Markolf KL, Dunbar AM, Hannani K. Mechanisms of load transfer in the cadaver forearm: role of the interosseous membrane. *J Hand Surg Am.* 2000; 25(4), 647-682.

52. Tomaino M, Elfar J. Ulnar Impaction syndrome. *Hand Clinics.* 2005; 21(4), 567-575.

53. Knowles NK, Gladwell M, Ferreira LM. An intra-bone axial laod transducer: development and validation in an in-vitro radius model. *J Exp Orthop.* 2015; *2*(1), 19.

54. Sachar K. Ulnar-side wrist pain: evaluation and treatment of triangular fibrocartilage complex tears, ulnocarpal impaction syndrome, and lunotriquetral tears. *J Hand Surg Am.* 2008; 33(9), 1669-1679.

55. Ferreira LM, Greeley GS, Johnson JA, King GJ. Load transfer at the distal ulna following simulated distal radius fracture malalignment. *J Hand Surg Am.* 2015; 40(2), 217-223.

56. Markolf KL, Lamey D, Yang S, Meals R, Hotchkiss R. Radioulnar load-sharing in the forearm. A study in cadavera. *J Bone Joint Surg Am.* 1998; 80(6), 879-888.

57. Dunning CE, Lindsay CS, Bicknell RT, Patterson SD, Johnson JA, King GJ. Supplemental pinning improves the stability of external fixation in distal radius fractures during simulated finger and forearm motion. *J Hand Surg Am*. 1999;24(5):992-1000.

58. Werner FW, Palmer AK, Somerset JH, et al. Wrist joint motion simulator. *J Orthop Res*. 1996;14(4):639-646.

59. Iglesias D. Development of an in-vitro passive and active motion Simulator for the investigation of wrist function and Kinematics. *Electron Thesis Diss Repos*. 2015.

Chapter 2

2 *Design and Development of an Experimental Measurement System for Examining In Vitro Load Magnitudes and Sharing in the Distal Forearm*

Overview

This chapter focuses on the design and development of two modular implants capable of simulating clinically relevant length change deformities of the distal radius and ulna bones. These implants will be employed in the biomechanical testing of common forearm deformities in a laboratory setting. An overview of the application of an active wrist motion testing simulator and optical tracking system for forearm motion are also discussed.

2.1 Distal Forearm Bone Implant Development

As described in Chapter 1 (Section 1.5), understanding forearm bone loads is an integral part of optimizing rehabilitation protocols, surgical techniques, and improving biomechanical models. Biomechanical studies examining native and pathological forearm bone loads during active motion, with simulated changes in bone length and varied wrist and forearm joint angles have not been reported. A greater understanding of the forces through the distal radius and ulna will improve the diagnosis and treatment of common clinical presentations of altered forearm bone geometries including distal radial fractures, Kienbock's disease, ulnar impaction syndrome, distal radius malunions, and wrist arthroplasty.[1-5] Although previous studies have examined the effect of altered radial and ulnar lengths under static loading scenarios these studies have not quantified the associated distal forearm bone loads during active simulated wrist and forearm motion.[6-9]

Previous studies have employed simple load cell implant designs to examine forearm bone loads and load sharing.[6, 10-12] These designs have been invasive, geometrically inaccurate and disruptive of surrounding soft tissues thereby decreasing their ability to reliably and accurately quantify forearm bone loads. The majority of previous designs feature an offset load cell configuration producing a potential bending moment at the osteotomy. [6, 10-12] Therefore, an adjustable implant that allows for *in vitro* radial and ulnar load measurement with minimal soft tissue disruption and anatomic load cell placement is required for improved experimental load cell measurements.

A modular implant described herein allowed for simple transition between clinically relevant changes in forearm bone length. These implants were developed to examine native load sharing with wrist joint angle, forearm rotation angle and forearm bone length being the independent variables. Simulating active wrist and forearm motions allowed common bone length deformities be accurately and reproducibly studied to determine their effect on distal forearm bone loading. Active wrist flexion/extension, radial/ulnar deviation, forward/reverse dart throw, and forearm pronation/supination were simulated and both radial and ulnar loads were simultaneously measured. Clinically relevant

forearm bone length changes were evaluated in the same specimen to allow for a repeated measures experimental design.

The aim of the implants (Figures 2.1, 2.2) was to lengthen and shorten the radius and ulna with the incorporation of uniaxial load cells to quantify distal forearm load transmission. The radius implant utilized plate fixation distally and intramedullary fixation proximally while the ulna implant employed intramedullary fixation both distally and proximally. Both implants were inserted using alignment spacers, which were later removed and replaced with the modular implants containing the uniaxial load cells.

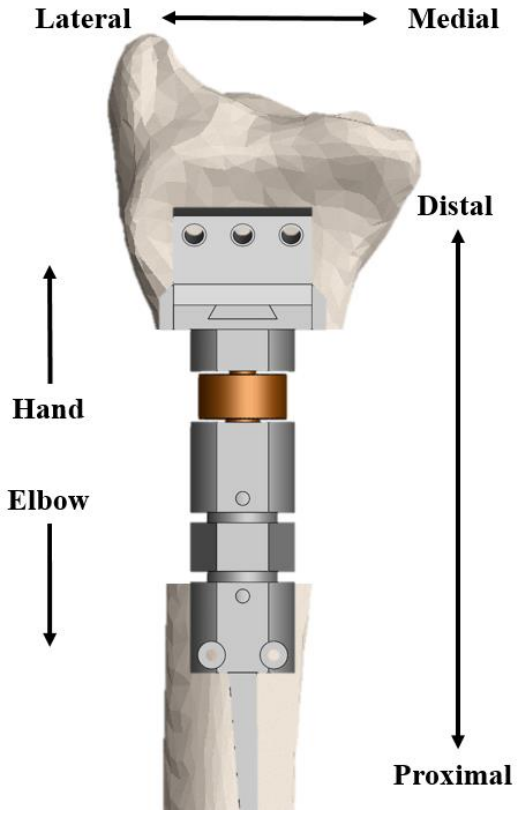

Figure 2.1: Distal Radius Implant. *A volar view of the surgically inserted radial implant is shown. The distal radius implant was designed and used for biomechanical testing and examination of distal axial radial bone loads. The central turnbuckle mechanism allows for modular bone length changes.*

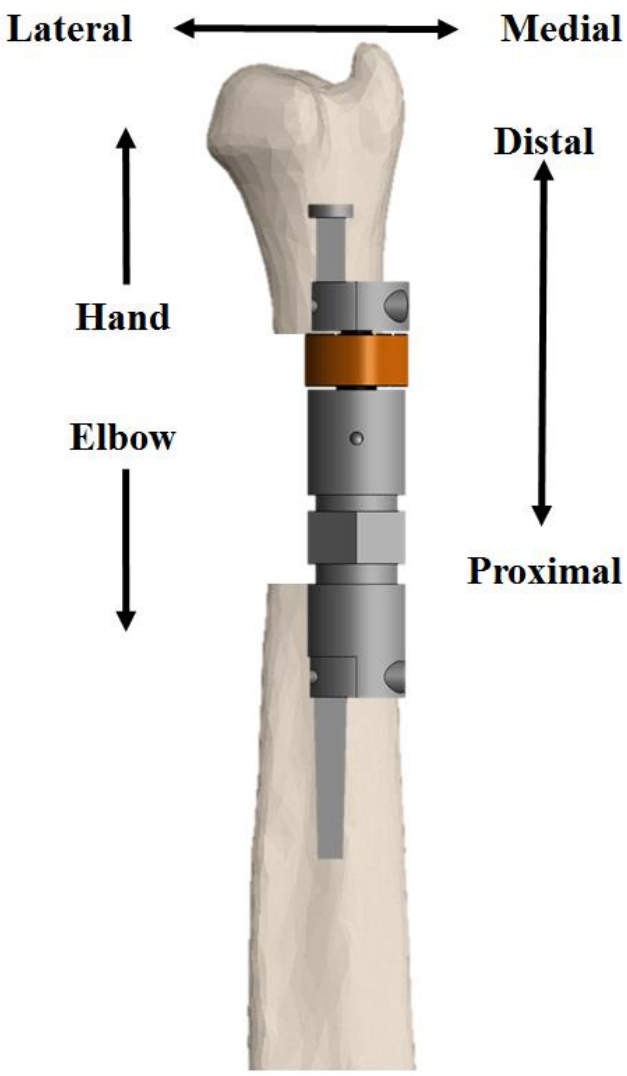

Figure 2.2: Distal Ulna Implant. *A volar view of the surgically inserted ulnar implant is shown. The distal ulna implant was designed and used for biomechanical testing and examination of distal axial ulnar bone loads. The central turnbuckle mechanism allows for modular bone length changes.*

One ***uniaxial load cell*** (Honeywell Model 11) was incorporated into both the modular radius and ulna implant appliances to measure axial loads through the each bone (Chapter 1, Figure 1.21) (Honeywell, Golden Valley, MN, 2008). Honeywell's Model 11 subminiature load cell measures both tension and compression. Load cell position was offset dorsally from the modular implant appliance axis to better align with the biomechanical axis of the radial bone. In the ulnar implant, the uniaxial load cell was threaded into the proximal junction and fixed with medium steel epoxy in the same fashion as the in the radial implant. The load cell was fit into pre-existing threads and held in place by a mating threaded cap, two perpendicular #2-56 screws and the associated compressive force.

Two implantation spacers were designed and machined from stainless steel to aid in the implantation of the modular radius (Figure 2.3) and ulna implants (Figure 2.4). The implantation spacers were machined to be the exact length of the modular appliance component when set to its neutral length. During implantation, the spacers were used to allow fixation of the stems using bone cement (Simplex P ,75% Methylmethacrylate-stryrene copolymer, 15% polymethylmethacrylate, 10% Barium Sulfate,Stryker Medical, Kalamazoo, MI, 2016) while maintaining a bone bridge to ensure optimal implant positioning while maintaining the anatomical alignment of the bones. The bone bridges were removed after the cement had set (Section 2.2.1.1, Figure 2.16 (B)). After the implantation was complete and the arm had been mounted on the active motion simulator the spacers were exchanged for the modular appliances. These spacers have the same mating interfaces as their respective modular appliances to assure a seamless transition between the spacers and the measurement devices.

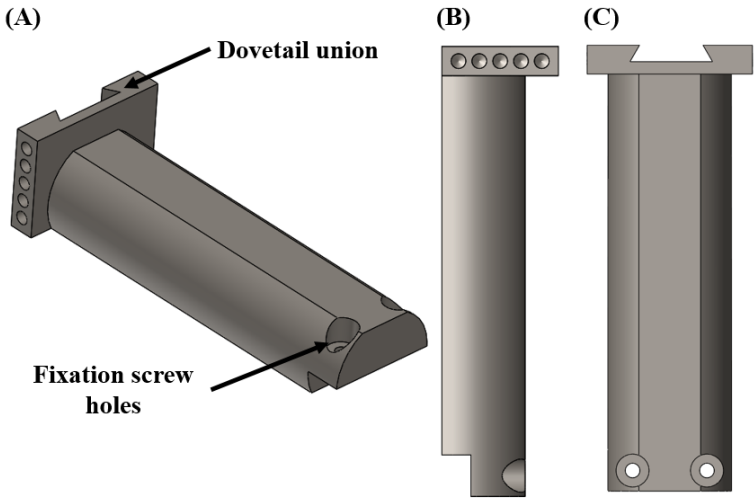

Figure 2.3: Implantation Spacer for Modular Radial Device. *An isometric view of the radial implant spacer (A) is shown along with a lateral view (B), and a volar view (C). The radial spacer was designed to replace the modular radius implant device to protect it from being damaged during surgical implantation. The mating interfaces are the same as those of the modular radial appliance.*

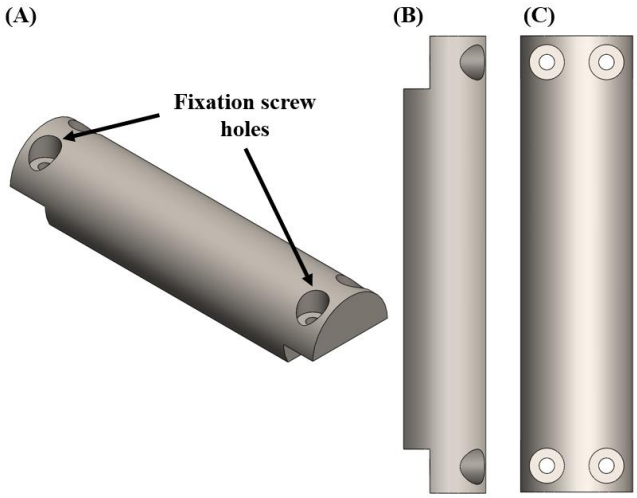

Figure 2.4: Implantation Spacer for Modular Ulnar Device. *An isometric view of the ulnar implant spacer (A) is shown along with a lateral view (B), and a volar view (C). The ulnar spacer was designed to replace the modular radius implant device to protect it from being damaged during surgical implantation. The mating interfaces are the same as those of the modular ulnar appliance.*

2.1.1 *Distal Radius Implant Design and Function*

The experimental distal radius implant (Figure 2.5) was developed to examine the effect of common clinical conditions such as distal radial fractures, Keinbock's disease and distal radial malunions on the axial loads experienced in the distal radius. Stainless steel was used for its strength and its compatibility with the material properties of the uniaxial load cells used to ensure that the steel threads of the load cell did not strip the mating threads of the implant, as would occur with a softer metal. Intramedullary measurements of the distal radius were taken on an in-house database of CT scans to ensure device would fit varying sizes of specimen (Appendix B). The distal plate was modeled from a commercial distal radial fixation plate (Volar Distal Radius Plate, Synthes North America, West Chester, PA). Similarly, a distal volar tilt of 22˚ was used for the distal radial plate geometry.

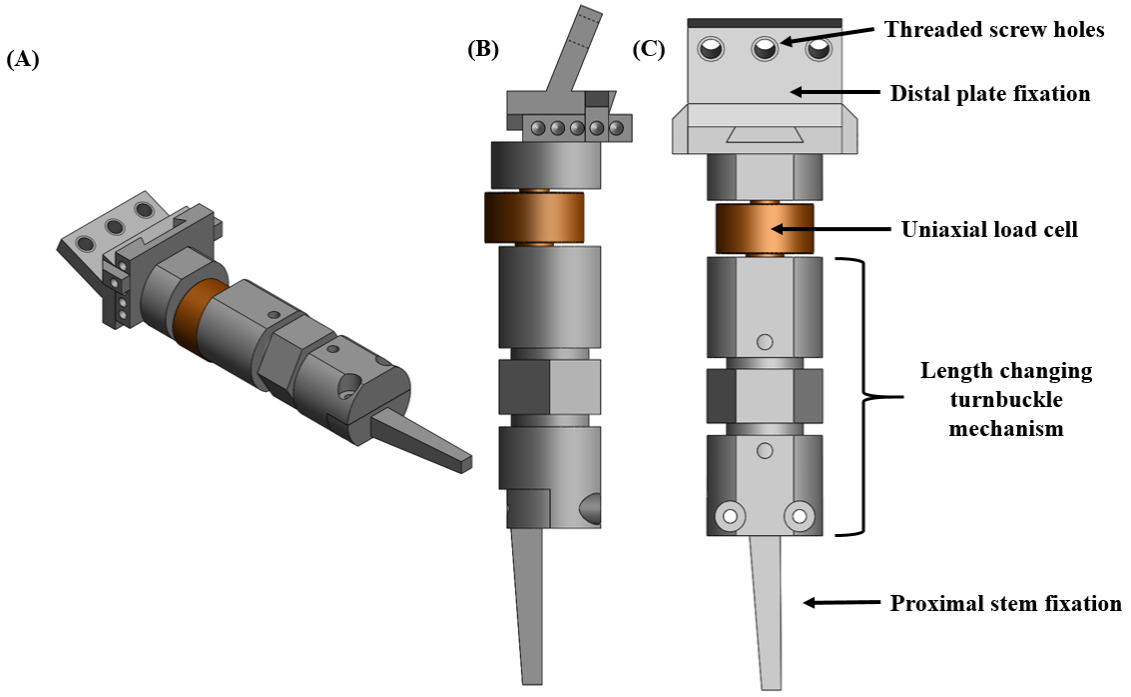

Figure 2.5: Outline of the Modular Distal Radius Implant Components. *An isometric view of the assembled radial implant hardware (A) is shown along with a lateral view (B), and a volar view (C). There are four main components - the distal fixation plate, the uniaxial load cell, the turnbuckle mechanism and the proximal fixation stem.*

The distal radius implant is comprised of the distal fixation plate, the modular implant appliance, and the proximal intramedullary stem. The modular implant is comprised of removable a uniaxial load cell and turnbuckle mechanism. Radial bone length changes are achieved by the rotation of the hexagonal component of the ***turnbuckle mechanism*** (Figure 2.6). The hexagonal component has reverse threaded posts on either size, allowing its rotation to act as a turn-buckle, a common mechanical appliance. Clockwise rotation generates bone lengthening and counter clockwise rotation generates shortening. The posts were threaded with 1.5 mm pitch in the left and right directions. This ensured that one sixth of a turn would generate 0.25mm of lengthening at both the proximal and distal posts, 0.5mm overall. Radial loads were measured at radial lengths of -4mm to +3mm at 1mm length change increments.

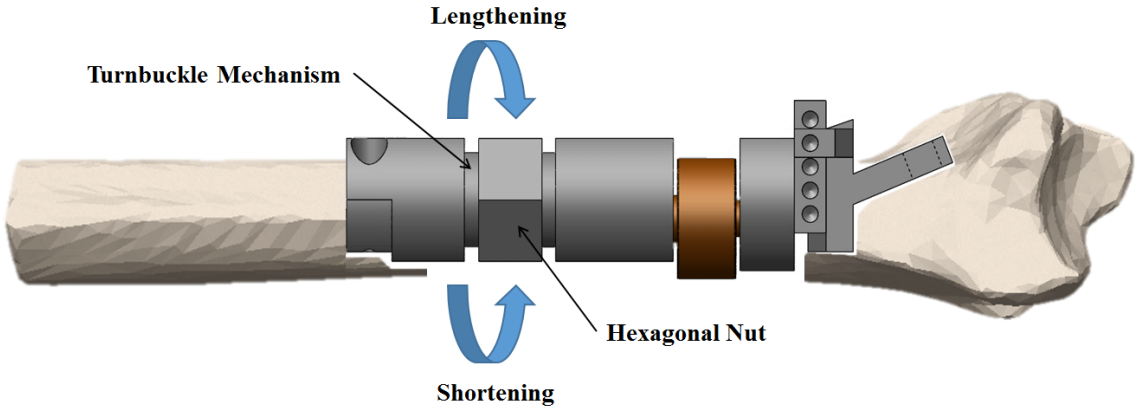

Figure 2.6: Distal Radius Implant Length Change Adjustments. *A medial view of the surgically inserted radial implant is shown. The distal radial implant allows for both radial lengthening and shortening. Length changes of 0.5mm where achieved through a sixth of a turn of the hexagonal component. Clock-wise motion results in bone lengthening, and counter clock-wise motion results in shortening.*

The ***distal radial plate*** was designed with a 22^{o} volar angulation as suggested by previous literature (Figure 2.7).[13-16] This shape mimics average distal radius geometry of the volar distal radius allowing the best fit. [13-16] Three holes were included in the distal radial plate to allow for screw fixation. The holes were threaded to avoid pre-load induced by compressive bolt force and to increase fixation strength using locking screws. Screws were threaded through the implant and affixed in the underlying bone augmented with bone cement. A dove tail union was included on the proximal side of the radial plate to allow for the spacer and modular implant to be easily exchanged after implantation and before testing.

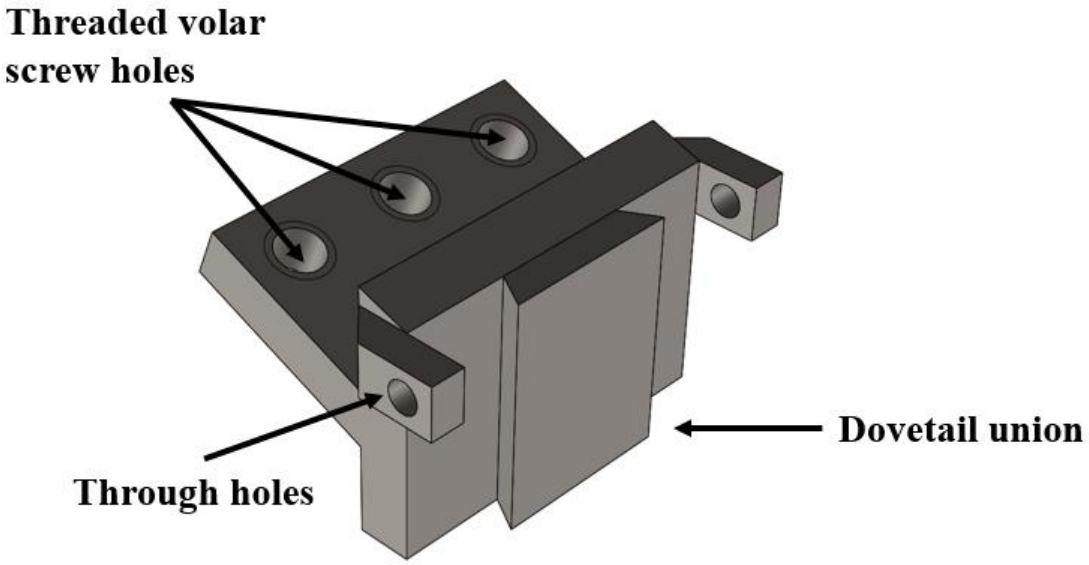

Figure 2.7: Distal Radial Plate Implant Component. *The three threaded screw holes allow for volar screw fixation without pre-loading due to compressive bolt force. Two through holes, on the medial and lateral aspects, allow for the y-axis of the dovetail union to be rigidly fixed to the spacer and modular implant appliance.*

The ***proximal intramedullary stem*** (Figure 2.8) was designed to provide fixation of the implant to the proximal radius. A stem had a 5˚ angle to better accommodate the natural curve of the radius. The stem was roughened and fixation was achieved with bone cement. The stem was fixed to rest of the implant with two perpendicular #2-56 screws.

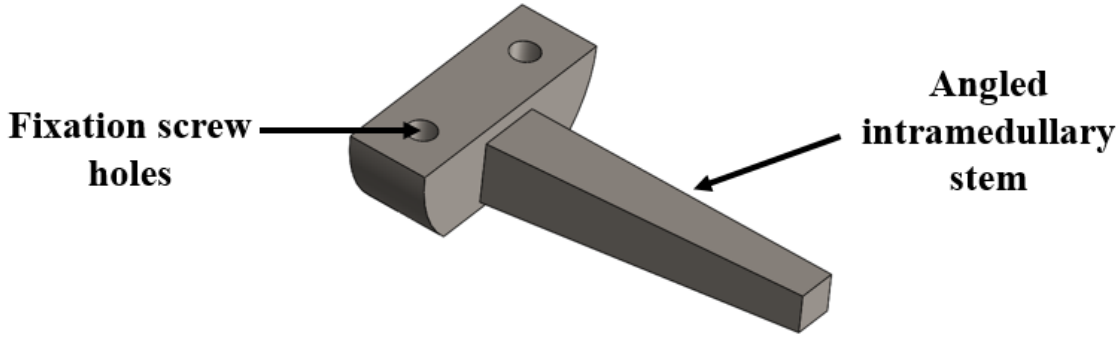

Figure 2.8: Proximal Intramedullary Stem. *Proximal fixation was achieved with an intramedullary stem fixated with Simplex B Bone cement. The stem had a 5˚ angle to accommodate for the natural curvature of the central radius.*

A flat stainless steel plate and commercial hose clamp were used to inhibit rotation of the turnbuckle mechanism (Figure 2.9). The plate lies adjacent to the hexagonal nut and the flat surfaces of both mating modular pieces throughout implantation and testing. The hose clamp was tightened to induce a compressive force between the plates the flat surfaces of the implants creating a rigid implant. The hose clamp was loosened and shifted from the hexagonal nut (Figure 2.6) when incremental length changes of the bone were required.

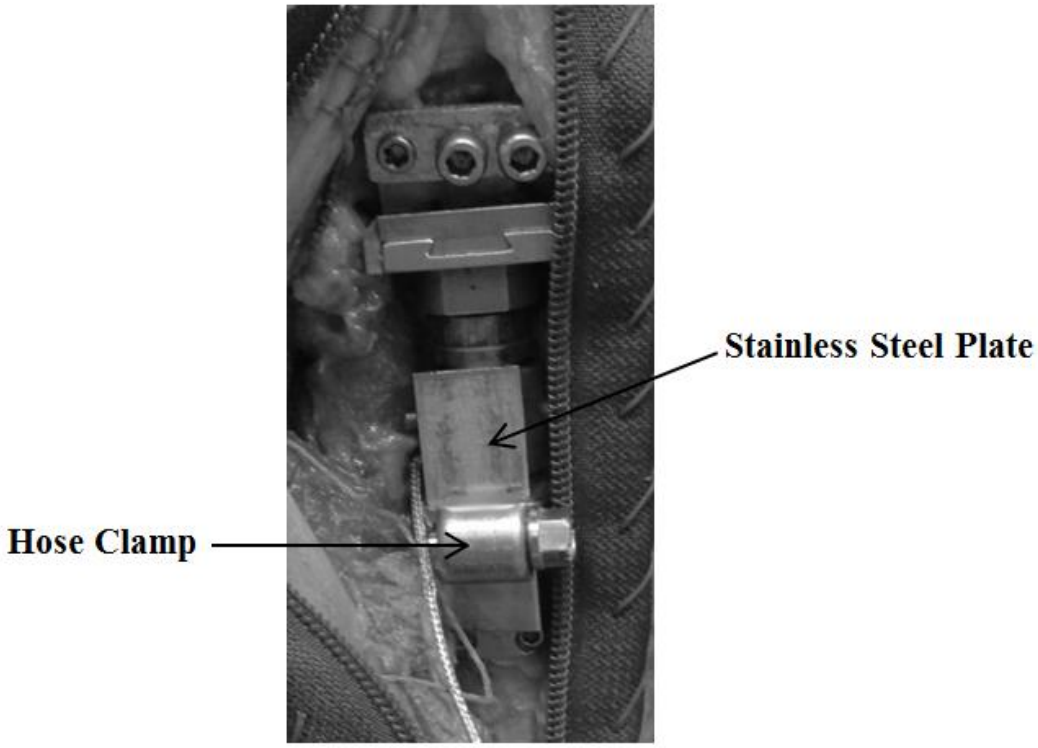

Figures 2.9: Radial Implant with Plate and Hose Clamp. *In order to constrain unwanted rotational movement of the experimental devices, stainless steel plates were placed against the flat surfaces of the radial and ulnar devices and held in place with compressive force provided by the tightened hose clamp.*

2.1.2 *Overview of Radius Implant Components*

The modular appliance, uniaxial load cell, distal radial plate, and proximal intramedullary stem act together to simulate and measure the effect of common distal radial injuries and deformities. This device adjusts to produce -4mm and +4mm of radial length variance at 1mm increments. The implant design allows for the easy exchange between the implantation spacer and the modular appliance. The modular appliance attaches with a dovetail union distally and two perpendicular screws proximally. Engineering drawings and specifications are included in Appendix D.

2.1.3 *Distal Ulna Implant Design and Function*

The modular distal ulnar implant (Figures 2.10, 2.11) was developed to examine the effect of common clinical conditions such as ulnar impaction syndrome and distal ulnar fractures. The features are similar to the radial device as described in the previous sections. Like the radial implant, the ulnar implant was machined from stainless steel. Intramedullary measurements of the distal ulna were taken to ensure device would fit varying sizes of specimen (Appendix B). The distal ulnar implant is comprised of the distal fixation stem, the removable uniaxial load cell and turnbuckle mechanism, and the proximal fixation stem. Ulnar bone length changes of -4mm to +4mm at 1mm increments were achieved using the same turnbuckle apparatus previously described for the radius.

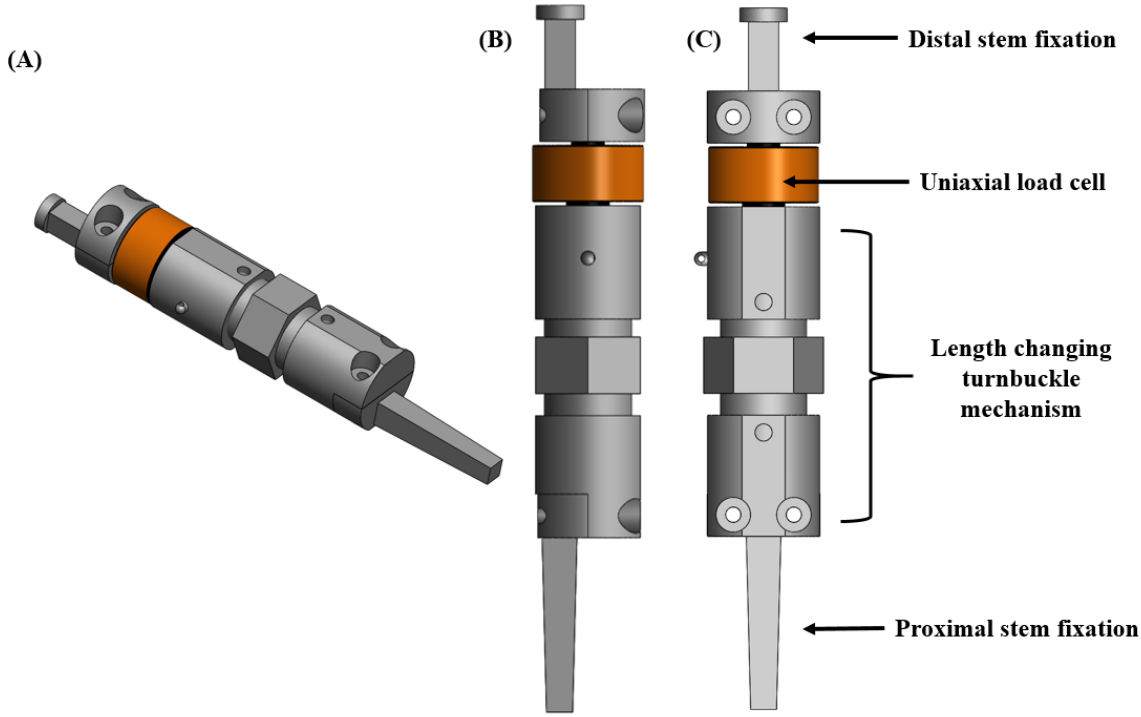

Figure 2.10: Outline of the Modular Distal Ulna Implant Components. *An isometric view of the assembled ulna implant hardware (A) is shown along with a lateral view (B), and a volar view (C). There are four main components - the distal fixation stem, the uniaxial load cell, the turnbuckle mechanism and the proximal fixation stem.*

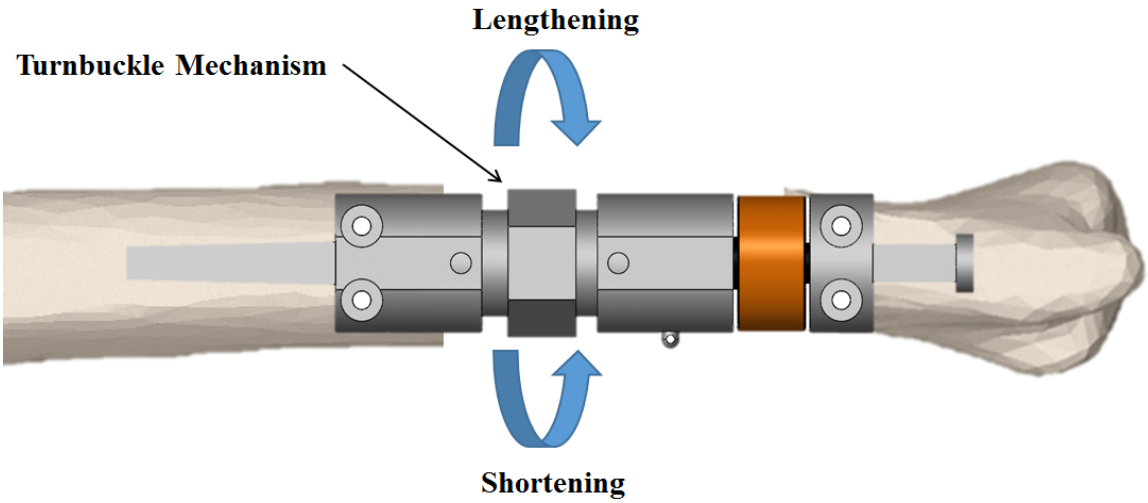

Figure 2.11: Distal Ulna Implant Length Change Adjustments. *A lateral view of the surgically inserted ulna implant is shown. The distal ulna implant allows for both ulna lengthening and shortening. Length changes of 0.5mm where achieved through a sixth of a turn of the hexagonal component. Clock-wise motion results in bone lengthening, and counter clock-wise motion results in shortening.*

Bone fixation of the ulna implant was achieved with ***intramedullary stems*** at both the distal and proximal interfaces (Figures 2.12, 2.13). The distal ulna stem has a circular addition on the distal end to provide a press fit in the trabecular bone. Bone cement was used in the distal and proximal medullary spaces to ensure rigid implant fixation. Both intramedullary stems were connected to the modular implant appliance using two perpendicular #2-56 screws. The distal intramedullary stem received the distal pins of the uniaxial load cell which was held in place with medium weight epoxy and compressive force from the adjacent implant piece.

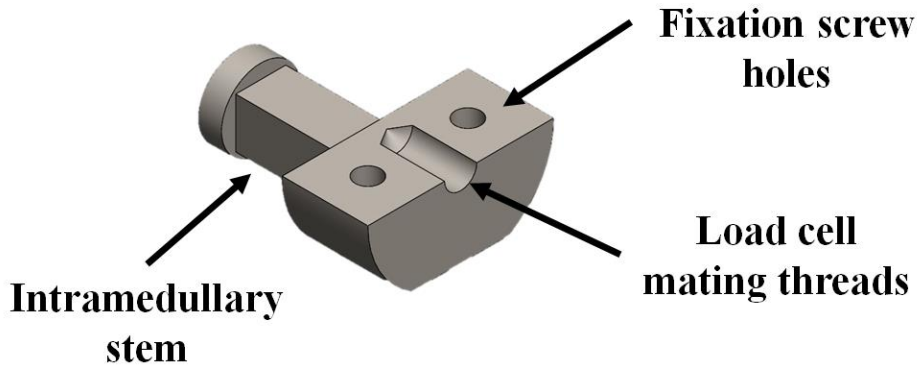

Figure 2.12: Distal Ulna Implant Length Change Adjustments. *Distal fixation was achieved with an intramedullary stem fixated with bone cement. The load cell was set into mating threads and held in place with medium weight epoxy and compressive force from the adjacent implant piece.*

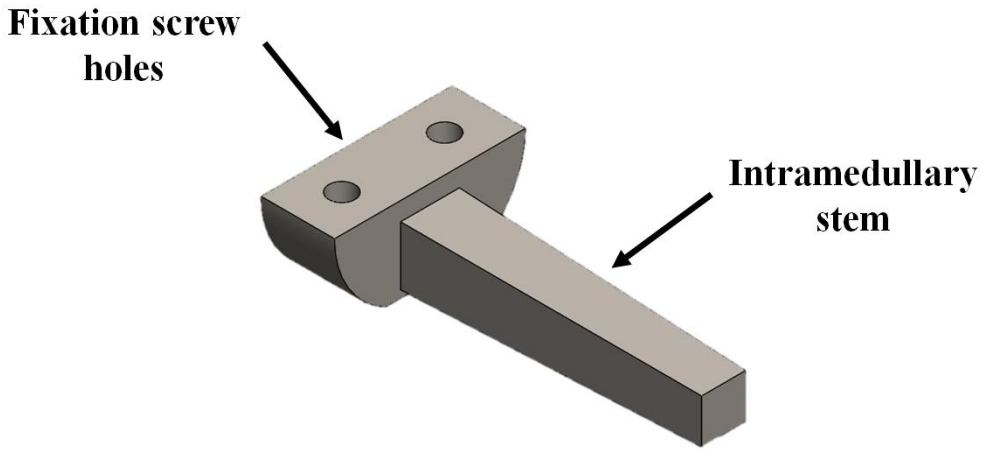

Figure 2.13: Distal Ulna Implant Length Change Adjustments. *Proximal fixation was achieved with an intramedullary stem fixated with bone cement.*

2.1.4 *Overview of Ulna Implant Components*

The modular appliance, uniaxial load cell, and distal and proximal intramedullary stems act together to simulate and measure the effect of common distal ulna injuries and deformities. The modular implant appliance adjusts to simulate -4mm and +4mm of ulnar length variance at 1mm increments. The implant design allows for the easy exchange between the implantation spacer and the modular appliance. The modular appliance attaches with two perpendicular screws both the distal and proximal interfaces. Engineering drawings and specifications are included in Appendix D.

2.2 Biomechanical Testing

An existing active motion wrist simulator was employed to generate wrist and forearm motion (Figure 2.14). The simulator actuates wrist and forearm motion through optical feedback and synchronized loading of tendons through using custom LabVIEW software (National Instruments Corporation, Austin, TX). Tone loads of 8.9 N were applied to seven tendons, biceps, pronator teres (PT), flexor carpi radialis (FCR), flexor carpi ulnaris (FCU), extensor carpi ulnaris (ECU), extensor carpi radialis brevis (ECRB) and extensor carpi radialis longus (ECRL) (Chapter 1, Section 1.1.4, Figure 1.12). Additional motion controlled loads were applied to the tendons and were used to achieve target joint angels. Optical trackers (Figure 2.15) were secured to the third metacarpal, radius and ulna to track wrist and forearm motion joint motion (Optotrak Certus; Northern Digital, Waterloo, ON, Canada).

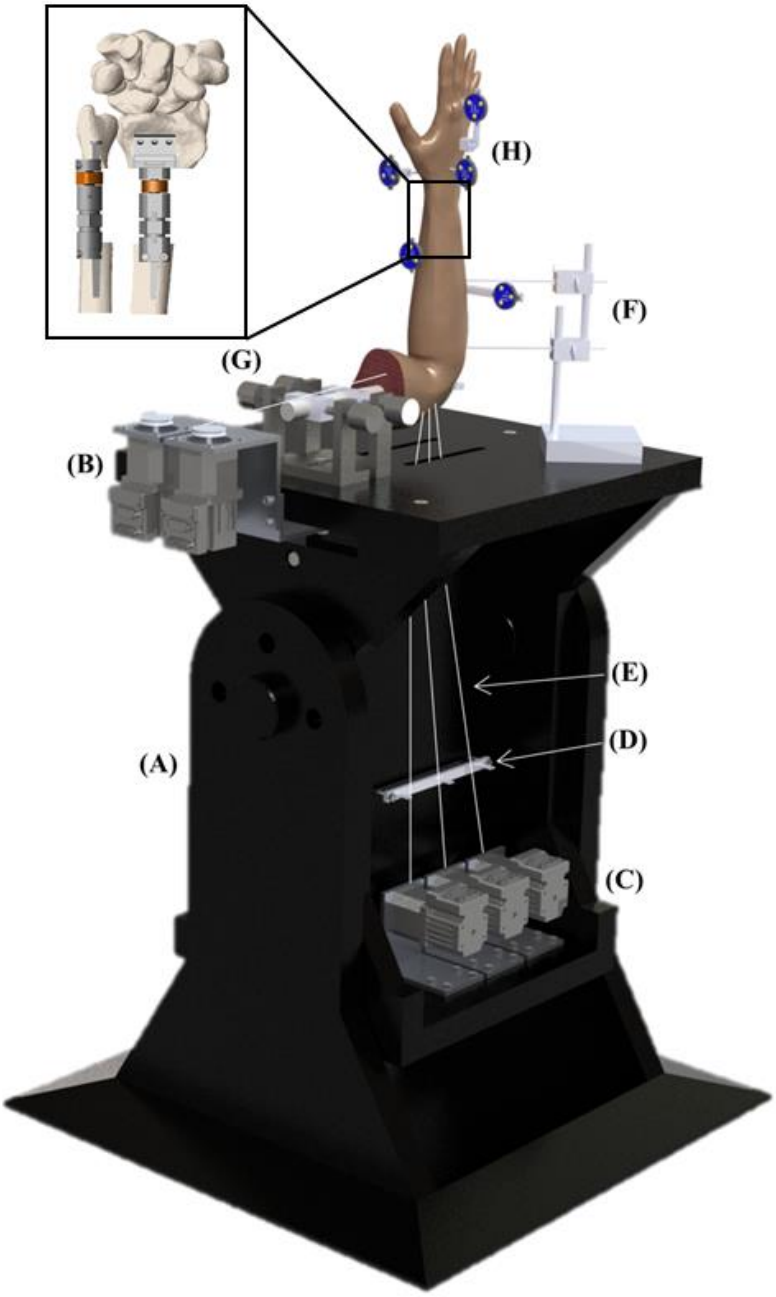

Figure 2.14: Active Wrist Motion Simulator. *The in vitro active motion simulator in capable of loading seven forearm muscles to generate wrist flexion-extension, radioulnar deviation and forearm pronation supination: (A) structural base of simulator (B) Biceps servomotor (C) servomotor manifold responsible for applying tendon loads which generate joint motion, (D) cable guide ensures an uninterrupted path for cabled from specimen to SmartMotor manifold, (E) suture cables connect muscles tendons to corresponding SmartMotor (F) ulnar support tower acts to maintain forearm in 90° of flexion (G) humeral clamp rigidly fixes humerus to simulator, (H) optical trackers record motion and provide real-time feedback of joint position.*

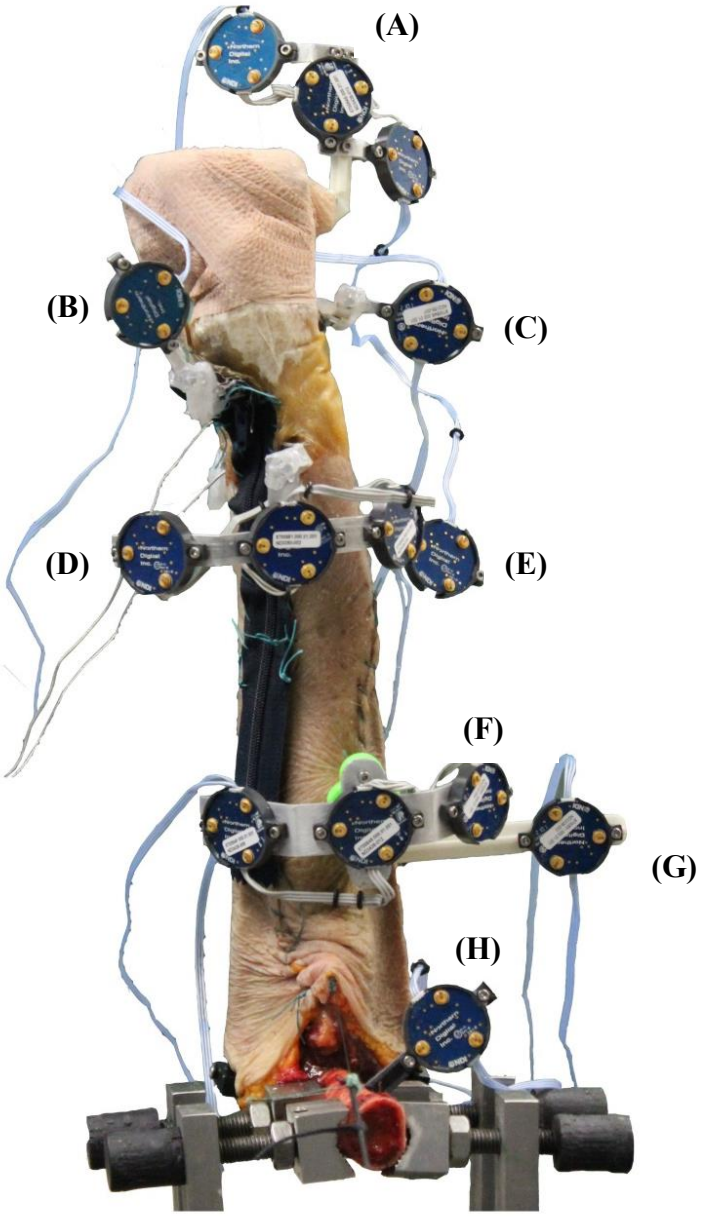

Figure 2.15: Optical Tracker Configuration. *Optical trackers were rigidly fixed to bones to record kinematics and give real-time feedback of joint position. A configuration of three tracker ridged bodies was used to track rotational movement of the radius. Optical trackers were fixed to the: (A) third metacarpal tracker, (D) distal radius, (E) distal ulna, (F) proximal radius, and (G) proximal ulna. Data from the (B) scaphoid, (C) lunate and (H) humerus was collected for use in an additional study.*

2.2.1 *Implant Procedure*

2.2.1.1 *Radial Implantation Procedure*

A volar incision was made to access the radial bone surface with minimum soft tissue disruption (Figure 2.16). An oscillating saw was used to perform a 52mm volar radius osteotomy to prepare space for the implant. A dorsal bone bridge was left connecting the distal and proximal ends of the osteotomy to ensure anatomic alignment of the bone after implantation. A cutting guide was 3D printed from nylon to allow precise bone removal. The distal aspect of the cutting guide mimicked the volar angulation of the radius and had identical holes to the distal radial plate to allow for predrilling of holes for the plate fixation screws. The radial osteotomy was performed as distal as possible while still proximal to the DRUJ to avoid joint disruption. Cancellous bone in the intramedullary canal was cleared using a burr to make space for the proximal fixation stem. Bone cement, was injected into the distal radial metaphysis and proximal intramedullary canal. The proximal fixation stem was pressed into the bone canal and secured to the spacer with two #2-56 screws. The distal plate fixation screws were then inserted into wet bone cement filling the trabecular bone. The plate was fixed to the spacer along the Y-axis with two perpendicular screws. The spacers were replaced with the modular implants after the specimen had been mounted on the simulator.

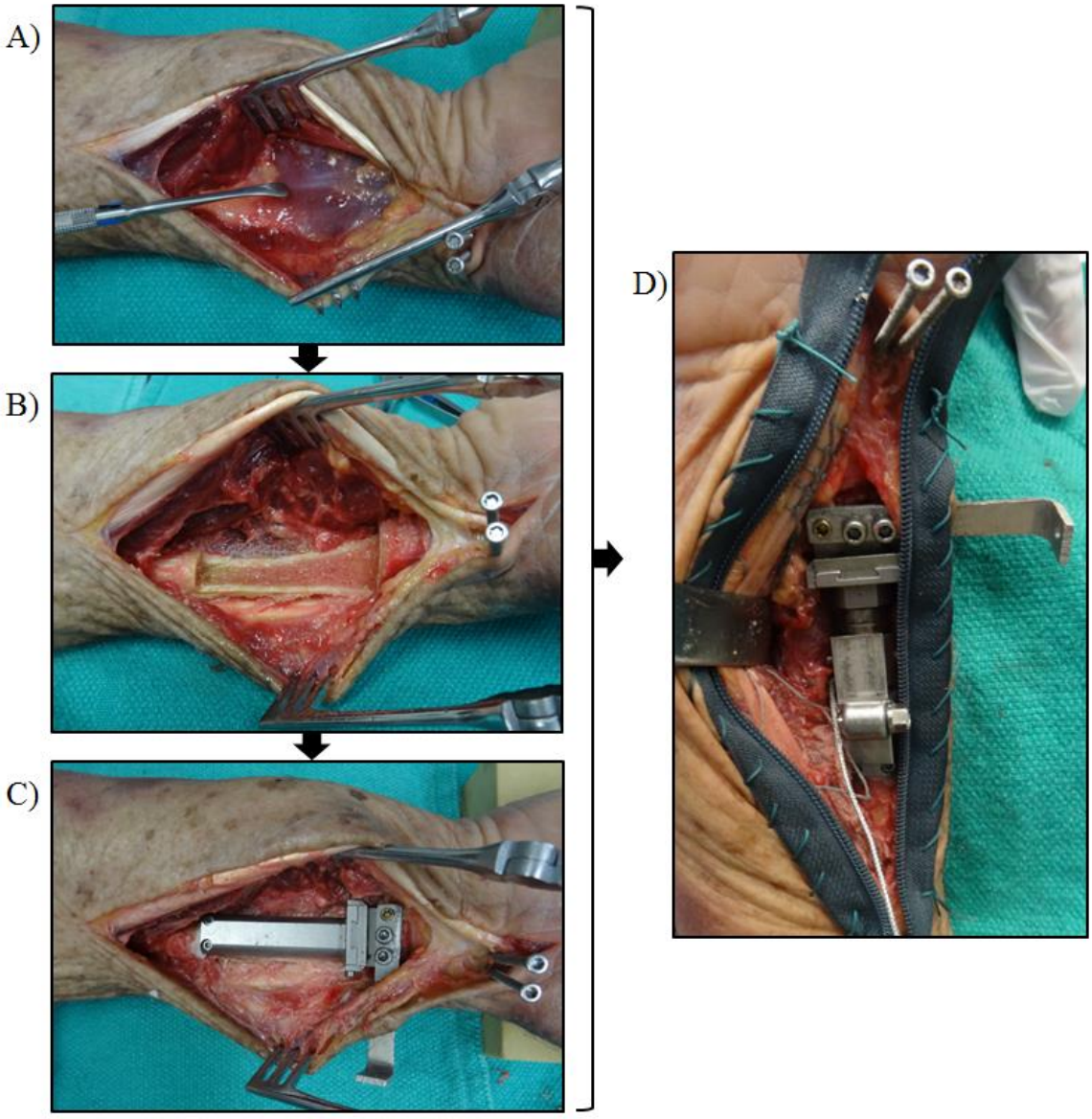

Figure 2.16: Radius Device Implantation Procedure. *(A) A volar incision was made to access the radius. (B) A radial osteotomy was performed to create space for the modular device. A bone bridge was left intact to ensure joint alignment after implantation. (C) The proximal stem and distal plate were fixed into place using bone cement. The implantation spacer was fixed in place with screws and the bone cement was left to set. (C) After the bone cement has set and the specimen has been mounted on the simulator, the implantation spacer was exchanged for the modular experimental device.*

2.2.1.2 *Ulnar Implantation Procedure*

A similar procedure was followed for implantation of the modular ulnar device (Figure 2.17). A medial incision was made to access the ulnar bone surface with minimal soft tissue disruption. An oscillating saw was used to perform a 50mm medial ulnar osteotomy. A lateral bone bridge was left connecting the distal and proximal ends of the osteotomy to ensure anatomic bone alignment after device implantation. A cutting guide was 3D printed from nylon to aid precise bone removal. The ulnar osteotomy was performed as distal as possible while avoiding DRUJ injury. The distal and proximal intramedullary canals were cleared with a motorized burr to make space for the fixation stems. Bone cement was injected into the distal and proximal bone canals and the fixation stems were pressed into place. Alignment of the two stems occurred when the spacer was secured to each stem with two #2-56 screws. The spacers were replaced with the modular implants after the specimen had been mounted on the simulator and prior to testing.

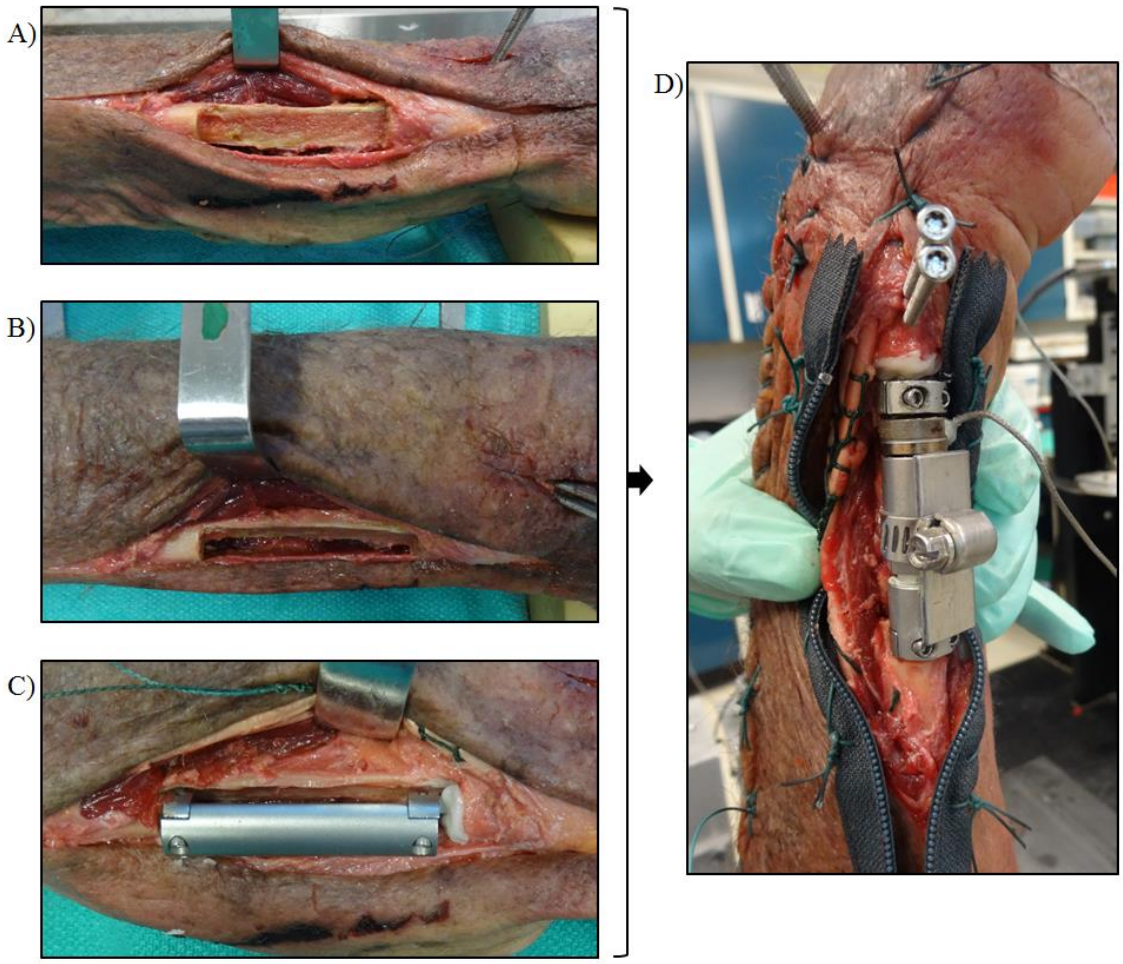

Figure 2.17: Optical Tracker Configuration. *(A) A medial incision was made to access the ulna. (B) A dorsal view of the ulnar osteotomy was performed to create space for the modular device. A bone bridge was left intact to ensure joint alignment after implantation. (C) The distal and proximal stems were fixed into place using Simplex B bone cement. The implantation spacer was fixed in place with screws and the bone cement was left to set. (C) After the bone cement has set and the specimen has been mounted on the simulator, the implantation spacer was exchanged for the modular experimental device.*

2.2.2 *Testing Protocol*

Following the implantation of the radial and ulnar devices, active wrist and forearm motion was simulated. Kinematic and load cell data was recorded for neutral and varying bone lengths. A repeated measures experimental design was employed to account for interspecimen variability in size and shape and to increase statistical power. The wrist simulator was used to generate reliable wrist and forearm motion. Optical trackers were used to quantify motion and provide position feedback to the simulator. A custom LabVIEW program was used for simulator control and data collection. Local coordinate systems were generated at the start of each testing day using anatomical skin markers. The joint angles calculated from these coordinate systems were used for kinematic reference.

2.2.3 *Methods*

Trials were completed to examine the repeatability of the combined tendon simulated motion and implant load readings. One fresh-frozen cadaveric upper limb was thawed for roughly 18 hours, and prepared for radial and ulnar device implantation. Osteotomies were performed on both the radius and ulna to make space for the modular implants. Bone bridges were left intact to maintain anatomical bone alignment after device implantation. Implants were rigidly fixed to the bones with bone cement following the implantation procedures previously outlined. Nylon line was sutured into the tendons of seven prime movers of wrist and forearm. The specimen was then mounted on the simulator with a humeral clamp and two threaded pins placed into the ulna, ensuring the elbow remained at 90˚. After mounting the specimen, the spacers were exchanged for the modular instrumented implants. Tendon cables were connected to smart motors and active motion was controlled by manipulating tendon forces.

Five cyclic flexion/extension, radioulnar deviation and dart throw motions were performed and compared separately. The intraclass correlation coefficient (ICC) was calculated for each set of five movements for statistical analysis.

2.2.4 *Results*

The modular experimental device produced reliable and repeatable bone load measurements. Repeatability was confirmed for the three wrist motions by conditioning the wrist tendons with five passive ranges of motion and five active wrist simulation trials for each individual motion pathway. Axial forearm bone loads were compared for each motion pathway. Repeatability trials for flexion motion (Figure 2.18) resulted in single measures ICC = 0.980 and ICC = 0.996 between the radial and ulnar axial load cells measurements respectively for the five consecutive motions. For ulnar deviation motion (Figure 2.19) the ICC for radial and ulnar load cell measurement were 0.978 and 0.999 proving to be repeatable. Axial load cell measurements were also repeatable for dart throw motion (Figure 2.20) single measures ICC = 0.984 in the radius and ICC = 0.996 in the ulna.

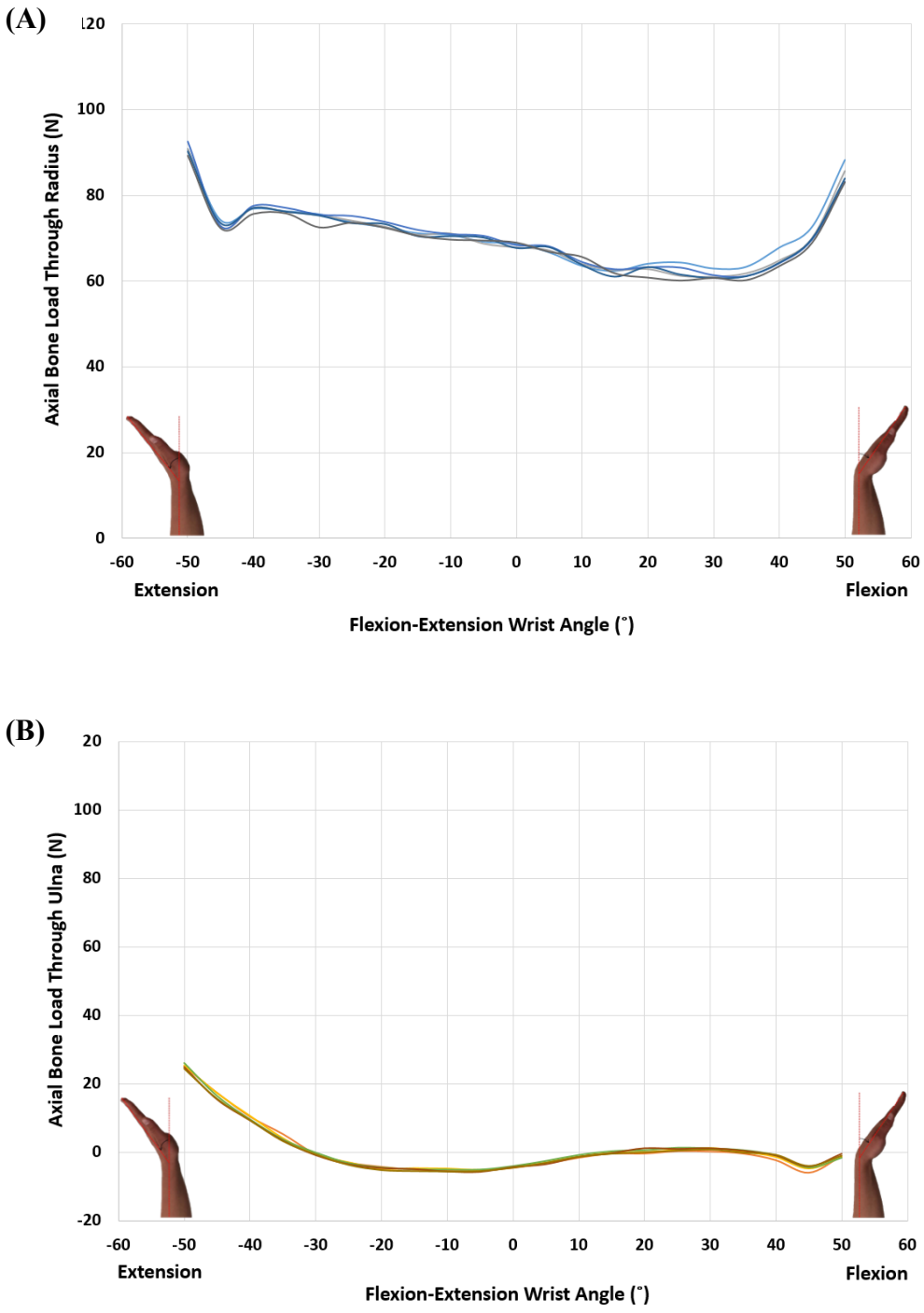

Figure 2.18: Repeatability of Axial Load Cell Measurements during Flexion Motion. *The repeatability of radial (A) and ulnar (B) axial load cell measurements of five trials of active flexion motion plotted against wrist angle in degrees of flexion-extension. Radial loads had an ICC=0.980 and ulnar loads an ICC=0.996for the five cyclic flexion motions. Standard deviations have been omitted for clarity.*

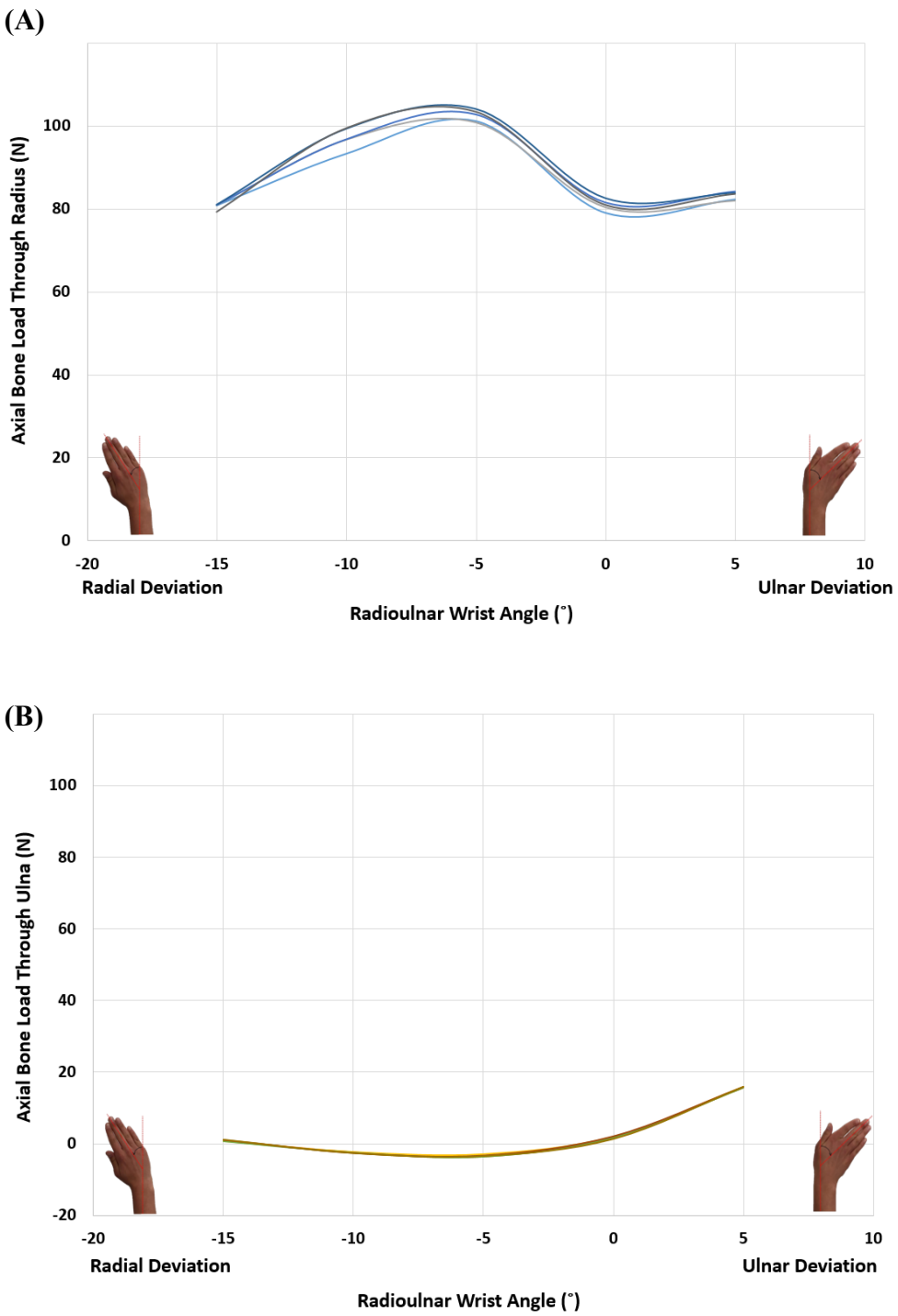

Figure 2.19: Repeatability of Axial Load Cell Measurements during Ulnar Deviation Motion. *The repeatability of radial (A) and ulnar (B) axial load cell measurements of five trials of active ulnar deviation motion plotted against wrist angle in degrees of radioulnar deviation. Radial loads had an ICC=0.978 and ulnar loads an ICC=0.999 for the five cyclic ulnar deviation motions. Standard deviations have been omitted for clarity.*

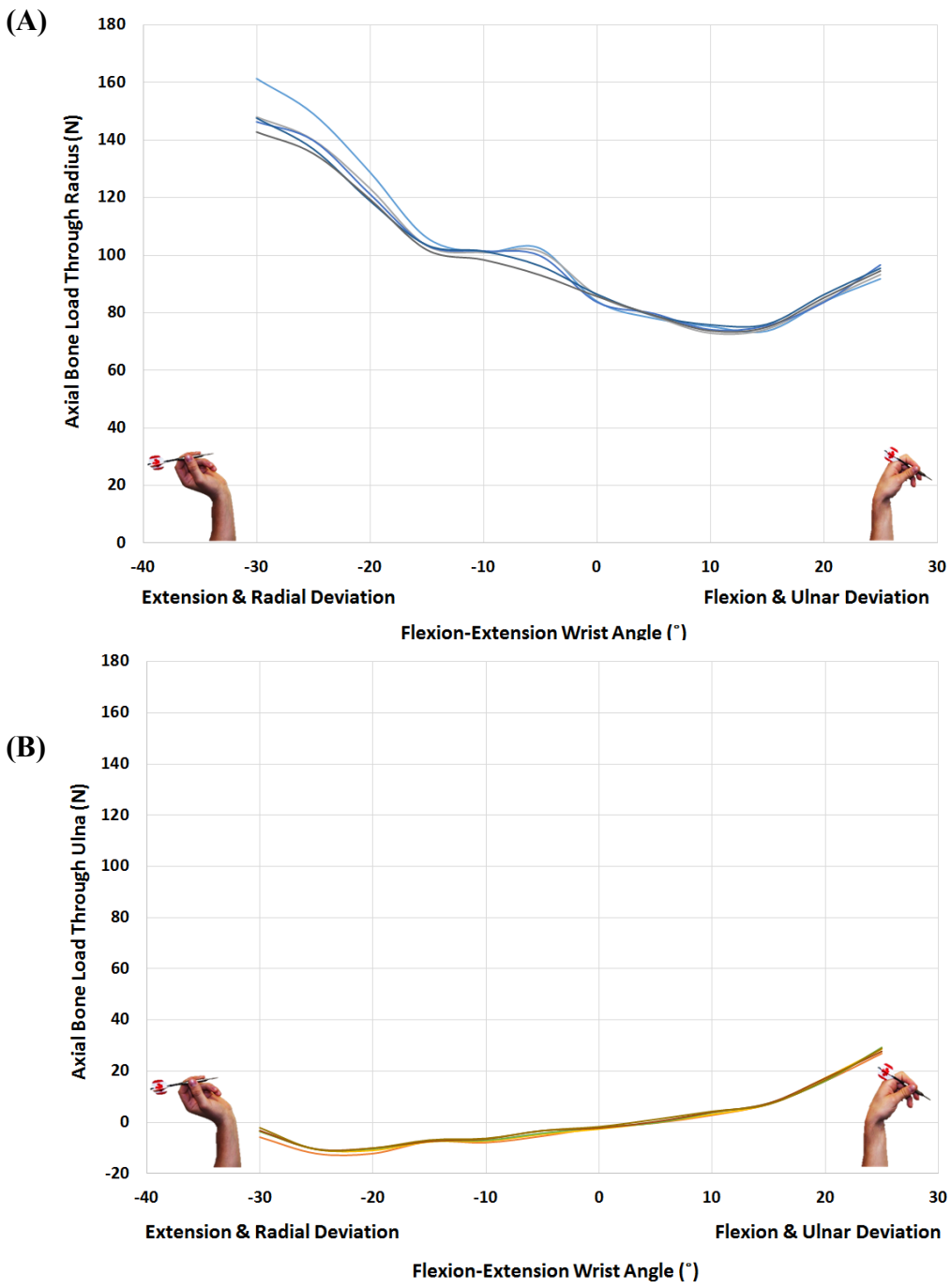

Figure 2.20 – Repeatability of Axial Load Cell Measurements during Dart Throw Motion. *The repeatability of radial (A) and ulnar (B) axial load cell measurements of five trials of active dart throw motion plotted against wrist angle in degrees of flexion-extension motion. Radial loads had an ICC=0.984 and ulnar loads an ICC=0.996 for the five cyclic forward dart throw motions. Standard deviations have been omitted for clarity.*

2.2.5 *Discussion and Conclusions*

Two instrumented modular implants were designed to simulate radial and ulnar length changes and measure axial bone loads in the distal forearm. The devices were surgically implanted with bone cement to allow for rigid bone fixation. Surgical cutting guides were designed and utilized to ensure the accurate bone removal and implant placement. The modular implants allow for reproducible changes in the lengths of the radius and ulna thereby simulating many common forearm injuries, disease and/or deformities.

The reliability of the combined implant and active motion simulation system was excellent. The lowest ICC reported was 0.978 in the radius during ulnar deviation, indicating very little variation in load cell measurements between the five cyclic movements. The measurements from the radial load cell had slightly lower reliability than the measurements from the ulnar load cell. This is intuitive as the distal radial articulations are much more intricate than those of the distal ulna. Overall, the results from the measurement system demonstrated the combined reliability of the simulator applied tendon loads and the load cell measurements from the radial and ulnar implants.

While other implants have been developed to examine loading in the distal forearm very little information about the reliability and repeatability of these devices is available. Obtaining accurate *in vitro* bone loads depends heavily on the instrument configuration used for measurement. A previous study conducted by *Knowles et al.* at the proximal radius has reported that the same load cell used herein, implanted along the radial axis using intramedullary fixation, to be highly reliable and accurate in measuring axial bone loads.[17] *Ferreira et al.* developed a distal ulnar implanted instrumented with a strain gauge load cell. During forearm pronation and supination they found their implant to have a maximum coefficient of variance of 1.0% and to be reproducible up to 4.7% in the desired direction of measurement.[18] They considered these values reliable and adequate for further experimental use, indicating that an ICC of 0.978 is excellent.

The effect of radial and ulnar length changes and joint position on axial forearm bone loads can be examined with great accuracy using the modular radial and ulnar implants employed herein. A better understanding of native distal forearm loads during active

motion will help improve existing biomechanical models and influence surgical techniques and rehabilitation protocols. Simulating various forearm injuries, diseases and deformities will help clinicians improve the treatment of their patients. The following chapters outline how the implants were employed in *in vitro* biomechanical studies to quantify natural bone loading during simulated active wrist and forearm motion and the effect of radial length changes during forearm pronation-supination motion.

2.3 References

1. Graham T. Surrgical correction of malunited fractures of the disal radius. *J Am Acan Orthop Surg.* 1997; 5, 270-281.

2. Cooney WP. *The Wrist: Diagnosis and Operative Treatment*. Vol 8. 2nd ed. (Kluwer W, ed.). Philadelphia, Balitmore, New York, Lodon, Buenos Aires, Hong Kong, Sydney, Tokyo; 2011.

3. Gliatis JD, Plessas SJ, Davis TR. Outcome of distal radial fractures in young adults. *J Hand Surg Br.* 2000; 25(6), 535-543.

4. Nakamura R, Horii E, Watanabe K, Nakao E, Kato H, Tsunoda K. Proximal row carpectomy versus limited wrist arthrodesis for advanced Kienbock's disease. *J Hand Surg Br.* 1998; 23(6), 741-745.

5. Friedman AL, Palmer AK. The ulnar impaction syndrome. *Hand Clin.* 1991; 7(2), 295-310.

6. Palmer AK, Werner FW. Biomechanics of the distal radioulnar joint. *Clinical Orthop.* 1984; (187), 26-35.

7. Markolf KL, Tejwani SG, Benhaim P. Effects of wafter resection and hemirection from the distal ulnar on load-sharing at the wrist: a cadaveric study. *J Hand Surg Am.* 2005; 30(2), 351-358.

8. Werner FW, Palmer AK, Fortino MD, Short WH. Force transmission through the distal ulna: effect of ulnar variance, lunate fossa angulation, and radial and palmar tilt of the distal radius. *J Hand Surg Am*. 1992; 17(3)

9. Greenberg JA, Werner FW, Smith JM. Biomechanical analysis of distal metaphyseal ulnar shortening osteotomy. *J Hand Surg Am.* 2013; 38(1), 1914-1919.

10. Sachar K. Ulnar-side wrist pain: evaluation and treatment of triangular fibrocartilage complex tears, ulnocarpal impaction syndrome, and lunotriquetral tears. *J Hand Surg Am.* 2008; 33(9), 1669-1679.

11. Markolf KL, Dunbar AM, Hannani K. Mechanisms of load transfer in the cadaver forearm: role of the interosseous membrane. *J Hand Surg Am.* 2000; 25(4), 647-682.

12. Ekenstam FW, Palmer AK, Glisson RR. The load on the radius and ulna in different positions of the wrist and forearm. A cadaver study. *Acta Orthop Scand.* 1984; 55(3), 363-365.

13. Gartland JJ, Werley CW. Evaluation of healed Colles' fractures. *J Bone Joint Surg Am.*1951; 33, 895-907.

14. Dowling JJ, Sawyer B. Comminuted Colles' fractures: evaluation and method of treatment. *J Bone Joint Surg Am.*1961; 43, 657-668.

15. Friberg S, Lunstrom B. Radiographic measurements on the radio-carpal joint in distal radial fractures. *Acta Radiol Diagn*. 1976; 17(6), 869-876.

16. Sckeck M. Long-term follow-up of treatment of comminuted fractures of the distal end of the radius by transfixation with Kirschner wires and cast. *J Bone Joint Surg Am.* 1962; 44-A, 337-351.

17. Knowles NK, Gladwell M, Ferreira LM. An intra-bone axial laod transducer: development and validation in an in-vitro radius model. *J Exp Orthop.* 2015; *2*(1), 19.

18. Ferreira LM, Greeley GS, Johnson JA, King GJ. Load transfer at the distal ulna following simulated distal radius fracture malalignment. *J Hand Surg Am.* 2015; 40(2), 217-223.

Chapter 3

3 *Loads in the Distal Radius and Ulna during Active Simulated Wrist Motion*

Overview

An in-vitro biomechanical study was conducted to examine distal radial and ulnar axial bone loads during simulated active wrist motion. Loads were collected throughout motion and analyzed with respect to joint position and the direction of the motion path. Loads through the distal radius and ulna were reported as magnitudes and as proportions of total distal forearm bone loading.

3.1 Introduction

As discussed in Chapter 1 (Section 1.5), a comprehensive understanding of load sharing at the wrist and distal forearm is critical for optimizing rehabilitation protocols, influencing surgical techniques, designing joint replacement systems and improving existing biomechanical models. The native biomechanics of the wrist and forearm are often altered by traumatic injuries and degenerative diseases such as wrist fractures, Keinbock's disease and ulnar impaction, as previously reviewed in Chapter 1(Section 1.3). These disorders often lead to ulnar sided wrist pain, weakness, stiffness and arthritis, due at least in part as a result of altered bone loading.[1-9] Before the biomechanics of pathological states can be examined, we must first gain a better understanding of healthy forearm bone load magnitudes and sharing.

Previous studies have examined forearm bone load sharing under static loading scenarios and have concluded that the radius carries a greater percentage of load than the ulna at the distal forearm. Currently the static forearm bone loading ratio is widely accepted as 80/20 for the radius and ulna respectively.[10-15] Only one other study has examined distal forearm load sharing during active range of wrist motion. They have a suggested an 87/13 radial to ulnar forearm load sharing ratio with the wrist in neutral position.[14] Significant differences in bone loading were found based on joint position in wrist flexion-extension motion (FEM) and radioulnar deviation (RUD). However, the effect of active motion on native load sharing is not well defined and additional studies are hence needed.

The objective of this current study was to examine the magnitude of bone loads and bone load sharing during active wrist motion to allow for a more complete understanding of loading at the distal forearm. Axial loads through the distal radius and ulna were examined during simulated active planar wrist FEM, RUD and multiplanar dart throw motion (DTM). Differences in forearm bone load were examined based on the direction and angle of wrist joint motion. It was hypothesized that direction and angle of motion will have significant effects on axial forearm bone loads, with the greatest changes occurring in RUD.

3.2 Materials and Methods[a]

3.2.1 *Specimen Preparation*

Nine fresh frozen cadaveric upper extremities, resected mid-humerus were used for biomechanical testing (74 ± 7, 9 male, 9 right). Computed tomography (CT) scans, fluoroscopic images were performed and medical histories were reviewed for each specimen to rule out previous forearm injuries, deformities and/or osteoarthritis. The specimens were thawed for approximately 18 hours. Ulnar variance was quantified using fluoroscopy. The radial and ulnar load measurement devices were surgically implanted in the distal forearm bones, being careful to leave all soft tissues intact (Figures 3.1 & 3.2). A volar radial osteotomy was performed and a dorsal bone bridge was left intact to assure the alignment of the distal and proximal bone segments were maintained during insertion of the device. Polymethylmethacrylate, bone cement was injected into the distal trabecular bone and proximal intramedullary canal to improve fixation and the distal plate and proximal stem were secured in place (Figure 2.16). A similar procedure was followed on the medial side of the ulna for device implantation. Ulnar device fixation was achieved with intramedullary stems both proximally and distally (Figure 2.17). The osteotomies were performed as distal as possible while still proximal to the DRUJ to avoid joint disruption. Nylon line (45kg test) was sutured into the tendons of the prime movers proximal to the extensor retinaculum and wrist: biceps, pronator teres (PT), flexor carpi radialis (FCR), flexor carpi ulnaris (FCU), extensor carpi ulnaris (ECU), extensor carpi radialis brevis (ECRB), and extensor carpi radialis longus (ECRL) (Ethicon, Somerville, NJ). Guides were secured to the medial and lateral humeral epicondyles and tendon lines were directed through them to maintain physiological lines of action.

[a] The methodology related to specimen preparation and some aspects of testing protocol are similar to those employed in Chapters 2 and 4. As this thesis is in manuscript format, the methods have been re-written and included herein.

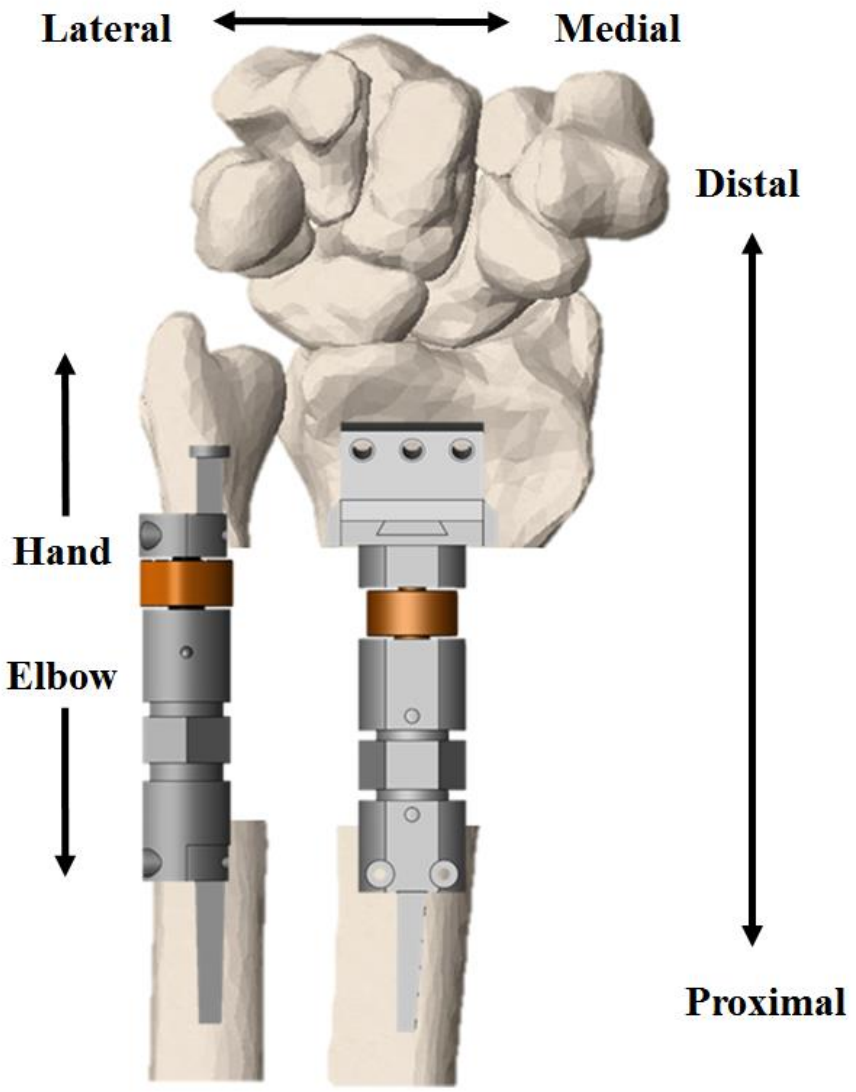

Figure 3.1: Computer Assisted Drawing of Implanted Experimental Devices. *Two experimental devices were implanted in the distal radius and ulna to measure axial loads through the distal forearm during active simulated wrist motion.*

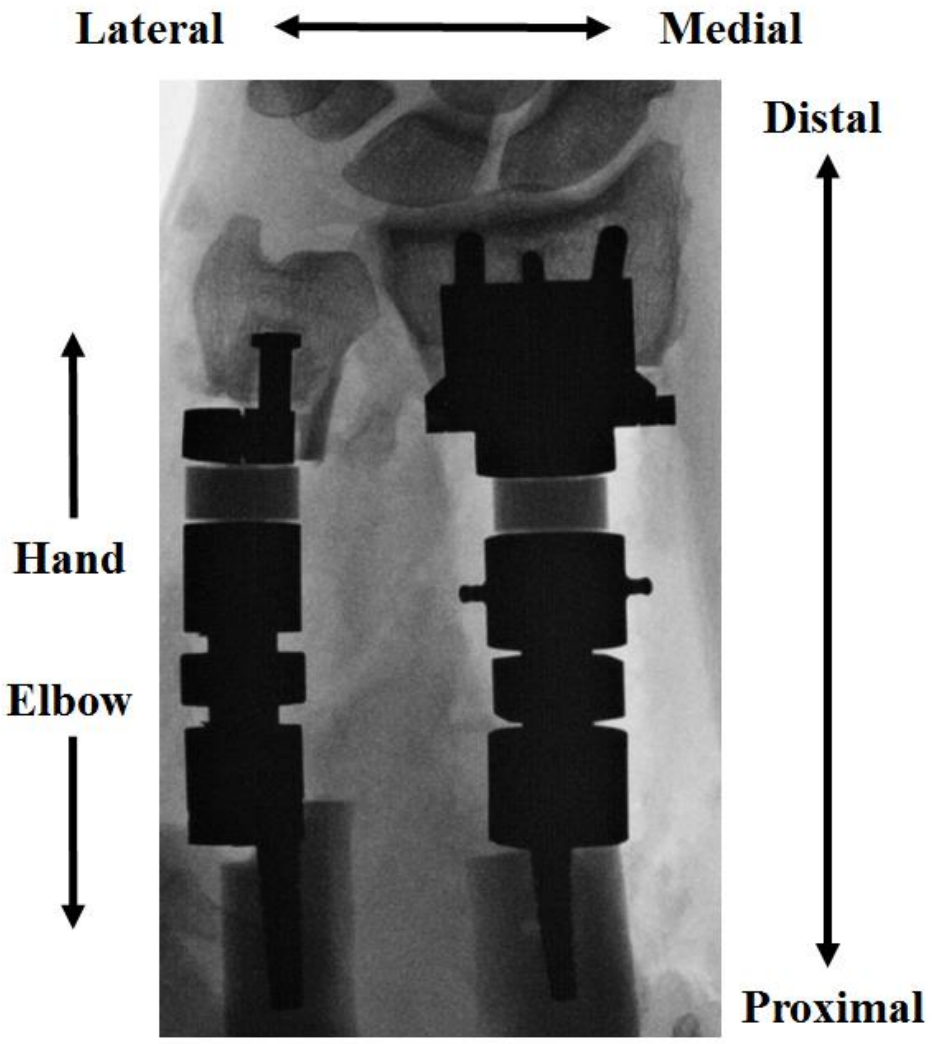

Figure 3.2: X-Ray Image Experimental Devices Implanted in a Cadaveric Specimen. *An X-Ray image was taken of the implanted experimental devices at neutral bone lengths to better depict plate and intramedullary stem fixation. Three dimensional printed nylon pacers were used in place of the load cells.*

Specimens were mounted on the wrist simulator using a humeral clamp and two perpendicular ulnar pins with the elbow at 90° (Figure 2.14). Tendon sutures were connected to smart motors (SM2316D-PLS2, Arumatics Corp, CA) located at the base of the wrist simulator. Optical trackers (Optotrak Certus; Northern Digital, Waterloo, ON, Canada) were secured to the dorsal distal aspect of the third metacarpal, the radius proximal to the PT insertion, the proximal ulna, the distal radius and ulna distal to the osteotomies to track wrist and forearm motion and collect kinematic data throughout testing. Fingers were flexed and secured using Coban Self-Adherent Wrap (3M, Elyria, OH, USA) to ensure clear line of site for the optical trackers.

3.2.2 *Testing Protocol*

Test-day coordinate systems were generated from skin markers for the radius, ulnar and third metacarpal. Neutral position was defined using the International Society of Biomechanics guidelines as 0° of wrist flexion, 0° of radioulnar deviation and 0° of forearm rotation. Joint motion was measured and recorded using the relative motion of the radial, ulnar and metacarpal coordinate systems. Two cyclic motions were completed at the rate of 5° of joint angulation per second for flexion-extension motion (-50° extension to 50° flexion) and forward and reverse dart throw motion (combined -30° extension and -10° radial deviation to 30° flexion and 10 ulnar deviation) and at 3° per second for radioulnar deviation (-10° radial deviation to 15° ulnar deviation) (Chapter 1, Figures 1.13 1.14, 1.15,). The first (pre-conditioning) cyclic movement was disregarded and the second cycle was analyzed. , . Individual motions were defined as a full range of motion in one direction, e.g. flexion was defined as -50° to 50° and extension as 50° to -50°. The length of the forearm bones was maintained at neutral throughout testing. The outcome variable of axial bone load in both the radius and ulna was recorded throughout testing at a sampling rate of 1000 Hz.

3.2.3 *Outcome Variables and Data Analysis*

Axial bone loads were continuously collected from the load cells implanted in the distal radius and ulna during FEM, DTM and RUD. Absolute bone loads were measured and the percentage of total bone load was calculated for both forearm bones to examine their individual contributions. International Society of Biomechanics guidelines were used to develop individual coordinate systems using skin markers for the radius, ulna and third metacarpal.[16] Wrist angle was calculated as the angle between the long axis of the radius and the long axis of the 3rd metacarpal with respect to the radial coordinate system. Individual motions pathways and the correlating radial and ulnar load cell measurements were discretized in 5° increments for data analysis and statistical purposes. Loads applied to the FCR, FCU, ECU, ECRB and ECRL tendons were also reported for the three wrist motions: FEM, RUD and DT. These were included for the purposes of interpretation of the bone loads, but not analyzed statistically as tendon loads were not a specific outcome variable.

3.2.4 *Statistical Methods*

A two-way repeated measures analysis of variance (ANOVA) was completed in SPSS 17.0 (SPSS Inc., Chicago IL, USA). The independent variables included: motion direction and wrist joint angle. The dependent variable was axial bone load. Individual analyses were completed for the radius and ulna during FEM, RUD and DTM. Additional pairwise comparisons were completed to examine the differences between individual joint angles. Statistical significance was considered $p<0.05$.

3.3 Results

3.3.1 *Radius and Ulna Loading during Flexion and Extension Motion*

The magnitudes of loads through the distal radius were significantly greater in planar extension compared to planar flexion ($p<0.001$) (Figure 3.3). Loads through the distal radius in planar extension were significantly greater than those in planar flexion at joint angles between -30° and 50° ($p<0.033$). Loads through the distal radius were significantly greater in planar extension than planar flexion at joint angles between 0° and 40° ($p<0.045$).

Axial loads at the distal radius showed a no significant change planar wrist flexion-extension throughout motion in both directions ($p=0.062$). Axial loads through the ulna were significantly higher in wrist extension ($p=0.005$) (Figure 3.3). Throughout planar wrist flexion-extension the magnitude of load through the radius was significantly greater than that through the ulna ($p<0.01$). The radius accounted for the largest proportion of forearm bone load throughout both forward and reverse dart throw motion, peaking in extension and radial deviation (94%) and reaching its minimum in flexion and ulnar deviation (72%). During planar wrist flexion distal ulnar loads were 27.8$\pm$20.5 N at -50° of extension, 7.5$\pm$10.6 N at 0° of wrist flexion and 8.4$\pm$7.8 N at 50° of wrist flexion. During planar wrist extension load transmission through the distal ulna averaged 26.8$\pm$19.9 N, 12.4$\pm$12.2 N, and 9.9$\pm$6.6 N at -50° of extension, 0° of flexion, and 50° of flexion, respectively.

Load sharing between the radius and ulna was the same in both planar flexion and extension ($p=0.912$).Therefore load sharing ratios will be presented for planar flexion herein. Load sharing between the radius and ulna varied during planar wrist flexion, however these changes did not reach statistical significance ($p=0.074$) (Figure 3.4 & 3.5). The radius bore a significantly larger proportion of total forearm load than the ulna throughout planar wrist flexion ($p<0.01$). At 50° of wrist extension the distal radius bore 80$\pm$9.1% of the total bone load and the distal ulna carried the remaining 20$\pm$9.1%. At 0°of wrist flexion the distal radius bore 89.9$\pm$14.3% of the load and the distal ulna 10.1$\pm$14.3% of the total bone load. At 50° of flexion the wrist experienced a similar bone

load proportion to the neutral wrist with 88.8±11.6 % of the total bone load through the radius and the remaining 11.2±11.6% through the ulna.

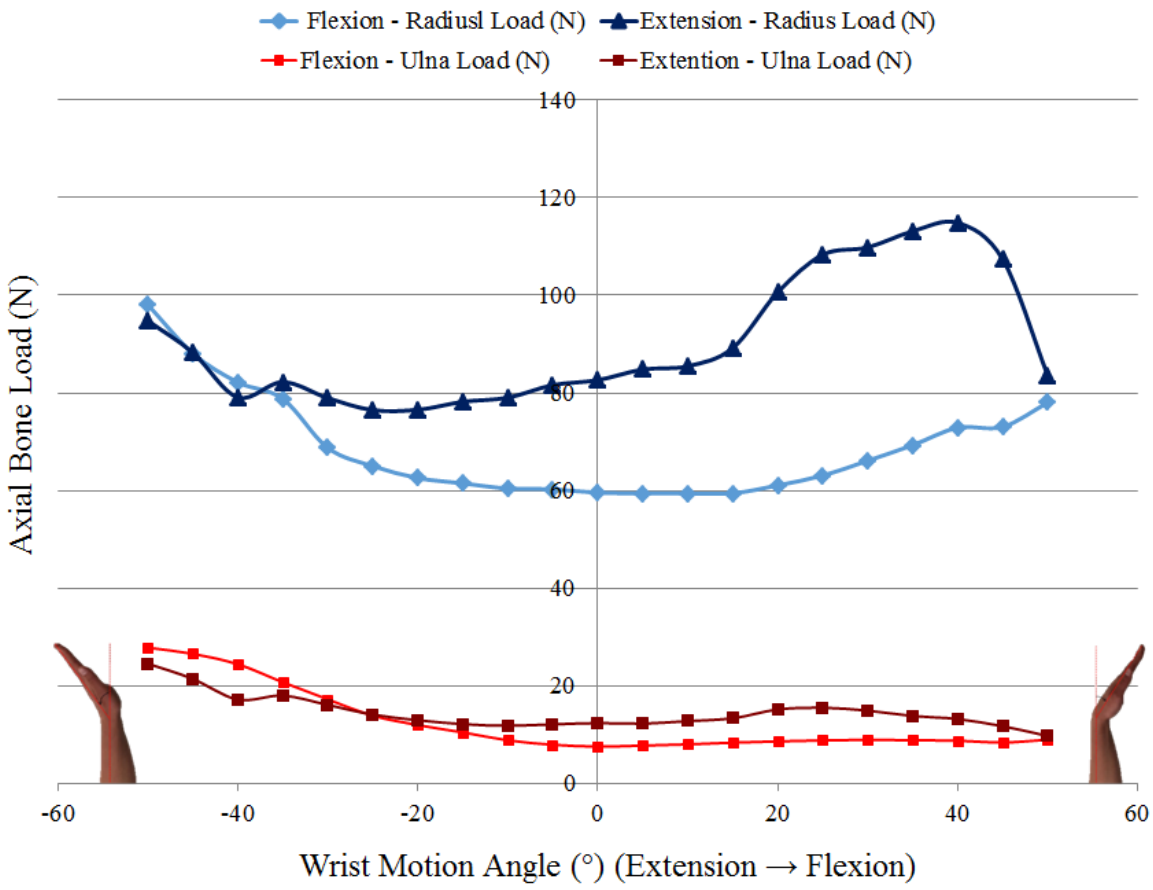

Figure 3.3: Axial Bone Loads through the Distal Radius and Ulna during Active Wrist Flexion and Extension Motions. *The graph illustrates the axial loads through the distal radius and distal ulna throughout wrist flexion and extension motions. Loads through the distal radius and ulna were significantly greater in planar wrist extension than in flexion ($p<0.001$). Radial loads were significantly greater in planar extension than flexion from -30° to 50° ($p<0.033$). Ulnar loads were significantly greater in planar extension from 0° to 40°. Loads were significantly greater through the radius than the ulna throughout all flexion-extension motions ($p<0.001$). Wrist flexion angle had no effect on load magnitudes ($p=0.142$). Standard deviations have been excluded from chart for clarity (During flexion: radius range: $\pm$5.8N to $\pm$37.7N; ulna range: $\pm$7.1N to $\pm$23.6N. During extension: radius range: $\pm$8.9N to $\pm$39.5N; ulna range: $\pm$6.5N to $\pm$39.5N).*

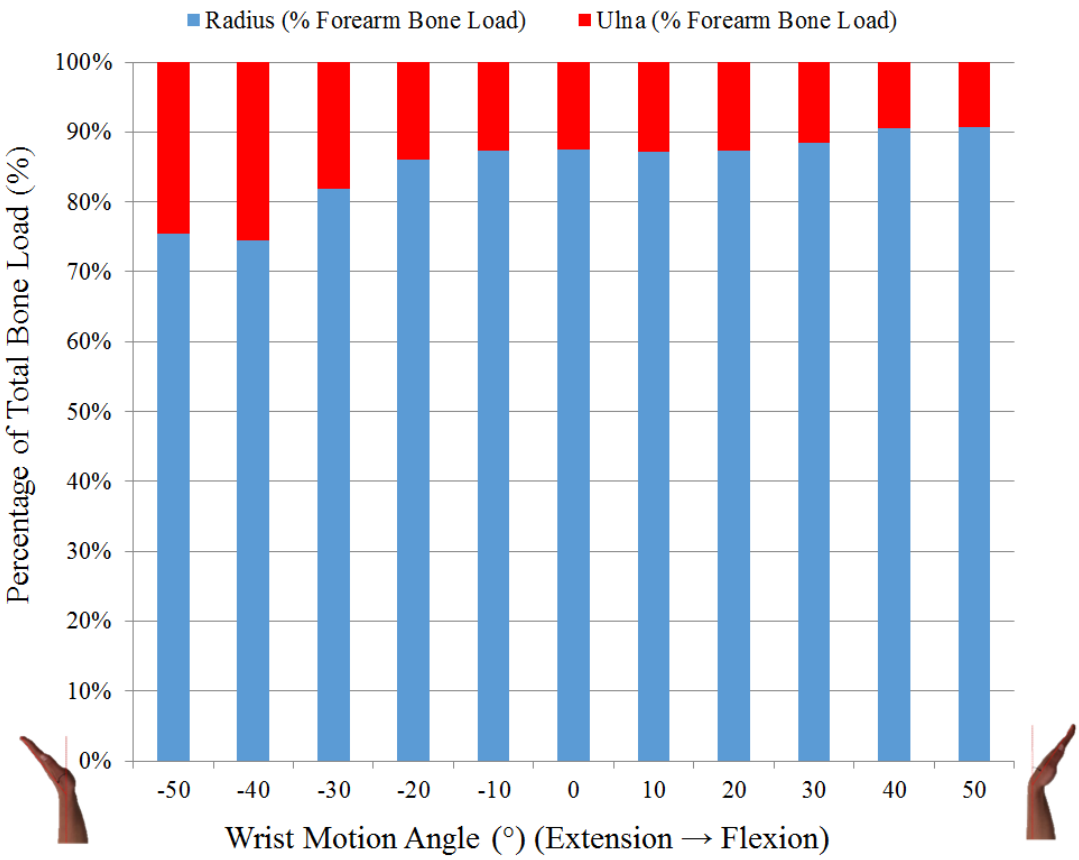

Figure 3.4: Proportion of Total Forearm Bone Load through the Distal Radius and Ulna during Active Wrist Flexion Motion. *The graph illustrates the proportion of total forearm bone load through the distal radius and distal ulna throughout planar wrist flexion from -50°of extension to 50° of flexion. Load sharing was similar throughout flexion (p=0.074). Standard deviations have been omitted for clarity. (Radius range: ±7.2% to ±15.9%; ulna range: ±7.2% to ±15.9%).*

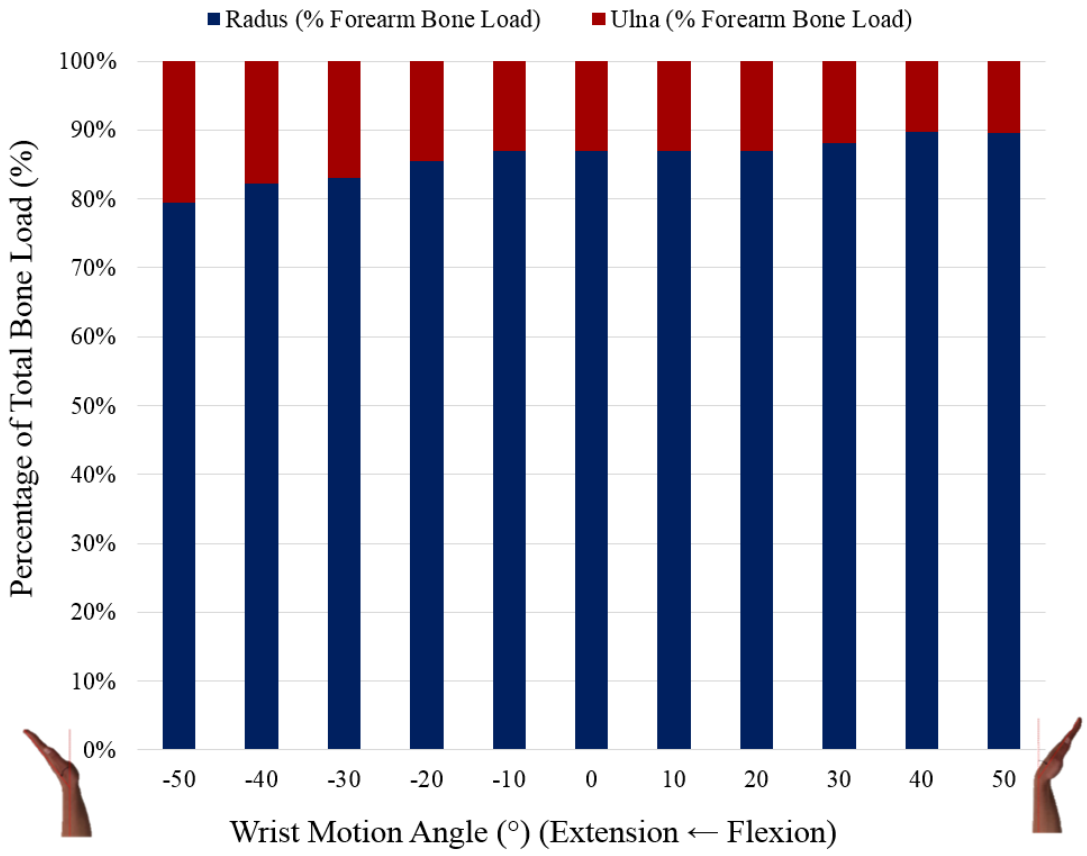

Figure 3.5: Proportion of Total Forearm Bone Load through the Distal Radius and Ulna during Active Wrist Extension Motion. *The graph illustrates the proportion of total forearm bone load through the distal radius and distal ulna throughout planar wrist flexion from 50° of flexion to -50°of extension. Standard deviations have been omitted for clarity. Standard deviations have been omitted for clarity. (Radius range: ±6.0% to ±10.6%; ulna range: ±6.0% to ±10.6%).*

Although not a specific outcome variable of this study, the mean tendon loads are presented to assist in the interpretation of the axial loads measured through the distal radius and ulna (Figure 3.6). During planar wrist flexion from -50° to 50°, loads in the extensor carpi ulnaris (ECU) (50.1±21.4 N to 14.2±8.6 N) and flexor carpi ulnaris (FCU) (37.0±13.9 N to 17.4±6.1 N) loads decreased, while flexor carpi radialis (FCR) (8.5±1.2 N to 42.5±26.6 N) and extensor carpi radialis longus (ECRL) (24.6±12.9 N to 40.2±21.3 N) loads increased. Tendon loading was more complex in planar wrist extension t, from 50° to -50°. As the wrist extended from 50° of flexion to roughly 30° of flexion loads in the extensor carpi radialis brevis (ECRB)(11.7±7.5 N to 32.8±6.6 N), ECRL (38.8±21.4 N to 47.3±24.1 N) and ECU (14.3±7.5 N to 40.3±10.0 N) spiked, slowly declining again as the wrist moved into neutral wrist position. Flexor carpi radialis loads decreased steadily from 50° to 0°(40.2±26.5 N to 11.24±1.4 N) and remained static. As the wrist extended from neutral position to full extension, 0° to -50°, ECU (27.1±8.4 N to 49.1±21.8 N) loads increased again.

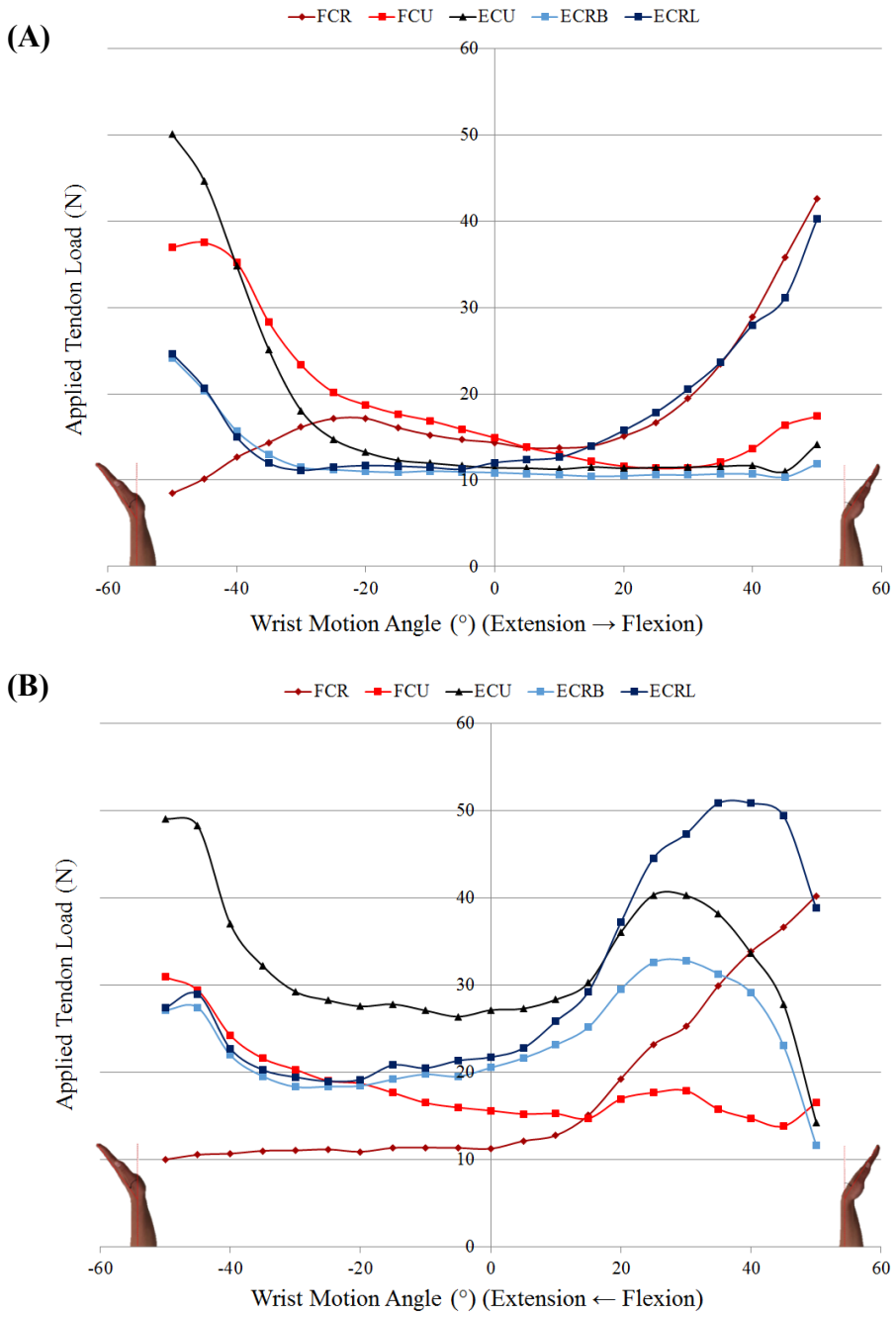

Figure 3.6: Applied Wrist Tendon Loads during Active Wrist Flexion-Extension Motion. *The graph illustrates the applied tendon loads of the FCR, FCU, ECU, ECRB and ECRL throughout wrist flexion (A) extension (B) motions from -50°of extension to 50° of flexion. Standard deviation bars have been omitted for clarity (During flexion: FCR range: ±1.2N to ±26.6N; FCU range: ±2.6N to ±13.9N; ECU range: ±2.1N to ±25.1N; ECRB range: ±0.5N to ±13.5N; ECRL range: ±1.8N to ±23.0N. During extension: FCR range: ±0.6N to ±26.5N; FCU range: ±4.0N to ±11.0N; ECU range: ±6.9N to ±21.8N; ECRB range: ±3.1N to ±12.7N; ECRL range: ±3.2N to ±25.1N.).*

3.3.2 *Radius and Ulna Loading during Radial-Ulnar Deviation*

The direction of radial-ulnar deviation motion did not have a significant effect on axial load magnitude through the distal radius ($p=0.546$) and ulna ($p=0.293$). Therefore results for loads changes will be presented for solely for planar ulnar deviation herein (Figure 3.7).

During planar ulnar deviation the magnitude of load through the distal radius ($p=0.043$) and ulna ($p=0.002$) changed significantly during motion (Figure 3.7). The magnitude of load through the distal radius was significantly greater than the load in the distal ulna ($p<0.001$) throughout motion. At 10° of radial wrist deviation the load through the distal radius was 104.6$\pm$48.0 N and 7.0$\pm$9.8 N through the distal ulna. At 0° of wrist deviation, or neutral wrist position, the distal radius measured 73.5$\pm$8.3 N and the distal ulna 9.7$\pm$10.4 N. At 15° of ulnar deviation, the distal radius and ulna were under 82.8$\pm$28.1 N and 28.1$\pm$23.7 N of compressive load respectively.

The direction of motion had no effect on distal forearm bone load sharing between the radius and ulna, therefore results for only planar ulnar deviation will be presented.($p=0.380$). Load sharing between the forearm bones changed significantly with active planar ulnar deviation of the wrist ($p=0.001$) (Figure 3.8 & 3.9). The proportion of load through the radius was significantly greater than that though the ulna for the full range of motion ($p<0.001$). In 10° of radial deviation the radius accounted for 92.0$\pm$12.1 % of total forearm bone load and the ulna the remaining 8.0$\pm$12.1 %. At 0° of wrist deviation, or neutral wrist position, 89.3$\pm$ 9.8 % and 10.7$\pm$9.8 % of the total forearm bone load was transmitted through the distal radius and ulna respectively. At 15° of ulnar deviation the proportion of total load transmission through the forearm bones in the radius lowered to 76.6$\pm$10.4 % and increased to 23.4$\pm$10.4 % in the ulna. While the overall change in load sharing between the radius and ulna was significant during planar ulnar deviation there were no significant differences between the pairwise comparisons of joint angles ($p>0.05$).

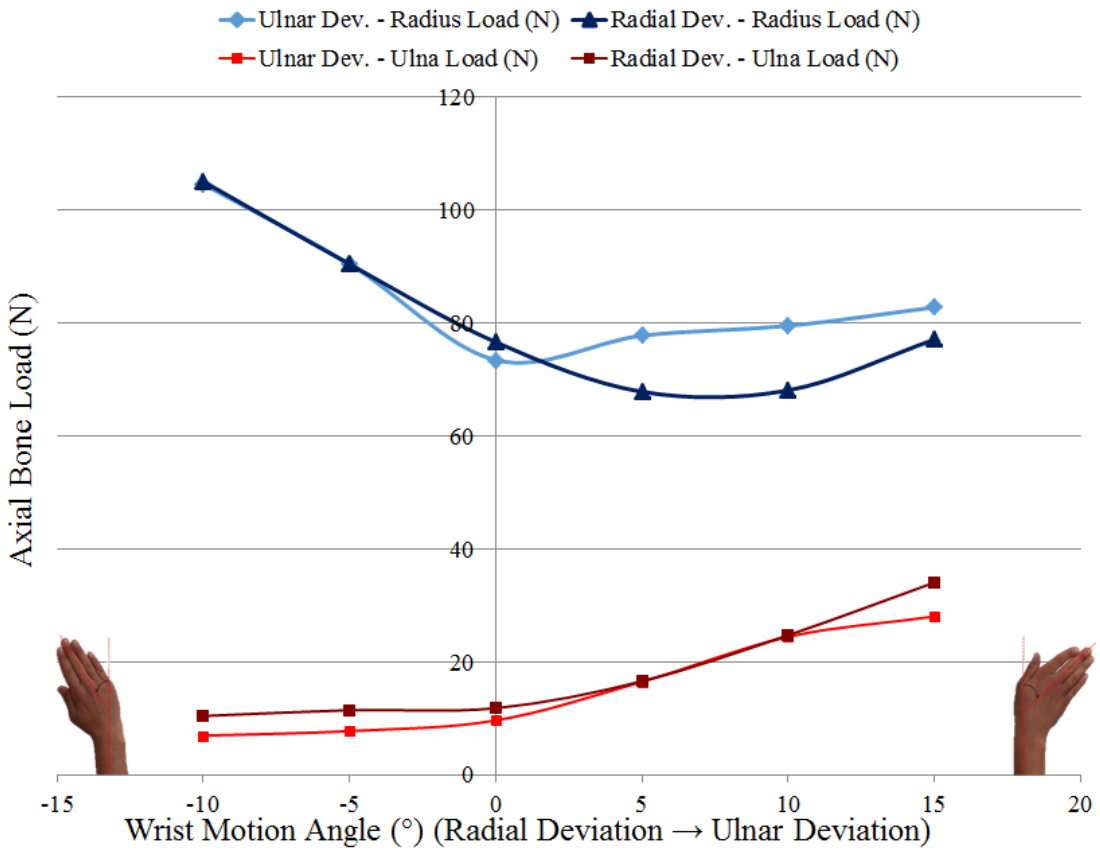

Figure 3.7: Axial Bone Loads through the Distal Radius and Ulna during Active Radial and Ulnar Deviation. *The graph illustrates the axial loads through the distal radius and distal ulna throughout active radial and ulnar deviation from -10°of radial deviation to 15° of ulnar deviation. The direction of motion did not have a significant effect (p=0.387). Loads through the radius were significantly greater than those through the ulna throughout radial and ulnar deviation (p<0.001). Wrist deviation angle had a significant effect on axial loads through the distal forearm (p=0.004). Standard deviations have been omitted for clarity (During ulnar deviation: radius range: ±8.3N to ±48.0N; ulna range: ±9.8N to ±18.6N. During radial deviation: radius range: ±17.3N to ±31.9N; ulna range: ±10.7N to ±25.0N).*

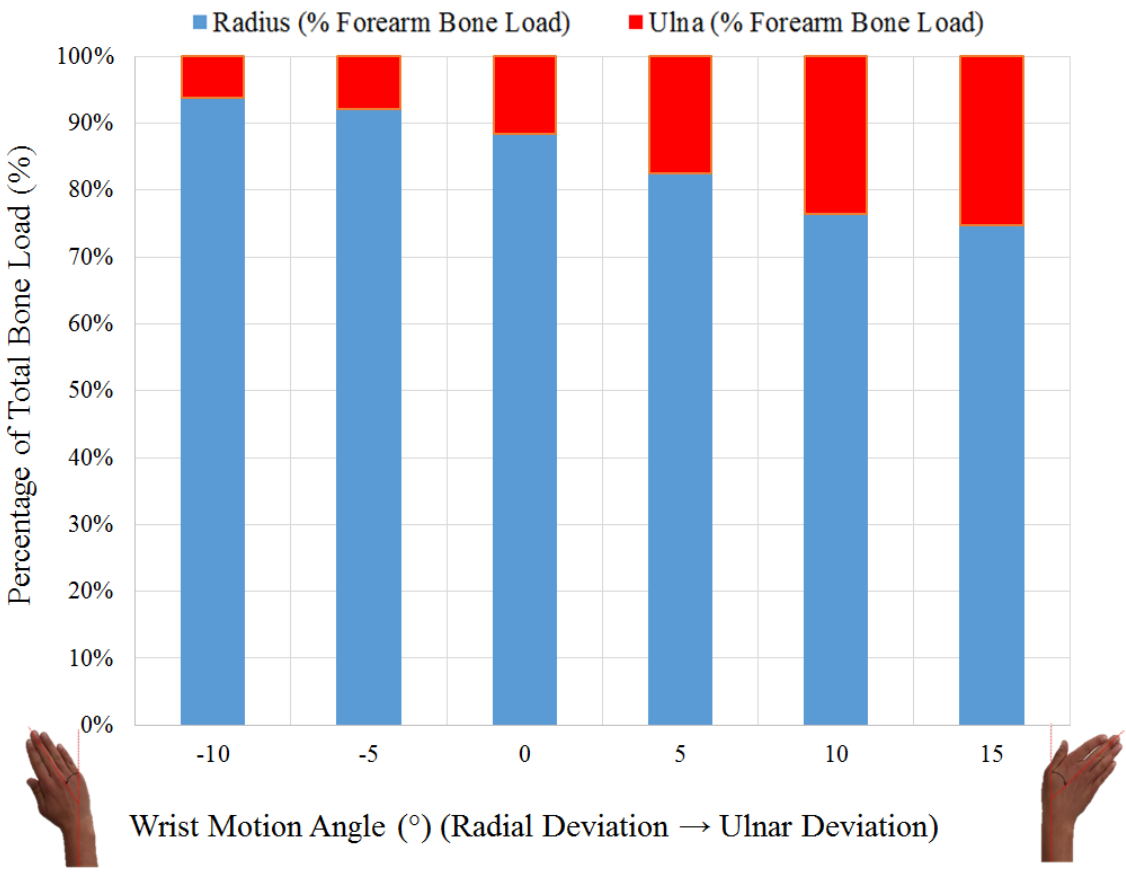

Figure 3.8: Proportion of Total Forearm Bone Load through the Distal Radius and Ulna during Active Wrist Ulnar Deviation. *The graph illustrates the proportion of total forearm bone load through the distal radius and distal ulna throughout ulnar deviation from -10°of radial deviation to 15° of ulnar deviation. Wrist deviation angle has a significant effect on forearm bone load sharing (p=0.001).Standard deviations have been omitted for clarity. (Radius range: ±9.0% to ±12.1%; ulna range: ±9.0% to ±12.1%).*

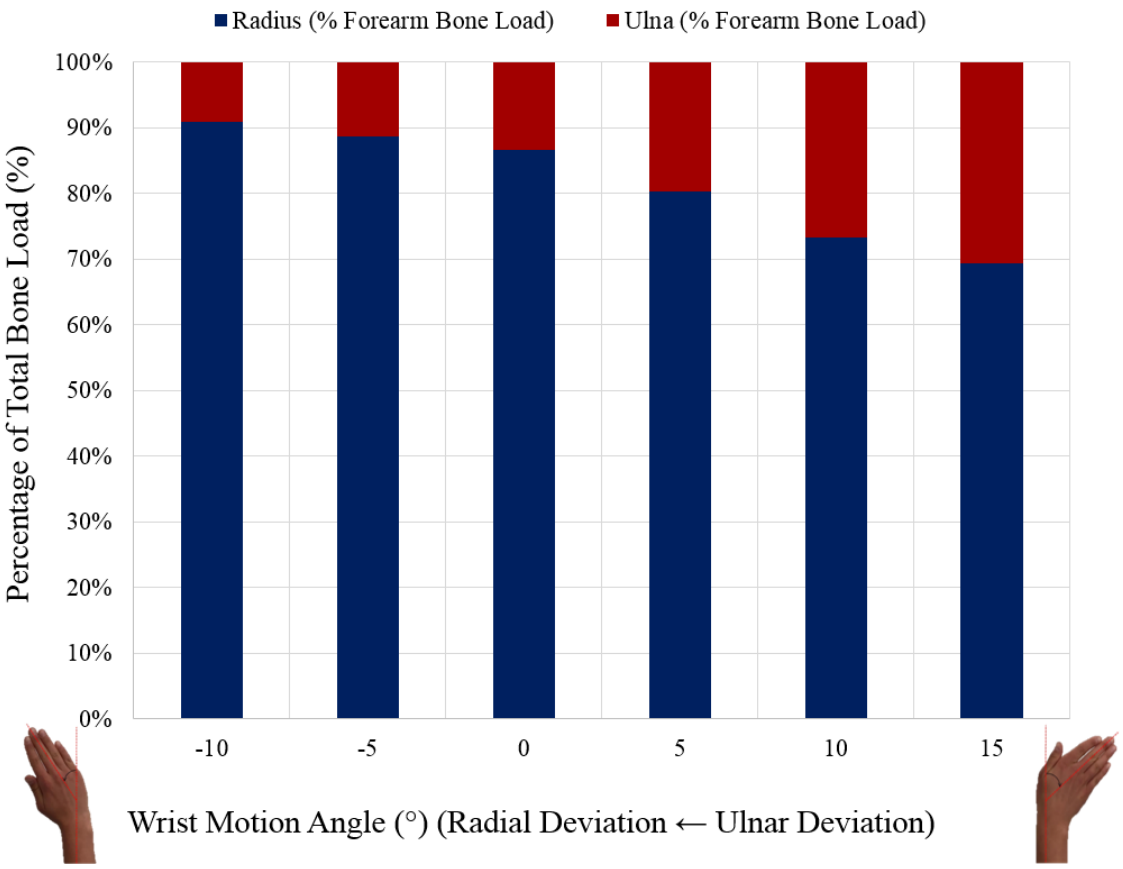

Figure 3.9: Proportion of Total Forearm Bone Load through the Distal Radius and Ulna during Active Wrist Radial Deviation. *The graph illustrates the proportion of total forearm bone load through the distal radius and distal ulna throughout radial deviation from 15° of ulnar deviation to -10°of radial deviation. Standard deviations have been omitted for clarity. (Radius range: ±7.8% to ±14.5%; ulna range: ±7.8% to ±14.5%).*

Although not a specific outcome variable of this study, tendon loads have been presented to help with the interpretation of the distal radius and ulna load measurements (Figure 3.10). Throughout planar ulnar deviation, -10° to 15°, ECU (15.9±5.6 N to 57.9±9.2 N) and FCU (13.4±5.7 N to 44.1±6.4 N) loads increased. Flexor carpi radialis loads decreased from -10° to 0° (20.4±16.2 N to 9.4±0.5 N) and remained static to 15°. During active planar radial deviation, ECU (47.6±26.7 N to 20.3±2.5 N) and FCU (33.5±17.8 N to 10.1±1.2 N) loads decreased from 15° to -10°, while FCU (9.0±0.7 N to 34.0±10.6 N) loads increased. Extensor carpi radialis longus loads increased from 5° to -10° (17.5±4.6 N to 42.6±13.3 N).

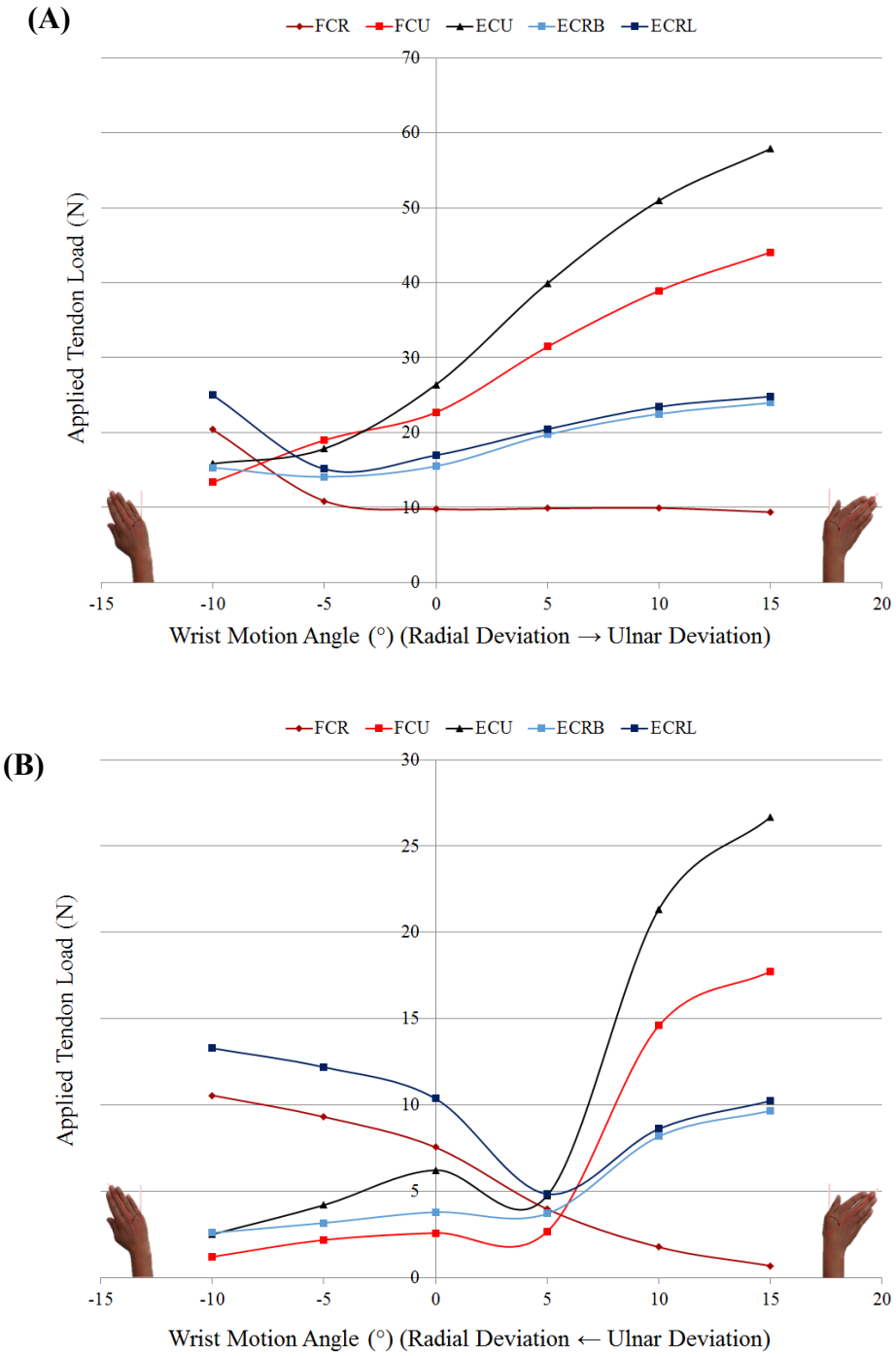

Figure 3.10: Applied Wrist Tendon Loads during Active Ulnar and Radial Deviation. *The graph illustrates the applied tendon loads of the FCR, FCU, ECU, ECRB and ECRL throughout ulnar deviation (A) and radial deviation from -10°of radial deviation to 15°of ulnar deviation. Standard deviation bars have been excluded for clarity. (During ulnar dev.: FCR range: ±0.5N to ±16.2N; FCU range: ±4.6N to ±7.4N; ECU range: ±5.6N to ±10.4N; ECRB range: ±2.1N to ±4.9N; ECRL range: ±2.6N to ±21.9N. During radial dev.: FCR range: ±0.7N to ±10.6N; FCU range: ±1.2N to ±17.8N; ECU range: ±2.5N to ±26.7N; ECRB range: ±2.6N to ±9.7N; ECRL range: ±4.9N to ±13.3N.).*

3.3.3 *Radius and Ulna Loading during Forward and Reverse Dart Throw Motion*

The direction of dart throw motion had a significant effect on load transmission through the distal radius ($p=0.003$) and ulna ($p=0.02$) (Figure 3.11). Loads through the distal radius were significantly greater in reverse DTM than those in forward DTM at -10° to 30° of wrist flexion ($p<0.032$). Loads through the distal ulna were significantly greater in reverse DTM than in forward DTM at 15° to 30° of wrist flexion ($p<0.047$).

The magnitude of load transmitted through the distal radius ($p=0.016$) and ulna ($p=0.001$) changed significantly throughout the forward and reverse DTM (Figure 3.11). The magnitude of distal radial loads was greater than distal ulnar loads throughout forward and reverse DTM ($p<0.001$). During forward DTM, axial loads through the distal radius were 109.6$\pm$55.2 N at -30° of wrist extension and -10° of radial deviation, 57.4$\pm$18.9 N at 0° of wrist flexion and ulnar deviation, and 64.4$\pm$16.4 N at 30° of wrist flexion and 10° of ulnar deviation. During reverse DTM loads through the radius averaged 105.7$\pm$30.7 N, 35.3+20.7 and 74.1$\pm$20.1 at -30° of wrist extension and -10° of radial deviation, 0° of wrist flexion and ulnar deviation and 30° of wrist flexion and 10° of ulnar deviation, respectively. Throughout forward DTM, axial loads through the distal ulna averaged 5.4$\pm$9.74 N at -30° of wrist extension and -10° of radial deviation, 11.5$\pm$8.3 N at 0° of wrist flexion and ulnar deviation and 25.2$\pm$9.8 at 30° of wrist flexion and 10° of ulnar deviation. During reverse dart throw motion loads through the distal ulna were 8.7$\pm$8.7 N, 19.2$\pm$7.7 and 34.1$\pm$15.9 at -30° of wrist extension and -10° of radial deviation, 0° of wrist flexion and ulnar deviation and 30° of wrist flexion and 10° of ulnar deviation, respectively.

The direction of motion at no effect on distal forearm bone load sharing therefore load sharing will be presented for solely forward DTM herein ($p=0.602$). Load sharing between the distal radius and ulna changed significantly throughout the DTM ($p<0.001$) (Figure 3.12 & 3.13). The proportion of load through the distal radius was higher than that through the ulna throughout the DTM ($p<0.001$). At -30° of wrist extension and -10° of radial deviation the distal radius accounted for 94.8$\pm$9. 3 % of total forearm bone load

and the distal ulna the remaining 5.2± 9.3%. At neutral wrist position, the distal radius and ulna transmitted 81.8±14.2 % and 18.2 ±14.2 % of total forearm load respectively. At 30° of wrist flexion and 10° of ulnar deviation the proportion of load sharing was 72.2±8.7 % through the distal radius and 24.8±8.7 % through the distal ulna.

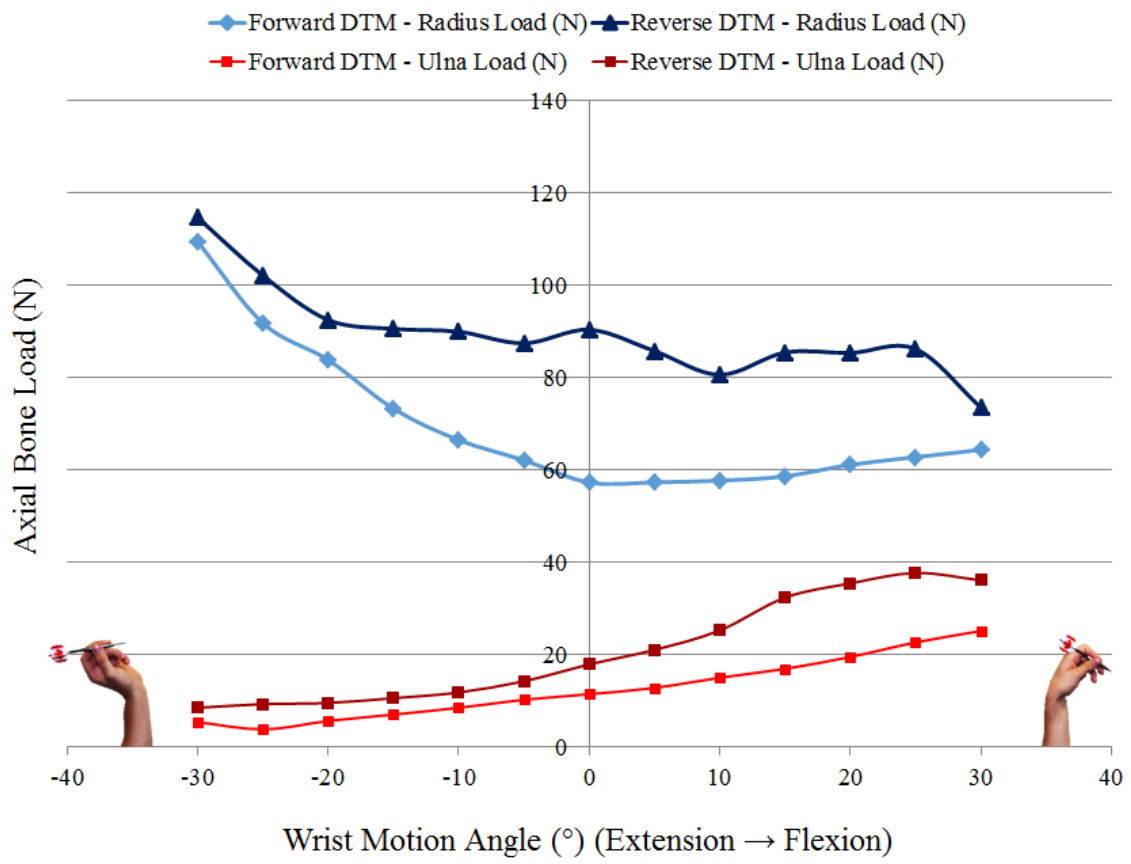

Figure 3.11 Axial Bone Loads through the Distal Radius and Ulna during Active Forward and Reverse Dart Throw Motion. *The graph illustrates the axial loads through the distal radius and distal ulna throughout forward and reverse dart throw motion from -30°of extension and 10° of radial deviation to 30° of flexion and 10° of ulnar deviation. Axial loads through the distal radius were significantly greater than those through the ulna throughout DTM ($p<0.001$). Loads through the distal radius and ulna were significantly greater in reverse DTM than in forward DTM ($p=0.017$). Radial loads were significantly higher in reverse than forward DTM from -10° to 30° ($p<0.032$) and ulnar loads were significantly greater from 15° to 30 ° ($p<0.047$). DTM angle had a significant effect on loads through the distal forearm bones ($p=0.001$). Standard deviations have been omitted for clarity (radius forward DTM. range: $\pm$10.5N to $\pm$55.3N; radius reverse DTM range: $\pm$20.2N to $\pm$43.1N; ulna forward DTM range: $\pm$6.7N to $\pm$6.7N; ulna reverse DTM range: $\pm$8.2N to $\pm$15.3N).*

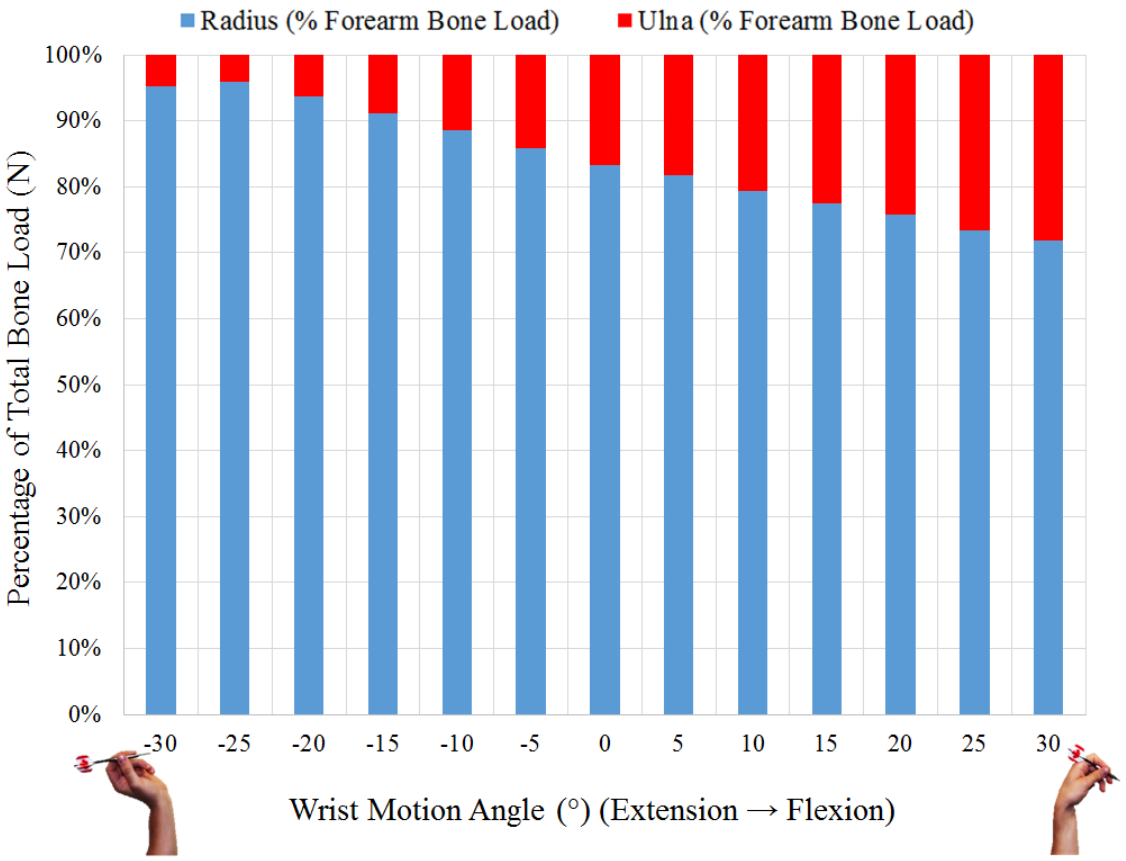

Figure 3.12: Proportion of Total Forearm Bone Load through the Distal Radius and Ulna during Active Forward Dart Throw Motion. *The graph illustrates the proportion of total forearm bone load through the distal radius and distal ulna throughout forward dart throw motion from -30°of extension and 10° of radial deviation to 30° of flexion and 10° of ulnar deviation. The proportion of load through the distal radius was greater than that through the ulna ($p<0.001$) and load sharing varied significantly with DTM angle ($p<0.001$). (Radius range: $\pm$7.9% to $\pm$14.2%; ulna range: $\pm$7.9% to $\pm$14.2%).*

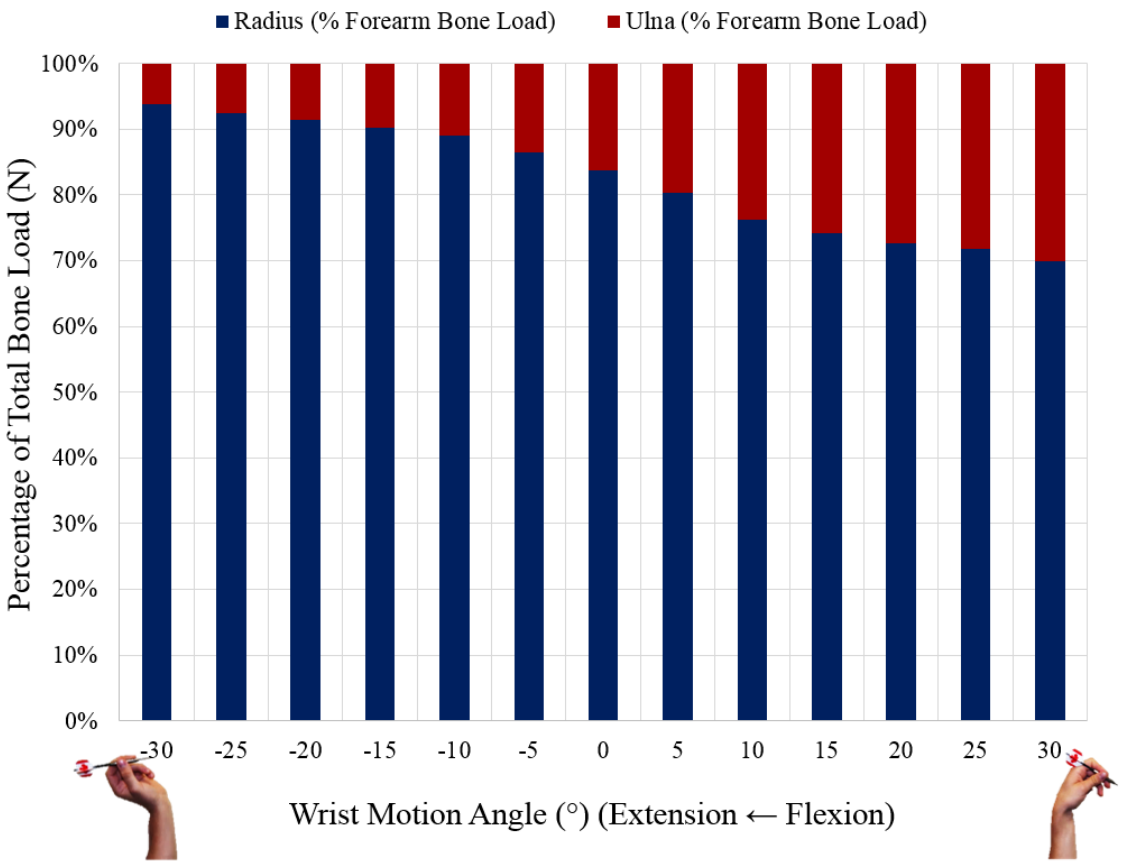

Figure 3.13: Proportion of Total Forearm Bone Load through the Distal Radius and Ulna during Active Reverse Dart Throw Motion. *The graph illustrates the proportion of total forearm bone load through the distal radius and distal ulna throughout reverse dart throw motion from 30° of flexion and 10° of ulnar deviation to -30°of extension and 10° of radial deviation. (Radius range: ±6.6% to ±11.6%; ulna range: ±6.6% to ±11.6%).*

Although tendon loading was not a specific outcome variable of the present study, mean tendon loads have been included to provide greater insight on axial load measurements through the distal radius and ulna (Figure 3.14). During forward DTM, -30° of wrist extension and -10° of radial deviation to 30° of wrist flexion and 10° of ulnar deviation, ECU (15.4±6.7 N to 40.6±18.3 N) and FCU (10.2±2.3 N to 35.73±14.6 N) loads steadily increased while FCR (26.6±18.4 N to 8.35±2.1 N) and ECRL (32.1±25.6 N to 15.1±5.1 N) loads decreased. In reverse DTM, ECU (61.3±26.3 N to 22.5±5.2 N) and FCU (36.9±17.2 N to 11.4±1.6 N) loads decreased from 25° to -30° of wrist flexion while FCR (9.7±1.3 N to 27.5±14.1 N) loads steadily increased from 30° to -30°.

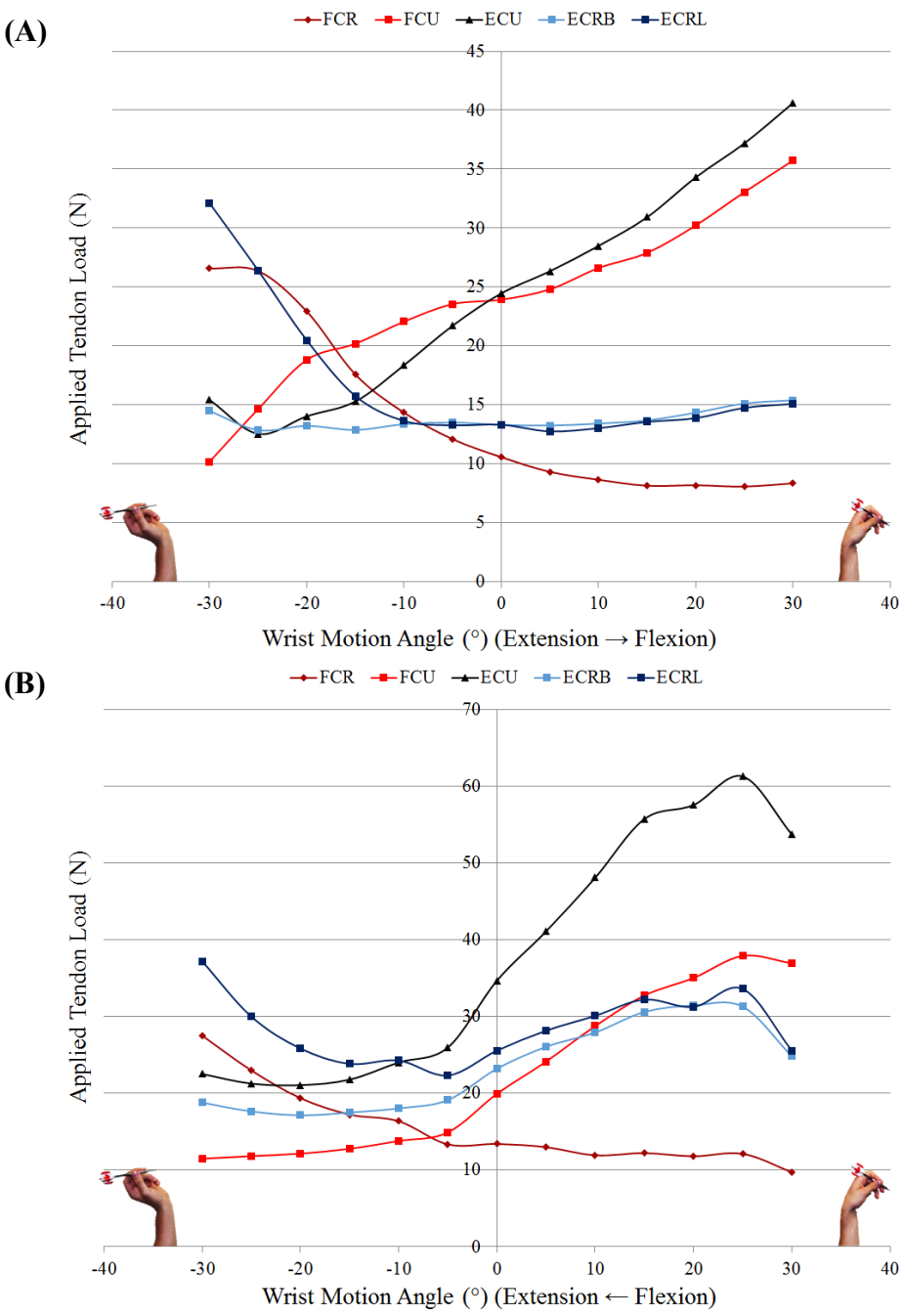

Figure 3.14: Applied Wrist Tendon Loads during Active Forward and Reverse Dart Throw Motion. *The graph illustrates the applied tendon loads of the FCR, FCU, ECU, ECRB and ECRL throughout forward DTM (A) and reverse DTM (B) from -30°of extension and 10° of radial deviation to 30° of flexion and 10° of ulnar deviation. Standard deviation bars have been omitted for clarity (During forward DTM: FCR range: ±1.9N to ±18.9N; FCU range: ±2.3N to ±14.6N; ECU range: ±3.4N to ±18.3N; ECRB range: ±1.5N to ±6.4N; ECRL range: ±2.8N to ±25.6N. During reverse DTM: FCR range: ±1.3N to ±14.1N; FCU range: ±1.1N to ±17.5N; ECU range: ±2.6N to ±28.9N; ECRB range: ±2.7N to ±11.5N; ECRL range: ±8.4N to ±18.4N.).*

3.4 Discussion

Traumatic injuries and degenerative diseases such as wrist fractures, Kienbock's disease and ulnar impaction cause changes in forearm bone length and angulation which can in turn lead to altered wrist joint loading and pain. Before we can diagnose and treat cases of altered wrist joint loading, we must first gain a better understanding of normal wrist biomechanics. Load magnitude and sharing through the distal forearm bones have been previously reported during static loading scenarios.[10-13, 15] This form of biomechanical testing is problematic because it does not necessarily simulate the loading that occurs during *in vivo* activities. However, there has been very little investigation on the effects of active wrist motion on *in vitro* distal forearm bone loading.[14] This study investigated the effect of simulated active wrist joint motion on load transfer through the distal radius and ulna. Loads were examined during planar wrist flexion-extension motion, planar radial and ulnar deviation, and multiplanar forward and reverse dart throw motion. *In vitro* axial loads through the distal radius and ulna were monitored continuously throughout wrist motion.

Load magnitudes through the distal radius and ulna were greater during planar wrist extension than during planar wrist flexion, particularly at positive flexion angles. The differences observed with respect to direction of wrist flexion-extension motion are thought to be caused by the tendon loads applied to achieve each active motion. There is a steep increase in ECU, ECRB and ECRL loads as the wrist starts to extend out of 50° of flexion indicating that the wrist extensors work to both initiate and complete wrist extension. In flexion, the FCU acts to initiate flexion and the FCR acts to complete wrist flexion. While wrist extensors are recruited synergistically throughout planar wrist extension, wrist flexors seem to be recruited only moderately to initiate and complete wrist flexion. These differences in tendon loading are postulated to be responsible for the significantly greater loads through the distal radius and ulna seen in extension compared to flexion. The muscle moment arms of the wrist flexors greater than the extensors and both vary with wrist position.[21, 22, 23, 24] Therefore less muscle activation is required by the flexors than the extensors to achieve the same amount of wrist flexion and extension

respectively. The increase in extensor muscle force may account for the increase in loads through the distal radius and ulna during extension seen in the current study.

The magnitude of loads through the distal ulna varied significantly with wrist flexion and extension. Axial loads through the ulna also peaked in extension and decreased by a magnitude of four by the time the wrist reached neutral position. Ulnar loads remained similar to neutral position as the wrist moved into flexion. During wrist extension, axial loads through the ulna increased as the wrist moved out of full flexion and decreased again slightly as the wrist extended further to neutral position. Loads through the ulna increased steeply as the wrist extended from neutral position to full simulated wrist extension. In daily living tasks the wrist is thought to go through a natural range of radioulnar deviation as it performs FEM.[18, 19, 20] In our simulation of planar FEM, the wrist was forcibly constrained in neutral radioulnar deviation via applied tendon loads. In extension the wrist tends to radially deviate, therefore in order to maintain neutral wrist radioulnar deviation the loads in the ECU must increase thereby increasing axial loads through the distal ulna. Our flexion and extension motion results, agree with those of *Trumble et al.* and *af Ekenstam et al*., who also reported distal ulna load magnitudes peaking in wrist extension angles and decreasing in wrist flexion angles under static loading.[11, 17] The ECU moment arm is smaller than that of the ECRB, likely causing the ECU to exert more force than the ECRB to achieve the same degree of joint motion.[25] This may explain the why we obverse more significant changes in distal ulnar loading than radial loading throughout FEM. While tendon loading seems to have played a key role in distal forearm loading there may also have been changes due to radiocarpal joint contact.

With regard to load transmission through the distal radius, the magnitude did not change significantly with respect to joint angle neither wrist flexion nor extension. There was a distinct trend to the loads transmitted through the distal radius during wrist flexion and extension. During wrist flexion, loads through the radius peaked in extension and then decreased as the wrist flexed towards neutral wrist position. Loads through the radius then increased slightly as the wrist reached full actuated flexion. During wrist extension, loads through the radius peaked in flexion and slowly decreased as the wrist moved to

neutral position, increasing again only slightly as the wrist moved into full simulated extension. As the wrist flexes and extends it naturally tends to ulnarly and radially deviate respectively as in a dart throw motion. Therefore, in our simulation, during flexion the applied ECRL force must increase to negate this and keep the wrist in neutral radioulnar deviation, thereby slightly increasing the load applied to the distal radius.

Load sharing did not change significantly with direction of wrist flexion and extension motion and will therefore be discussed only for wrist flexion herein. Load sharing between the distal radius and ulna did not change with respect to wrist angle throughout active wrist flexion. The radius consistently bore the majority of the axial load at every flexion angle with the lowest contribution in extension where it accounted for 80% of total forearm bone load and the ulna the remaining 20%. As the wrist flexed, the distal radius accounted for more forearm bone transfer with maximum distal radius contribution occurring at neutral (90%). *Harley et al.* reported similar changes in load sharing between the radius and ulna, with the peak load borne by the ulna occurring in extension and reaching 15$\pm$7%, compared to the 20$\pm$9.1% reported in the current study. [14] Despite of the different testing techniques used by *Harley et al.* and the current study similar results were observed. The key findings of our study confirm their results while adding load magnitudes to the current literature.

There was no difference in direction of motion between load magnitudes nor sharing during radial and ulnar deviation. Ulnar deviation has a much smaller motion arc and is therefore subjected to less gravity at extremes of motion. Radioulnar deviation was also simulated at a slower rate than FEM and DTM, 3°/sec as opposed to 5°/sec. It is speculated that a combination of these factors accounts for the similarity between radial and ulnar deviation motions. Due to their similar nature, only ulnar deviation will be discussed herein

With respect to radial-ulnar deviation, as the wrist progressed ulnarly, the magnitude of load transfer through the distal radius peaked in radial deviation and decreased towards neutral. These loads also increased again slightly as the wrist moved into ulnar deviation. This is counter intuitive, however is thought to be caused by the large tendon loads

required to reach full ulnar deviation. In ulnar deviation, the applied tendon loads of both the ECRL and ECRB increase by roughly 15N above the applied tone load. This suggests that radial deviating tendons are activated for wrist stability even though the wrist is moving ulnarly under the primary control of the FCU and ECU. Ulnar deviation motion of the wrist objectively produced the largest magnitude of loads in the distal ulna of any of the testing wrist motions. Load transfer through the distal ulna was the lowest in radial deviation and increased slightly as the wrist moved into neutral position. As the wrist continued from neutral position to full ulnar deviation the magnitude of the load through the ulna roughly tripled. This was likely due to a combination of tendon activation and the shifting of the carpus more towards the ulna.

All existing literature on the effect of radioulnar deviation on distal forearm loading supports these findings.[10, 11, 14, 17] The magnitudes of ulnar loads reported in the current study are similar to those reported by *Harley et al.* during active ulnar deviation.[14] Throughout ulnar deviation the radius accounted for the majority forearm bone transfer with the greatest proportion of radial load (92%) occurring in maximum simulated radial deviation. As the wrist ulnarly deviated the proportion of load through the radius steadily declined reaching a minimum of 76.5% of total forearm bone load. *af Ekenstam et al.* reported a similar load sharing ratio during radial deviation (91/9% radius to ulna) and ulnar deviation (76/24% radius to ulna) with static tendon loading.[17] *Harley et al*. reported a similar trend during dynamic wrist motion however with a less dramatic increase in proportion through the ulna during ulnar deviation ($18\pm9\%$).[14] The increase in radial loading during radial deviation may be due in part to the compression of the scaphoid against the scaphoid facet on the distal radius. This compression is induced by the wrist flexors and extensors that span the radiocarpal joint. Similarly, the increase in ulnar loading during ulnar deviation motion is thought to be caused by the compression of the triquetrum on the TFC induced active tendon loading. Increased compression of the triquetrum against the TFC would also explain the pain induced clinically when performing an ulnar deviation test for TFC tears.

Loads through the distal radius and ulna were significantly higher in reverse dart throw motion than in forward DTM. Similar to flexion-extension motion, the differences

between forward and reverse DTM were most significant in positive wrist flexion angles. As previously stated, muscles moment arms are known to be greater in flexion than extension.[21, 22, 23, 24] Therefore, the same phenomenon seen during FEM may be occurring during forward and reverse DTM, in which extensors must exert more force than flexors to achieve the same amount of joint motion in wrist extension and flexion, respectively. Therefore, the increased extensor muscle force may account for the increased loading through the distal radius and ulna during reverse DTM.

During both forward and reverse DTM, the magnitude of loads through the radius peaked in the combined extension and radial deviation position. As the wrist flexed and ulnarly deviated loads through the radius roughly halved as the wrist reached neutral position. Radial load transfer increased again slightly as the wrist flexed and ulnarly deviated further to the final position of the forward DTM. The magnitude of loads through the ulna was the lowest in the extended and radially deviated position and roughly doubled as the wrist moved to neutral. Loads through the ulna doubled again as the wrist moved to the final flexed and ulnarly deviated position. Load magnitude changes were more like those of ulnar deviation than to those of flexion. Reverse DTM objectively produced the largest radial loads of any of the tested wrist motions. The differences in distal forearm loading during forward and reverse dart throw motion are again thought to be caused by the tendon loads required to initiate and achieve these motions. Similar to flexion-extension motion, there was an increase in ECU loads in order to initiate the reverse dart throw motion. However, ECU loads then taper as the wrist extends further and ECRL loads increase to complete the combined extension-radial deviation motion, which is more similar to the tendon loading exhibited in radial deviation than in planar wrist extension. In forward dart throw motion, FCR loads peaked to initiate the motion and then quickly decreased to allow for ulnar deviation. The ECU and FCU then increased in parallel to generate the flexion-ulnar deviation position that terminates forward dart throw. Overall, the tendon loads required to produce forward and reverse dart throw motion more similarly mimic those of radial and ulnar deviation than those of flexion and extension.

The radius accounted for the largest proportion of forearm bone load throughout both forward and reverse dart throw motions, peaking in extension and radial deviation (94%)

and reaching a minimum in flexion and ulnar deviation (72%). These results are of interest because DTM is thought to be a more physiologically representative form of wrist flexion.[18,19,20] In both forward and reverse DTM, load magnitudes and sharing between the two forearm bones followed the same trend as of radial and ulnar wrist deviation rather than flexion and extension.

The increased loads and proportion of total forearm load through the ulna during DTM may explain ulnar sided wrist pain that often occurs during repetitive wrist flexion-extension.[27] High ECU involvement in dart throw motion may also explain the increased incidence of wrist tendonitis in workplaces that require repetitive wrist motions, such as factory work.[27, 28] There have been no previous studies conducted to examine the effect of a multiplanar motion on loads through the distal radius and ulna. This aspect of our study is particularly novel and provides a better understanding of the effect of the combined extension-radial deviation and flexion-ulnar deviation generated by DTM. Our results suggest that repetitive physiologic flexion-extension motion, represented in this study by DTM, should be avoided to decrease the risk and incidence of ulnar sided wrist pain and wrist extensor tendonitis.

The distal forearm load sharing at neutral wrist position was 90% through the radius and 10% through the ulna during wrist flexion and ulnar deviation. A number of studies have examined load sharing in distal forearm at neutral wrist position and have reported the proportion of total forearm bone load through the ulna to be roughly 18% of the total forearm bone load.[10,11,12,13] Additional studies have examined load sharing at neutral wrist position during quasistatic and active wrist motion and have shown that the proportion of total forearm bone load through the ulna decreased to 13-14% under these circumstances.[14,15] The further decrease in the proportion of total forearm bone load through the ulna in thought to have occurred due to soft tissue retention and variable tendon loading. Our study, unlike many previous studies, left almost all soft tissues intact. The loads measured through the load cells only accounted for roughly half of the applied tendon loads inferring that the remaining proportion of load was transferred through soft tissues or dissipated in the tendons themselves. Increased proportion of total

distal forearm bone load through the radius may also be explained by the tendon loading employed by the active motion simulator.

This study provided new information about how load sharing in the distal forearm is affected by active wrist motion. Over the three wrist motions tested, distal radius load magnitudes objectively peaked in combined extension and radial deviation position from dart throw motion. Distal radius load magnitudes were the lowest during each motion when the wrist was in neutral joint position. Distal ulna loads were observed to peak in planar wrist extension. Total forearm load was divided between the distal radius and ulna and the proportion of load through each bone was calculated. The proportion of load through the radius was always greater than that of the ulna. Distal radial load proportions were observed to be lowest in the flexed ulnarly deviated position generated by the dart throw motion. These observations have important implications for rehabilitation protocols and post-surgical recommendations. Wrist bracing and rehabilitation positions can now be altered to minimize or maximize load magnitudes and proportions through the forearm bone of concern. In cases of ulnar impaction, wrist should be braced in neutral wrist flexion with slight radial deviation. For cases of wrist extensor tendonitis, our results suggest that range of motion should be limited to -20° to 20° of wrist flexion and extension to avoid the high tendon loads reported during initiation of flexion-extension motions.

This study has also improved our understanding of basic wrist biomechanics and can be used to improve biomechanical models in the future. Previously, an overall load sharing ratio of 80/20 between the distal radius and ulna was widely accepted and taught clinically. This study has shown that this is not always the case and that load sharing is dependent on wrist position. Hence, classic teaching that the 80:20 loading ratio predominates is not fully accurate. Instead, we observed a 90:10 load sharing ratio at neutral wrist position and variable load sharing ratios dependent on wrist position.

The study presented in this chapter has limitations. Due to the nature of cadaveric research our sample size was small. However, statistical significance was achieved for most comparisons and therefore our study was sufficiently powered. Wrist flexion and

ulnar deviation were actuated as fully planar motions, not accounting for the more typical complex multiplanar motions during activities of daily living. Forearm bone loads were collected strictly through the long axis of the radius and ulna. Off axis loads were not measured. Physiologic loads occur in all directions of the wrist joint. The axial bone loads are more indicative of radiocarpal joint forces than they are of distal radioulnar joint loads. Wrist motions were performed actively through applied physiologic tendon loads.[29] However, these loads are merely an estimation of *in vivo* loads generated during simple loading scenarios. Therefore, we do not know how closely the loads applied with the active wrist motion simulator represent *in vivo* tendon loads. No resisted joint motion or simulated object lifting was performed.

This study has several strengths. The direction of motion was accounted for and load magnitudes were reported in both directions of wrist flexion-extension, radioulnar deviation and dart throw motions. Wrist flexion was simulated from 50° of extension to 50° of flexion, whereas previous static and dynamic loading studies have only examined simulated wrist motion from 30° of extension to 50° of flexion.[14, 30, 31, 32] Active wrist motion was simulated to more closely represent *in vivo* loading, which has only been reported by one other research group.[14] Loads were collected continuously for all joint angles throughout the three simulated wrist motions. Load magnitudes were also reported for both forearm bones separately as well as proportions of total forearm bone load. All incisions were closed throughout testing to maintain tissue hydration and the viscoelastic behavior of *in vivo* soft tissues. The experimental devices used for collecting axial bone loads were critically designed and evaluated to ensure that measurements were reliable and repeatable, while being in-line (i.e. concentric) with the long axes of both the distal radius and the ulna. Unlike other studies, the experimental devices were discrete, located anatomically and allowed for retention of all soft tissues, excluding the distal interosseous membrane.[10-15] Highly accurate optical motion tracking was employed, allowing for real time joint angle feedback. Lastly, a multiplanar dart throw motion was examined. The dart throw motion simulated a more physiologic form of wrist flexion and extension allowing for a better representation of daily living and working tasks.[18, 19, 20]

3.5 Conclusions

The current study supports the hypotheses that axial loads through the distal radius and ulna fluctuate during flexion-extension motions and forward and reverse dart throw motions. The greatest load magnitudes through the radius occurred in the combined extension-flexion and radioulnar deviation positions simulated during dart throw motion, the most common wrist motion in daily activities. Axial loading through the distal ulna reached similar maximums in ulnar deviation and wrist extension. The forearm bone load magnitudes and proportions produced by the forward and reverse dart throw motions were more similar to the loading patterns during radial and ulnar deviation than those during wrist flexion and extension. This study provides a more detailed explanation of the loads occurring in the healthy wrist during active wrist motion and has implications for improved rehabilitation protocols and surgical recommendations.

3.6 References

1. Adams BD. Effects of radial deformity on distal radioulnar joint mechanics. *J Hand Surg Am.* 1993; 18(3), 492-498.

2. Fernandez DL. Correction of post-traumatic wrist deformity in sdults by osteotomy, bone-grafting and internal fixation. *J Bone Joint Surg Am.* 1982; 64(8), 1164-1178.

3. Fernandez DL. Radial osteotomy and Bowers arthroplasty for malunited fractures of the distal end of the radius. *J Bone Joint Surg Am.* 1988; 70(10), 1538-1551.

4. Jupiter JB, Ring D. A comparison of early and late reconstruction of malunited fractures of the distal end of the radius. *J Bone Joint Surg Am.* 1996; 78(5), 739-748.

5. Cooney WP, Dobyns JH, Linscheid RL. Complications of Colles' fractures. *J Bone Joint Surg Am.* 1980; 33(4), 895-907.

6. Gartland JJ Jr, Werley CW. Evaluation of healed Colles' fractures. *J Bone Joint Surg Am.* 1951; 33(4), 895-907.

7. Gliatis JD, Plessas SJ, Davis TR. Outcome of distal radial fractures in young adults. *J Hand Surg Br.* 2000; 25(6), 535-543.

8. Beckenbaugh RD, Shives TC, Dobyns JH, Linscheid RL. Kienbock's disease: the natural history of Kienbock's disease and consideration of lunate fractures. *Clin Orthop Relat Res.* 1980; 149, 98-106.

9. Friedman AL, Palmer AK. The ulnar impaction syndrome. *Hand Clin.* 1991; 7(2), 295-310.

10. Palmer AK, Werner FW. Biomechanics of the distal radioulnar joint. *Clinical Orthop.* 1984; (187), 26-35.

11. Trumble T, Glisson RR, Seaber AV, Urbaniak JR. Forearm force transmisison after surgical treatment of distal radioulnar joint disorders. *J Hand Surg Am.* 1987; 12(2), 196-202.

12. Markolf KL, Tejwani SG, Benhaim P. Effects of wafter resection and hemirection from the distal ulnar on load-sharing at the wrist: a cadaveric study. *J Hand Surg Am.* 2005; 30(2), 351-358.

13. Werner FW, Palmer AK, Fortino MD, Short WH. Force transmission through the distal ulna: effect of ulnar variance, lunate fossa angulation, and radial and palmar tilt of the distal radius. *J Hand Surg Am*. 1992; 17(3)

14. Harley B, Pereria M, Werner F, Kinney D, Sutton L. Force Variations in the Distal Radius and Ulna: Effect of Ulnar Variance and Forearm Motion. *J Hand Surg Am.* 2015; 40(2), 211-216.

15. Greenberg JA, Werner FW, Smith JM. Biomechanical analysis of distal metaphyseal ulnar shortening osteotomy. *J Hand Surg Am.* 2013; 38(1), 1914-1919.

16. Wu G, van der Helm FCT, Veeger HEJD, et al. ISB recommendation on definitions of joint coordinate systems of various joints for the reporting of human joint motion--Part II: shoulder, elbow, wrist and hand. *J Biomech*. 2005; 38(5):981-992.

17. Ekenstam FW, Palmer AK, Glisson RR. The load on the radius and ulna in different positions of the wrist and forearm. A cadaver study. *Acta Orthop Scand.* 1984; 55(3), 363-365.

18. Palmer AK, Werner FW, Murphy D, Glisson R. Functional wrist motion: a biomechanical study. *J Hand Surg Am.* 1985; 10(1), 39-46.

19. Werner FW, Green JK, Short WH, Masaoka S. Scaphoid and lunate motion during a wrist dart throw motion. *J Hand Surg Am.* 2004; 29(3), 418-422.

20. Waters MS, Wener FW, Haddad SF, McGrattan ML, Short WH. Biomechanical Evaluation of Schaphois and Lunate Kinematics FOllowing Selective Sectioning of Protions of the Scapholunate Interosseous Ligament. *J Hand Surg Am.* 2006; 41(2), 208-213.

21. Ramsay JW, Hunter BV, Gonzalez RV. Muscle moment arm and normalized moment contributions as reference data for musculoskeletal elbow and wrist joint models. *J Biomech.* 2009; 42(4), 463-473.
22. Gonzalez RV, Buchanan TS, Delp SL. How muscle architecture and moment arms affect wrist flexion-extension moments. *J Biomech.* 1997; 30(7), 705-712.
23. Loren GJ, Shoemaker SD, Burkholder TJ, Jacobson MD, Friden J, Lieber RL. Human wrist motors: biomechanical design and application to tendon transfers. *J Biomech*. 1996; 29(3), 331-342.
24. Hooke AW, Pettersson K, Sagerfors M, An KN, Rizzo M. *J Wrist Surg*. 2015; 4(2), 121-127.
25. Hermann AM, Delp SL. Moment arm and force-generating capacity of the extensor carpi ulnaris after transfer to the extensor carpi radialis brevis. *J Surg Am*. 1999; 24(%), 1083-1890.
26. Erhart S, Schmoelz W, Arora R, Lutz M. The biomechanical effects of a deepened articular cavity during dynamic motion of the wrist joint. *Clin Biomech.* 2012; 27(6), 557-561.
27. Rettig AC. Athletic injuries of the wrist and hand: part II: overuse injuries of the wrist and traumatic injuries to the hand. *Am J Sports Med.* 2004; 32(1), 262-273.
28. Armstrong TJ, Radwin RG, Hansen DJ, Kennedy KW. Repetitive trauma disorders: Job evaluation and design. *Human Factors*. 1986; 28, 325-336.

29. Palmer AK, Glisson RR, Werner FW. Ulnar variance determination. *J Hand Surg Am.* 1982; 7(4), 376-376.
30. Werner FW, Palmer AK, Somerset JH, et al. Wrist joint motion simulator. *J Orthop Res*. 1996;14(4):639-646.

31. Greenberg JA, Werner FW, Smith JM. Biomechanical Analysis of the Distal Metaphyseal Ulnar Shortening Osteotomy. *J Hand Surg Am.* 2013; 38(10), 1919-1924.
32. Werner FW, Short WH, Palmer AK, Sutton LG. Wrist tendon forces during various dynamic wrist motions. *J Hand Surg Am.* 2010; 35(4), 628-632.

Chapter 4

4 *Effect of Radial Length Changes on Axial Bone Loads through the Distal Radius and Ulna during Active Forearm Rotation*

Overview

A biomechanical study was conducted to examine the effect of radial lengthening and shortening on axial loads through the distal radius and ulna throughout forearm rotation. Radial lengths were simulated between -4mm of radial shortening and +3mm of radial lengthening and loads were collected continuously throughout forearm rotation. Axial loads through the distal radius and ulna were analyzed with respect to radial length and forearm rotation angle.

4.1 Introduction

As discussed in Chapter 1 (Section 1.3) common clinical wrist disorders often result deformities and malunions of the distal forearm bones. In most people the relative length of the radius and ulna at the wrist (often termed ulnar variance) are similar.[1] Differences in radial and ulnar lengths are common complications and presentations of distal radial fractures, Kienbock's disease and ulnar impaction syndrome.[1] Distal radius fractures often heal with residual radial shortening.[2,3] Kienbock's disease, avascular necrosis of the lunate bone, is often associated with a long radius relative to the ulna.[4,5] Ulnar impaction syndrome typically has a relatively long ulna with respect to the radius.[4,6,7] Forearm position has also been shown to cause changes in ulnar variance; the radius migrates proximally as the arm pronates.[8,9] It is important to understand the effect of changes in forearm bone length on distal radius and ulna loading in order to better diagnose and treat traumatic wrist injuries and degenerative diseases and to improve rehabilitation techniques and protocols.

Previous biomechanical studies have shown that changes in radial length effects load transmission through the distal radius and ulna under static loading scenarios, as previously discussed in Chapter 1 (Section 1.5).[1, 10, 13] These studies rigidly fixed the arms into position and applied static axial loads as radius lengths were altered. *Bu et al.* reported that as the radius was shortened with respect to the ulna the proportion of load through the radius decreased and that through the ulna increased.[10] *Palmer et al.* quantified the magnitude of loads through the distal ulna with changes in radial length and found they increase significantly with only 2mm of radial shortening.[12] Researchers have interpreted these studies to suggest that natural ulnar variance should therefore affect loads through the distal ulna and load sharing between the two forearm bones.[13,14] However, there has been very little correlation found between natural ulnar variance and the magnitude of load transmitted through the distal ulna.[15, 16]

While the effect of radius length on axial load transmission under constrained static loading has been reported, the effect during simulated dynamic motion remains poorly understood. Simulated active motion likely better represents the loading environment that the wrist will see during normal activities of daily living. The biomechanical implications

of static loading studies on radius length and load transmission through the distal radius and ulna have already been applied directly to clinical applications. For example, the treatment of Kienbock's disease with a radial shortening osteotomy or ulnar lengthening.[17, 18] Therefore, an additional examination of the effect of radius length on axial load transmission during dynamic simulated forearm motion is important to optimize existing biomechanical models and improve surgical recommendations.

Forearm pronation has been shown to increase loading through the distal ulna and proportion of total bone load that goes through the distal ulna. *Trumble et al*. and *af Ekenstam et al*. both reported increased loads through the distal ulna when the forearm was in pronation while under compressive static loading.[8, 9] The increase in load transmission though the ulna during forearm pronation is thought to be due to a change in the ulna's position with respect to the radius during forearm rotation. The ulna becomes longer relative to the radius in forearm pronation and shorter relative to the radius in forearm supination.[13, 20] Therefore it is important to examine the combined effect of forearm rotation and radial length change to determine any compounding effects.

In light of the above, the objective of the current study was to quantify the effect of forearm rotation angle, direction of motion and radial length changes on axial load transmission during simulated active forearm rotation. Axial loads through the distal radius and ulna were measured during active forearm rotation with the wrist in neutral position for varying radial lengths. Differences in loads through the radius and ulna were examined based on angle of forearm rotation, direction of motion and radial length changes between -4mm to +3mm in 1mm increments. It was hypothesized that increasing the radial length will increase radial loads and decrease ulnar loads and decreasing radial length will increase ulnar loads and decrease radial loads. It was also hypothesized that ulnar loads will increase as the forearm pronates and radial loads will increase in supination.

4.2 Materials and Methods[b]

4.2.1 *Specimen Preparation*

Six fresh frozen cadaveric upper extremities resected mid-humerus were used (73±8 years, 6 males, 6 right arms). Computed tomography scans and specimen medical history were examined to exclude any specimen with previous wrist injuries and/or degenerative diseases such as osteoarthritis. Specimens were thawed for 18 hours before testing. The experimental devices were then implanted in the distal radius and ulna, as previously described in Chapters 2 and 3. A volar osteotomy was performed on the distal radius. The radial implant was fixed in place by a distal plate and a proximal intramedullary stem held in place by bone cement. A similar procedure was performed on the medial aspect of the distal ulna and the implant was fixed with bone cement utilizing intramedullary stems both distally and proximally. Implants were placed as distal was possible without distal radioulnar joint disruption to measure loads through the distal radius and ulna. Bone bridges were left intact to maintain anatomic alignment of the forearm bones during implantation. Tendons of the wrist and forearm were sutured distal to the musculotendinous junction using 45kg strength nylon line: flexor carpi radialis (FCR), flexor carpi ulnaris (FCU), extensor carpi ulnaris (ECU), extensor carpi radialis brevis (ECRB), extensor carpi radialis longus (ECRL), biceps brachii, and pronator teres (PT) (Ethicon, Somerville, NJ). Tendon guides were fixed to the medial and lateral epicondyles of the humerus and tendon sutures were passed through them to maintain the physiologic lines of action of each muscle.

After the experimental devices were surgically implanted and the tendons lines were sutured, the specimens were mounted on the active wrist motion simulator (Chapter 2, Figure 2.14). The upper extremities were fixed to the simulator with a humeral clamp and two ulnar pins secured the elbow in 90° of flexion. The suture lines from the seven wrist and forearm prime movers were attached to servomotors at the base of the simulator

[b] The methodology related to specimen preparation and some aspects of testing protocol are similar to those employed in Chapters 2 and 3. As this thesis is in manuscript format, the methods have been re-written and included herein.

(SM2316D-PLS2, Arumatics Corp, CA). Optical trackers were attached to the proximal radius, proximal ulna and 3rd metacarpal to measure wrist joint angle throughout testing (Optotrak Certus; Northern Digital, Waterloo, ON, Canada). Optical trackers were also attached to the distal radius in semicircle configuration to measure and record forearm position throughout forearm rotation. The fingers were flexed and secured with Coban wrap (3M, Elyria, OH, USA) to maintain a clear line of sight between the trackers and the camera.

4.2.2 *Testing Protocol*

Test day joint coordinate systems were generated for the radius, ulna and 3rd metacarpal using anatomic skin markers per International Society of Biomechanics guidelines.[19] Forearm rotation angle was calculated as the rotation of the radius around the fixed ulna. Tone loads of 8.9N were applied to all forearm tendons, including: FCR, FCU, ECU, ECRB, ECRL, bicep brachii, and PT. Biceps brachii loads generated forearm supination and PT loads generated forearm pronation. Applied loads of the wrist flexor and extensor tendons were controlled by wrist joint angle and acted to maintain the wrist in neutral position throughout forearm rotation. This led to variable tendon loading dependent on radial lengths and forearm rotation. The upper extremities performed two cyclic motions of pronation-supination at a rate of 5° per second. The first cyclic motion was disregarded and the second was analyzed. Specimens were put through a range of motion from -35°of supination to 35° of pronation. Tendons of wrist flexors and extensors acted to keep the wrist in neutral position (i.e. 0° of wrist flexion and 0° of wrist deviation). Individual motions were defined as a full range of motion in one direction, i.e. pronation was from -35° to 35° of forearm rotation and supination was 35° to -35° of forearm rotation. Forearm rotation was completed for each incremental radial length change from -4mm to +3mm; +4mm was not possible due to soft tissue constraints.

4.2.3 *Outcome Variables and Data Analysis*

Load magnitudes were collected continuously from the implanted load cells throughout forearm rotation Forearm bone load proportions were calculated from the direct load measurements. Test day coordinate systems were joint angles were used to determine the joint position throughout forearm rotation. Loads were then discretized in 5° increments of joint motion for data analysis and statistical purposes.

4.2.4 *Statistical Methods*

A three-way repeated measures analysis of variance (ANOVA) was completed in SPSS 17.0 (SPSS Inc., Chicago IL, USA). The independent variables were forearm rotation angle direction of motion and radial length, and. The dependent variable was axial bone load. Analysis was completed for pronation-supination motion from -30° of supination to 30° of pronation in 5° increments. Additional pairwise comparisons were completed to examine the differences between individual joint angles and radial lengths. Statistical significance was considered $p<0.05$.

4.3 **Results**

4.3.1 ***Radius and Ulna Loading during Pronation-Supination Motion***

The direction of forearm rotation had no significant effect on load transmission through the distal ulna ($p=0.949$); load transmission through the distal radius was greater in supination ($p=0.048$) (Figure 4.1). Axial loads through the distal radius were significantly greater in supination (from -35° to 0°) than in pronation (0° to 35°) ($p=0.022$).

The magnitude of load transmitted through the distal radius ($p=0.132$) and ulna ($p=0.359$) were similar throughout forearm rotation (Figure 4.1). The loads through the distal radius remained significantly higher than those through the distal ulna throughout rotation ($p<0.001$).

The direction of rotation significantly altered load sharing between the distal radius and ulna ($p=0.048$) (Figure 2). The proportion of total forearm bone load through the radius was greater in forearm supination than in pronation. Load sharing between the distal radius and ulna remained consistent throughout forearm rotation ($p=0.351$)). The proportion of load through the distal radius was significantly higher than that through the distal ulna during forearm rotation ($p=0.002$).

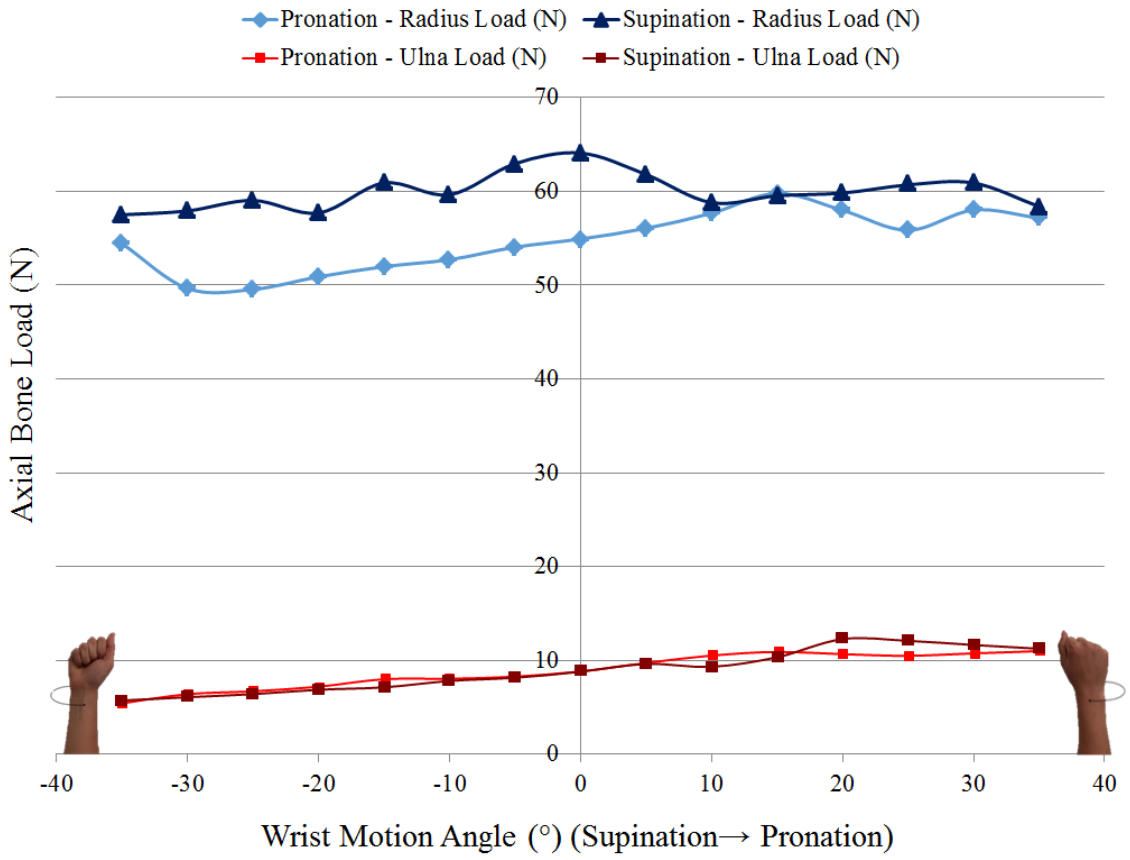

Figure 4.1: Axial Bone Loads through the Distal Radius and Ulna during Active Forearm Pronation and Supination. *The graph illustrates the axial loads through the distal radius and distal ulna from -35°of supination to 35° of pronation. Loads through the distal radius (p=0.132) and ulna (p=0.359) did not change significantly with forearm rotationLoads through the radius were significantly greater than those through the ulna throughout forearm rotation (p<0.001). Loads through the radius are significantly greater in supination than pronation from - 35° to 5° (p<0.022). Standard deviations have been omitted for clarity (During pronation: radius range: ±8.8N to ±21.9N; ulna range: ±7.7N to ±16.5N. During supination: radius range: ±7.7N to ±22.6N; ulna range: ±8.9N to ±14.4N).*

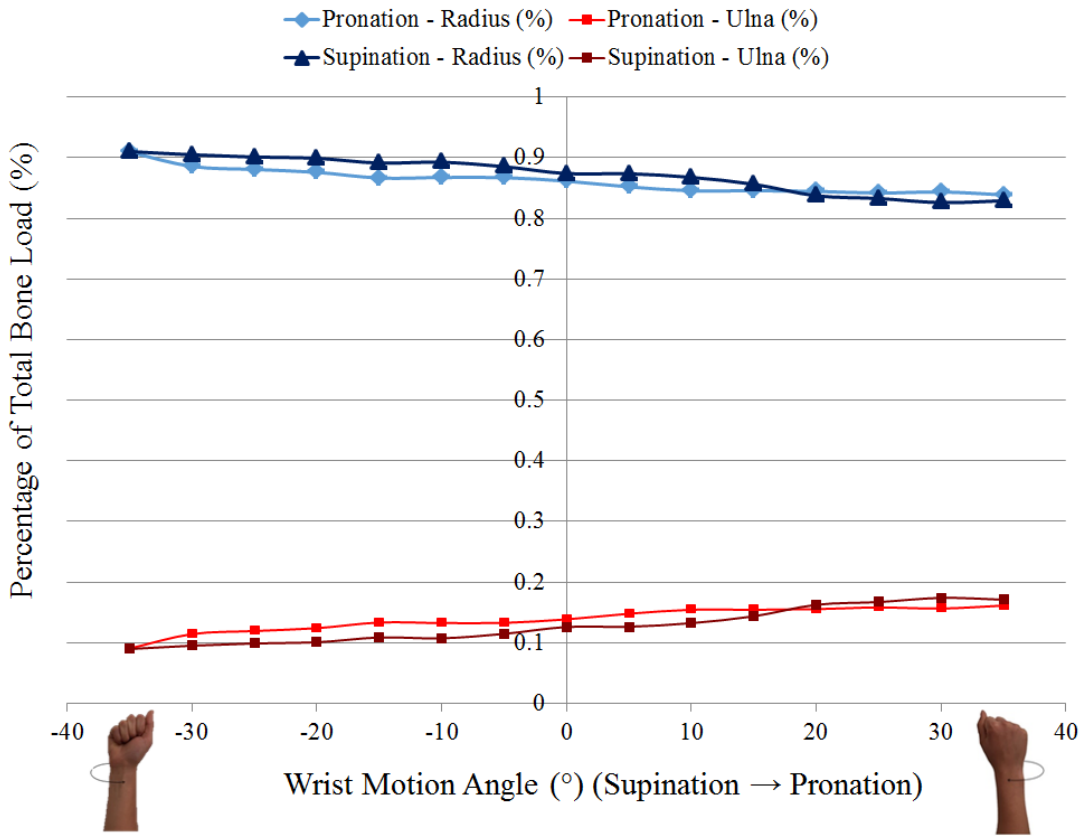

Figure 4.2: Proportion of Total Forearm Bone Load through the Distal Radius and Ulna during Active Forearm Rotation. *The graph illustrates the proportion of total forearm bone load through the distal radius and distal ulna from -35°of supination to 35° of pronation. The proportion of total forearm bone load through the radius is significantly greater in supination than in pronation. The proportion of total forearm bone load through the radius was significantly greater than that through the ulna throughout forearm rotation ($p<0.001$). Loads sharing did not change significantly throughout forearm pronation ($p=0.820$). Standard deviations have been omitted for clarity (radius range: $\pm$7.9% to $\pm$43.5%; ulna range: $\pm$7.9% to $\pm$43.5%).*

4.3.2 *Effect of Radial Length Change on Axial Load Transmission through the Distal Radius Loading during Active Forearm Pronation*

The general trends for radial length changes were the same in pronation and supination, therefore the effect of radial length change will be presented for forearm pronation only. Changes in radial length had a significant effect on axial load transmission through the distal radius ($p<0.001$) (Figure 4.3). Loads through the distal radius remained constant throughout forearm rotation angle when length changes were present ($p=0.360$) (Figure 4.4). As radial lengths increased incrementally, loads through the radius increased in a quasi-linear fashion. Radial loads were lowest with -4mm of radial shortening and the highest with +3mm of radial lengthening. Axial load transmission through the radius did not change significantly with forearm rotation at any radial length from -4mm of shortening to +3mm of lengthening ($p>0.05$)(Figure 4.3 and 4.4).Loads at -4mm of radial shortening were significantly lower than those at +1 ($p=0.031$), and +3mm ($p=0.006$) of radial lengthening, independent of forearm rotation at -35° of supination Loads through the radius were significantly less with -4mm of shortening than +1mm of lengthening ($p=0.024$) at neutral forearm rotation and +3mm of lengthening at 35° of forearm rotation. Axial loads through the distal radius with +3mm of radial lengthening were significantly greater than those through the distal radius with: -4mm ($p=0.006$) of radial shortening at -35° of supination, -2mm ($p=0.033$) and -3mm ($p=0.039$) of radial shortening at 0° of forearm rotation, and -1mm, ($p=0.050$) -3mm ($p=0.023$), and -4mm ($p=0.048$) of radial shortening at 35° of pronation.

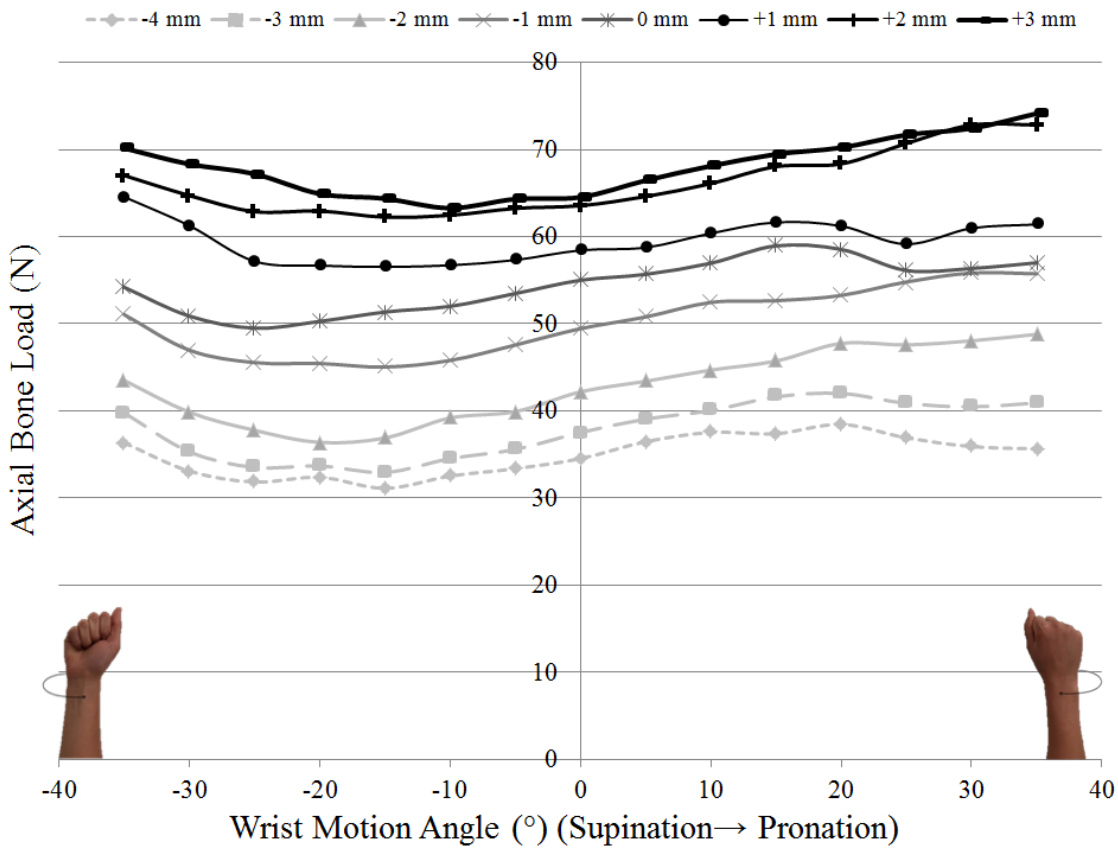

Figure 4.3: Axial Bone Loads through the Distal Radius at Varying Radial Lengths throughout Active Forearm Pronation. *The graph illustrates the axial loads through the distal radius at eight different increments of radial length from -35°of supination to 35° of pronation. Radial loads did not change throughout with forearm rotation (p=0.132). Radial length had a significant effect on the magnitude of load transmission through the distal radius (p<0.001). Standard deviation bars have been omitted for clarity (-4mm range: ±12.2 to ±18.1N; -3mm range: ±9.7N to ±13.2N; -2mm range: ±8.4N to ±12.9N; -1mm range: ±7.8 to ±13.5N; 0mm range: ±0.4N to ±18.5N; +1mm range: ±7.3N to ±19.0N; +2mm range: ±12.1N to ±17.8N; +3mm range: ±10.3N to ±20.7N).*

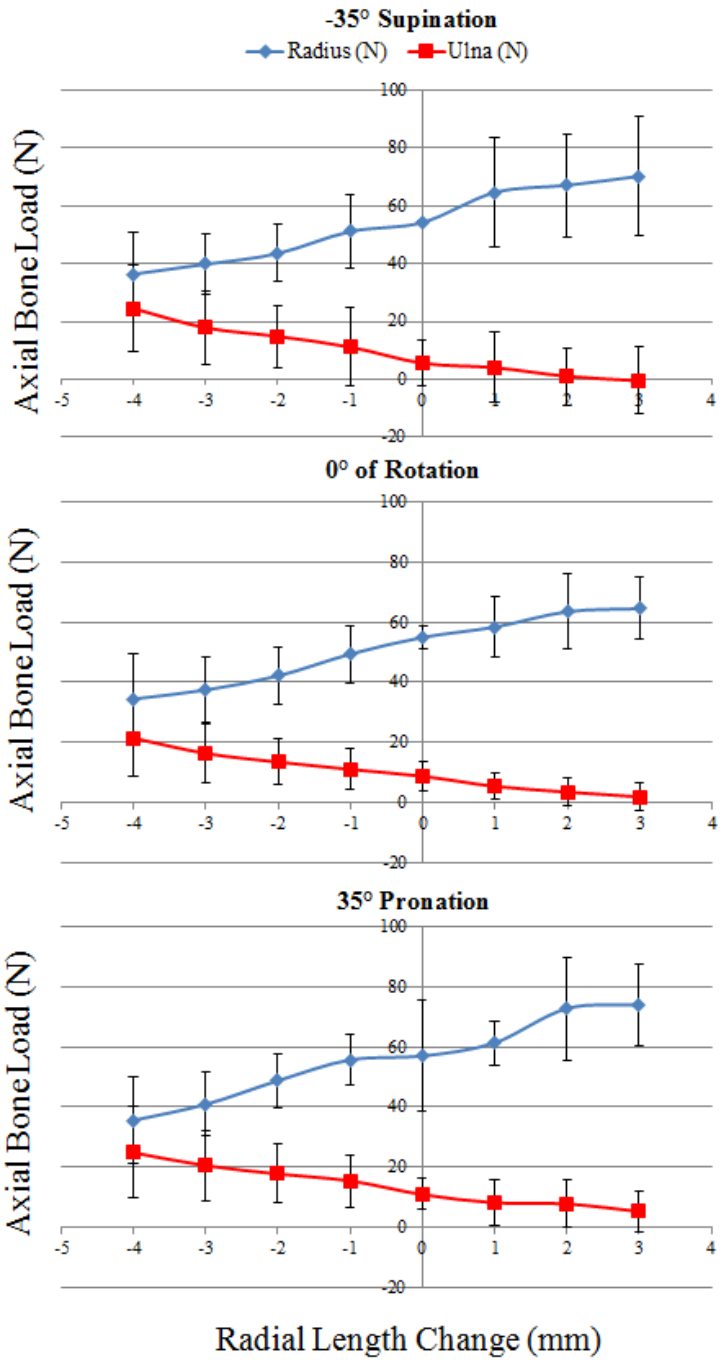

Figure 4.4: Axial Bone Loads through the Distal Radius and Ulna with 8mm of Radial Length at -35° of supination, 0° of forearm rotation and 35° of pronation. *The graph illustrates the axial loads through the distal radius and distal ulna at discrete angles of pronation-supination motion. The x-axis is the length of the radius and the y-axis is the load through the distal radius and ulna in Newtons. Figure 4.4 has been included to show a comparison of distal forearm load magnitudes and provide graphical depiction of ± one standard deviation. Radial length change had a significant effect on distal radial ($p<0.001$) and ulnar ($p=0.002$) loads, however forearm rotation angle did not ($p=0.360$, $p=0.142$)*

4.3.3 *Effect of Radial Length Change on Axial Load Transmission through the Distal Ulna during Active Forearm Pronation*

The direction of forearm rotation did not significantly affect the magnitudes of load through the ulna; therefore data for pronation will be presented herein (p=0.949). Radial bone length had a significant effect on load transmission through the distal ulna (p=0.002). Loads through the distal ulna did not change significantly with respect to forearm rotation angle (p=0.142) (Figure 4.5). As radial lengths increased incrementally load transmission through the distal ulna decreased in a quasi-linear fashion (Figure 4.4). Axial loads through the ulna peaked with -4mm of radial shortening and reached a minimum with +3mm of radial lengthening. At -3mm of radial shortening the effect of radial length change was dependent on forearm rotation. In -35° supination, axial loads through the distal ulna were significantly greater at -3mm of radial shortening than +2mm (p=0. 35) and +3mm (p=0.025) of radial lengthening. In neutral forearm rotation and 35° of forearm pronation, radial shortening had no significant effect on load transmission through the distal ulna. Axial loads through the distal ulna at +3mm of radial lengthening were significantly lower than those at -2mm (p=0.022,) and -3mm (p=0.035) at -35° of supination and at -1mm (p=0.030) and -2mm (p=0.028) at neutral forearm rotation. Radial lengthening had no effect distal ulnar loading at 35° of forearm pronation.

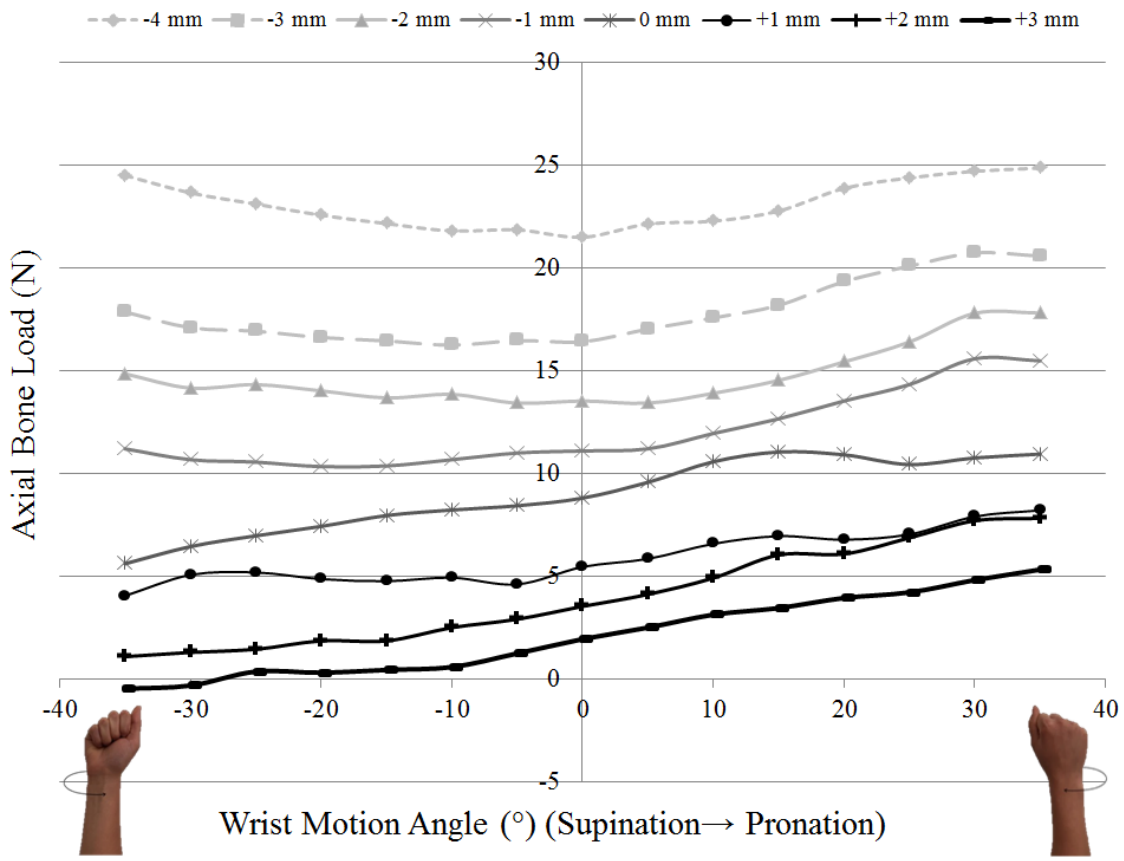

Figure 4.5: Axial Bone Loads through the Distal Ulna at Varying Radial Lengths throughout Active Forearm Pronation. *The graph illustrates the axial loads through the distal ulna at eight different increments of radial length change from -35°of supination to 35° of pronation. Radial length had a significant effect on magnitudes of load transmission at the distal ulna ($p<0.001$). At neutral forearm rotation, loads through the ulna were significantly lower with +3mm of lengthening than with -1mm ($p=0.049$), -2mm ($p=0.027$), -3mm ($p=0.027$) and -4mm of radial shortening. Standard deviations have been omitted for clarity (-4mm range: $\pm$9.5 to $\pm$18.5N; -3mm range: $\pm$7.5N to $\pm$17.0N; -2mm range: $\pm$7.3N to $\pm$12.3N; -1mm range: $\pm$5.5N to $\pm$12.4N; 0mm range: $\pm$7.9N to $\pm$14.9N; +1mm range: $\pm$4.8N to $\pm$11.0N; +2mm range: $\pm$3.9N to $\pm$9.8N; +3mm range: $\pm$3.8N to $\pm$10.0N).*

4.3.4 *Effect of Radial Length Change on Load Sharing between the Distal Radius and Ulna during Active Forearm Pronation-Supination Motion*

The direction of pronation-supination motion a significantly effected distal forearm load sharing, however the general trend remained the same and therefore only load sharing in pronation will be presented herein ($p=0.048$). Radial length change had a significant effect on load sharing between the distal radius and ulna ($p<0.001$) (Figure 4.6). The proportion of total forearm bone load through the distal radius was the least with -4mm of radial shortening and the greatest with +3mm of radial lengthening. The proportion of total forearm bone load decreased through the radius and increased through the ulna as the arm moved from supination to pronation, however this trend was not significant ($p=0.155$). Radial shortening had no effect on load sharing at any angle of forearm rotation. The proportion of load through the radius was significantly greater with +3mm of lengthening than with -2mm ($p=0.001$), radial shortening, at only neutral forearm rotation.

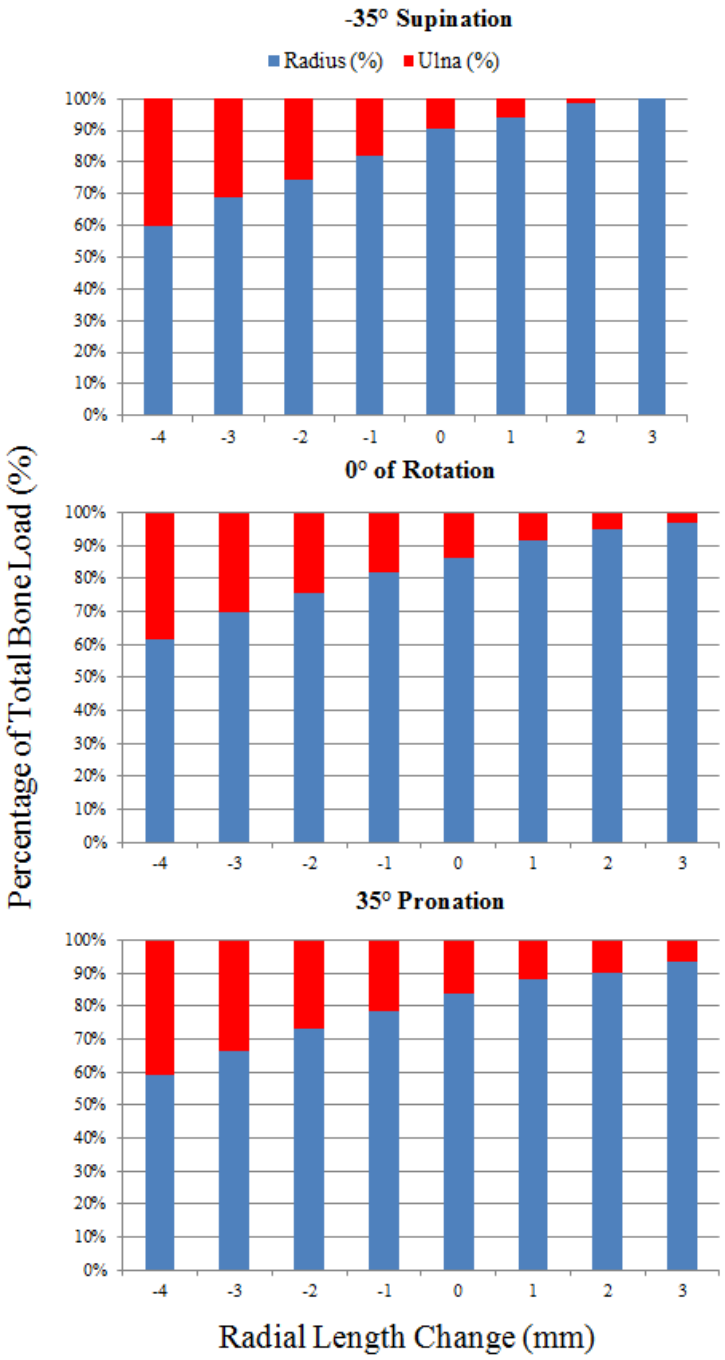

Figure 4.6: Proportion of Total Forearm Bone Load through the Distal Radius and Ulna at Varying Radial Lengths throughout Active Forearm Pronation. *The graph illustrates the proportion of total forearm bone load through the distal radius and distal ulna at eight different radial lengths throughout active forearm pronation from -35°of supination to 35° of pronation. Radial length had a significant effect of load sharing at the distal forearm ($p<0.001$). (-4mm range: $\pm$13.5% to $\pm$22.5%; -3mm range: $\pm$9.7% to $\pm$14.1%; -2mm range: $\pm$9.3% to $\pm$17.3%; -1mm range: $\pm$5.9% to $\pm$22.4%; 0mm range: $\pm$7.9 to $\pm$43.5N; +1mm range: $\pm$5.0% to $\pm$27.0%; +2mm range: $\pm$5.0% to $\pm$22.7%; +3mm range: $\pm$4.4% to $\pm$32.6%).*

4.4 Discussion

The effect of radial length changes on load transmission through the distal radius and ulna has been previously investigated for constrained static loading. Static joint loading is a valuable form of biomechanical testing; however it is not a fully indicative of *in vivo* loads through the distal forearm during daily living. There is a void of literature on the effect of radial length changes on *in vivo* and *in vitro* loads through the distal forearm. As noted earlier, radial length changes frequently occur due to traumatic injuries and degenerative diseases such as distal radial fractures, Kienbock's disease and ulnar impaction (Chapter 1, Section 1.3). The malalignment of the distal radioulnar joint may cause altered joint loading and further wrist pain.[4-7] An improved understanding of the altered wrist biomechanics caused by radial length changes will improve the diagnosis and treatment of the disorders from which they resulted. This current study examined the effect of direction of motion, forearm rotation angle and radial length change on distal forearm loading under active forearm rotation. *In vitro* loads were collected at the distal radius and ulna continuously throughout forearm rotation.

At native radial length, the magnitude of load through the distal radius ($p=0.132$) and ulna ($p=0.359$) remained similar throughout forearm rotation. *Trumble et al.* and *af Ekenstam et al.* reported increased loads through the ulna with forearm pronation and have attributed this phenomenon to the change in ulnar position as the forearm rotates.[8,9,13,20] The lack of a significant change in forearm rotation on ulnar loads in the population tested is likely due a small sample size, variability in loads between specimens and the limited rotation achieved.

There were no significant changes in forearm bone load sharing throughout rotation ($p=0.351$). In forearm supination the radius bore 91.0% the axial bone load and as the forearm pronated the ulna contributed more to forearm bone load and the proportion of bone load sharing through the radius decreased to 83.9% in end pronation. These small differences may be due to the previously described phenomenon of ulnar lengthening in forearm pronation.[13, 20]

Not surprisingly, the magnitude of load through the distal radius changed with changes in radial length throughout forearm rotation. Axial loads through the radius were the highest with +3mm of radial lengthening and were the lowest with -4mm of radial shortening. As radial length increased from -4mm to +3mm load magnitudes through the distal radius increased at an average of 5.2 N/mm throughout active forearm rotation. The greatest change in axial loads between radial lengths occurred between -2mm and -1mm of radial shortening (+17.4% at -35°, +17.2% at 0°, +14.2% at 35°) and the smallest between +2mm and +3mm of radial lengthening (+4.7% at -35°, +1.5% at 0°, 1.8% at 35°). Our results agree with those of *Markolf et al.* who reported significant changes in axial bone loads with as little as -2mm of radial shortening.[21] Our results are also consistent with those of *Bu et al.,* who reported an increase in the proportion of distal radial load with relative radial lengthening.[10] Load changes in the distal forearm caused by radial shortening have been linked to unfavorable clinical outcomes such as increased lunate contact, ulnar impingement, DRUJ pain and ulnar sided wrist pain.[11, 22, 23]

Equal magnitudes of radial shortening and lengthening did not produce the same magnitude of load change through the distal radius. At neutral forearm rotation, -3mm of radial shortening decreased radial loads by 59.3%, while +3mm of radial lengthening only increased loads by 17.3%. These results suggest that radial shortening has more of an effect on distal radius loading and should therefore be considered with caution. Forearm rotation angle had no effect at 0mm of radial length change. As the radius was lengthened or shortened more than 2mm, the effect of forearm rotation angle on loads transmitted through the radius was more prominent. This is thought to have occurred in part due to the tendon loads applied to the wrist flexors and extensors to maintain the wrist in neutral position. Radial shortening caused an increase in the force required by the FCU and ECU to maintain neutral wrist position. Radial lengthening caused a lesser increase in FCR and ECRL loads than the increase in tendon loads induced by radial shortening.

Axial load transmission through the distal ulna changed significantly with changes in radial length throughout active forearm rotation. Loads through the distal ulna were the highest with -4mm of radial shortening and were the lowest with +3mm of radial

lengthening. As the radial length increased from -4mm to +3mm the loads through the radius decreased an average of 3.0 N/mm throughout forearm rotation. *Shepard et al.* completed a similar study with static loading and concluded that each mm of radial lengthening increased ulnar loads by ~9%/mm.[24] The current study found changes in ulnar loads to be closer to 28%/mm increase with respect to radial length change The largest decrease in axial loads through ulna occurred between +2mm and +3mm of radial lengthening (-141.5% at -35°, -45.0% at 0°, -31.9% at 35°) and the smallest change occurred between -3mm and -2mm of radial shortening (-16.8% at -35°, -17.9% at 0°, -13.1% at 35°). These results suggest that radial lengthening has a greater effect on loads through the distal ulna than radial shortening. *Pouge et al.* reported that 6mm of radial shortening causes ulnar impingement.[11] *Markolf et al.* and *Palmer et al.* both stated that as little as 2mm of radial shortening causes a significant increase in loads through the distal ulna in neutral wrist position and static loading.[12,21] As the radius was shortened the FCU and ECU loads increased to keep maintain neutral wrist position during active forearm rotation. The change in tendon loading may account for the increase in axial loads through the ulna which occur with radial shortening.

In general, bone loads through the distal radius and ulna appeared to have a quasi-linear relationship with changes in radial length (Figure 4.2). This is interesting from a biomechanical perspective as it allows for better estimates of the changes induced by disorders that causes changes in radial length such as wrist fractures and Kienbock's disease as well as improves the understanding of native forearm mechanics.

Load sharing between the radius and ulna were included to improve the comparison to current literature and to account for the possible effects of simulator differences. The proportion of load through the radius increased with radial lengthening and decreased with radial shortening. With -4mm of radial length change the load sharing ratio was 62%/38% between the distal radius and ulna at neutral forearm rotation in the current study. *Shepard et al.* reported a 50%/50% ratio with -5mm of radial shortening and neutral forearm position.[24] *Markolf et al.* reported similar findings, reporting equal load sharing between the radius and ulna with -4mm of radial shortening.[25] The current study suggests that radial shortening may have a lesser effect under dynamic tendon loads that

it does under static compressive loads. The active loading employed in the current study more closely mimics *in vivo* joint loading than axial static loading. Therefore, it can be postulated that radial shortening has a lesser an effect on distal forearm loading sharing than previously thought from early static loading studies. With +3mm of radial lengthening, the radius accepted 97% of total compressive forearm bone load in neutral forearm rotation and 100% of forearm bone load in supination. *Bu et al.* reported 92-96% of load transmission through the radius with +3mm of radial lengthening at neutral wrist and forearm position.[10] *Markolf et al*. stated that with +4mm of radial lengthening the radius accepted 94% and 97% of total forearm bone load in varus and valgus elbow position respectively.[26] Again, our results suggest that dynamic loading produces a slightly higher proportion of radial loading than that during static loading (Chapter 3, Section 3.3).

The study presented in this chapter has limitations, as previously noted in Chapter 3. Forearm bone loads were collected strictly along the long axis of the bones. *In vivo* loading occurs in all dimensions rather than uniaxially as measured in this study. The loading presented in this study is therefore more indicative of radiocarpal joint loads than it is of distal radioulnar joint loads. Forearm motion was performed actively through applied tendon loads. These loads were an estimation of *in vivo* tendon loads during simple, unloaded forearm motion. Additionally, the pronator quadratus was not activated to assist with forearm pronation. *Gordon et al.* have shown that the pronator quadratus plays an important role in distal radioulnar joint loading and should therefore be considered in biomechanical modeling of the wrist and forearm.[27] However, the pronator quadratus acts perpendicular to the loads measured and in the current study and therefore would probably have very influence on the results presented. The cadaveric specimens were mounted on the simulator in a vertical position. Loading will likely differ with the arm in horizontal and dependent positions due to the effects of gravity. The range of forearm rotation achieved with the simulator was 70°, only a small portion of the motion available in patients' 120-165°.[30] The specimens used in this study were older and therefore had stiffer joints commonly associated with decreased joint ranges of motion. The specimens were also quite obese. This caused impingement of the optical trackers, which in turn decreased the range of forearm rotation we could study.

This study has several strengths. First, the effect of the direction of forearm rotation was examined and axial loads through the distal radius and ulna were reported separately. Loads through the distal radius and ulna were collected continuously throughout active simulated forearm rotation and the magnitudes of loads and load sharing were reported. The experimental devices used to collect distal radius and ulna loads were designed and evaluated to ensure measurements were reliable and device function was repeatable. Previous studies employing load measuring devices have suffered from large amounts of soft tissue resection and devices to change bone length often lacked structural rigidity such as the use of external fixators. The devices used were discrete and to allow for exceptional soft tissue retention with all soft tissues, excluding a portion of the distal interosseous membrane, left intact. Load measuring devices were implanted at the anatomic location of interest avoiding the need for mathematical transformations to determine bone loading. All incisions were closed for the duration of the testing day to retain soft tissues hydration and maintain their viscoelastic behavior. Lastly, the study of radial length change during active forearm rotation has not been previously examined making this study a novel contribution to existing biomechanical literature.

4.5 Conclusions

The current study revokes the hypothesis that ulnar loads increase with forearm pronation. The current study supports the hypothesis that radial length changes will affect loads through the distal radius and ulna. Load transmission through the distal radius decreased with radius shortening and increased with radial lengthening. The inverse was true for loads through the distal ulna. Loads through the distal ulna increased with radial shortening and increased with radial lengthening. The direction of motion proved to significantly increase the magnitude of load transmission through the radius and forearm bone load sharing. The magnitude of load transmission through the radius and the proportion of total forearm bone load through the radius were greater in supination than in pronation. Direction of motion had no effect on load transmission through the ulna. To our knowledge this is the first study examining the effect of radial length changes on distal radius and ulna loading during active simulated forearm rotation. This study provides new insights to the effect of radial length change on distal forearm loading during active forearm rotation and has implications for improved diagnosis and treatment of common wrist injuries and conditions.

4.6 References

1. Adams BD. Effects of radial deformity on distal radioulnar joint mechanics. *J Hand Surg Am.* 1993; 18(3), 492-498.

2. Amadio PC, Botte MJ. Treatment of malunion of the distal radius. *Hand Clin*. 1987;3(4):541-561.
3. Bushnell BD, Bynum DK. Malunion of the distal radius. *J Am Acad Orthop Surg*. 2007;15(1):27-40.

4. Cooney WP. *The Wrist: Diagnosis and Operative Treatment*. Vol 8. 2nd ed. (Kluwer W, ed.). Philadelphia, Balitmore, New York, Lodon, Buenos Aires, Hong Kong, Sydney, Tokyo; 2011.

5. Beckenbaugh RD, Shives TC, Dobyns JH, Linscheid RL. Kienbock's disease: the natural history of Kienbock's disease and consideration of lunate fractures. *Clin Orthop Relat Res.* 1980; 149, 98-106.

6. Friedman AL, Palmer AK. The ulnar impaction syndrome. *Hand Clin.* 1991; 7(2), 295-310.

7. Cerezal L, Pinal F, Abascal F, Garcia-Valtuille R, Pereda T, Canga A. Imaging findings in ulnar-sided wrist impaction syndromes. *Radiographics.* 2002; 22(1), 105-121.

8. Trumble T, Glisson RR, Seaber AV, Urbaniak JR. Forearm force transmisison after surgical treatment of distal radioulnar joint disorders. *J Hand Surg Am.* 1987; 12(2), 196-202.

9. Ekenstam FW, Palmer AK, Glisson RR. The load on the radius and ulna in different positions of the wrist and forearm. A cadaver study. *Acta Orthop Scand.* 1984; 55(3), 363-365.

10. Bu J, Patterson RM, Morris R, Yang J, Viegas SF. The Effect of Radial Shortening on Wrist Joint Mechanics in Cadaver Specimens With Inherent Differences in Ulnar Variance. *J Hand Surg Am*. 2006;31(10):1594-1600.

11. Pogue DJ, Viegas SF, Patterson RM, et al. Effects of distal radius fracture malunion on wrist joint mechanics. *J Hand Surg [Am]*. 1990;15(5):721-727.

12. Palmer AK, Werner FW. Biomechanics of the distal radioulnar joint. *Clinical Orthop.* 1984; (187), 26-35.

13. Palmer AK, Glisson RR, Werner FW. Ulnar variance determination. *J Hand Surg Am.* 1982; 7(4), 376-376.

14. Markolf KL, Dunbar AM, Hannani K. Mechanisms of load transfer in the cadaver forearm: role of the interosseous membrane. *J Hand Surg Am.* 2000; 25(4), 647-682.

15. Harley B, Pereria M, Werner F, Kinney D, Sutton L. Force Variations in the Distal Radius and Ulna: Effect of Ulnar Variance and Forearm Motion. *J Hand Surg Am.* 2015; 40(2), 211-216.

16. Greenberg JA, Werner FW, Smith JM. Biomechanical analysis of distal metaphyseal ulnar shortening osteotomy. *J Hand Surg Am.* 2013; 38(1), 1914-1919.

17. Fernandez DL. Radial osteotomy and Bowers arthroplasty for malunited fractures of the distal end of the radius. *J Bone Joitn Surg Am.* 1988; 70(10), 1538-1551.

18. Jupiter JB, Ring D. A comparison of early and late reconstruction of malunited fractures of the distal end of the radius. *J Bone Joint Surg Am.* 1996; 78(5), 739-748.

19. Wu G, van der Helm FCT, Veeger HEJD, et al. ISB recommendation on definitions of joint coordinate systems of various joints for the reporting of human

joint motion--Part II: shoulder, elbow, wrist and hand. *J Biomech*. 2005; 38(5):981-992.

20. Epner RA, Bowers WH, Guilford WB. Ulnar variance – the efffect of wrist positiononing and roentgen filming technique. . *J Hand Surg Am.* 1982; 7(3), 298-305.

21. Markolf KL, Lamey D, Yang S, Meals R, Hotchkiss R. Radioulnar load-sharing in the forearm. A study in cadavera. *J Bone Joint Surg Am.* 1998; 80(6), 879-888.

22. Fernandez DL. Correction of post-traumatic wrist deformity in sdults by osteotomy, bone-grafting and internal fixation. *J Bone Joint Surg Am.* 1982; 64(8), 1164-1178.

23. Jenkins NH, Mintowt-Czyz WJ. Mal-union and dysfunction in Colles' fracture. *J Hand Surg Br.* 1988;13(3):291-293.

24. Shepard MF, Markolf KL, Dunbar AM. The effect of partial and total interosseous membrane transection on load sharing in the cadaver forearm. *J Orthop Res.* 2001; 19(4):587-592.

25. Markolf KL, Tejwani SG, Benhaim P. Effects of wafter resection and hemirection from the distal ulnar on load-sharing at the wrist: a cadaveric study. *J Hand Surg Am.* 2005; 30(2), 351-358.

26. Markolf KL, Tejwani SG, O'Neil G, Benhaim P. Load-sharing at the wrist following radial head replacement with a metal implant. A cadaveric study. *J Bone Joint Surg Am.* 2004; 86-A(5):1023-1030.

27. Gordon KD, Kedgley AE, Ferreira LM, King GK, Johnson JA. Effect of simulated muscle activity on distal radioulnar joint loading in vitro. *J Orthop Res.* 2006; 24(7):1395-1404.

Chapter 5

5 *General Discussion and Conclusions*

Overview

This chapter summarizes the objectives and hypotheses outlined in Chapter 1, along with the major conclusions of the biomechanical studies presented in Chapters 2, 3, and 4. The testing methodologies, strengths and limitations of each study are reviewed. Current and future directions of the work presented in this thesis are then discussed.

5.1 Summary

This research was aimed to improve the understanding of native distal forearm bone loading during active simulated wrist and forearm motion and to examine the effect of radial length changes on distal radius and ulna load magnitude and sharing. This work advances literature on the effects of flexion-extension motion, radioulnar deviation and pronation-supination motion and the effect of radial length changes. Additionally, these findings provided new information on the effect of dart throwers motion on distal forearm bone loading, as well as new insights on the effect of radial lengths changes during active simulated forearm pronation-supination motion. The specific objectives stated at the beginning of this thesis have been fulfilled through the completion of the biomechanical studies presented in Chapters 2, 3, and 4.

The objectives of this thesis as given in Chapter 1, Section 1.8, were:

1. To design and evaluate an experimental apparatus for examining *in vitro* axial distal forearm bone loads during active wrist flexion-extension, radial-ulnar deviation and dart throw motion and forearm pronation-supination;
2. To determine the effect of joint position and motion direction on forearm bone loading throughout active wrist flexion-extension, radial-ulnar deviation, and dart throw motion;
3. To determine the effect of radial length change, joint position and direction of motion on distal forearm load magnitude and forearm bone load sharing during active forearm pronation-supination.

The hypotheses and results of the individual studies performed in Chapter 2, 3 and 4 are summarized in the following sections.

5.1.1 *Chapter 2: Design and Development of an Experimental Measurement System for Examining In Vitro Load Magnitudes and Sharing in the Distal Forearm*

The first objective of this thesis was to design and evaluate two experimental devices capable of measuring axial loads through the distal radius and ulna during active wrist and forearm motion. It was determined that these devices had to be capable of measuring loads through the distal radius and ulna with excellent reliability, ICC>0.95, to be considered reliable for use in further biomechanical studies. Two uniaxial loads were incorporated into the implant design to help achieve axial load measurement. The implants also allowed for simple incremental changes between common clinically occurring forearm bone lengths to simulate the effect of wrist fractures, Kienbock's disease and ulnar impaction. Both devices were implanted using spacers and the bone bridge technique, both of which were later removed and replaced with the load sensing components. They were surgically implanted with bone cement to allow for rigid fixation. One cadaveric specimen was mounted on a custom active motion simulator to evaluate these devices. Testing consisted of five cyclic flexion-extension motions (FEM), radioulnar deviations (RUD) and dart throw motions (DTM).

The repeatability of the combined implant and active motion simulation system was exceptional. The lowest intraclass correlation coefficient (ICC) reported for all three active wrist motions was 0.978. These results indicate very little variation in load cell measurements between the five cyclic trials. These findings represent the combined reliability of the applied tendon loads from the active motion simulator and the load cell measurements from the implants. Therefore, load measurements obtained from the experimental devices during future biomechanical studies can be considered reliable throughout different testing parameters. Additionally, the experimental devices allowed for reproducible changes in the lengths of the radius and ulna, thereby succeeding in simulating many common forearm injuries, diseases and/or malformities.

5.1.2 *Chapter 3: Loads in the Distal Radius and Ulna during Active Simulated Wrist Motion*

The second objective was to determine the effect of joint angle on forearm bone loading throughout active planar wrist flexion-extension (FEM), planar wrist radial-ulnar deviation (RUD), and multiplanar dart throw motion (DTM). It was hypothesized that axial loads would change with wrist and forearm motion with the greatest changes occurring in RUD. The experimental devices, evaluated in Chapter 2, were utilized for this biomechanical testing. The devices were implanted in the distal radius and ulna of nine cadaveric specimens using the bone bridge technique. Specimens were then mounted on the custom wrist motion simulator and tendon loads were applied to produce the aforementioned motions.

The results from this study supported the hypothesis that axial loads through the distal radius and ulna change based on wrist joint angle and forearm rotation angle. However, the greatest changes in load did not occur during RUD but instead during the combined extension-radial deviation and flexion-ulnar deviation positions simulated during DTM. Axial loads through the distal radius peaked in combined extension-radial deviation. Loading through the distal ulna peaked during wrist extension and ulnar deviation. This study provides new insight on distal forearm bone loading during the physiologic dart throw motion. The load magnitudes and distal forearm bone load sharing proportions produced by the dart throw motion resembled the loading patterns during ulnar deviation rather than those during wrist flexion. These finding imply that the tendons producing radioulnar deviation have a greater effect than those generating flexion-extension motion on magnitude of load transfer and load sharing through the distal forearm bones. This provides a more complete explanation of the axial loading that occurs in the healthy distal radius and ulna during active wrist motion. This work has implications for both optimizing rehabilitation protocols and improving surgical recommendations.

5.1.3 *Chapter 4: Effect of Radial Length Changes on Axial Bone Loads through the Distal Radius and Ulna during Active Forearm Rotation*

The third objective of this thesis was to determine the effect of radial length, forearm rotation angle and direction of motion on distal forearm loading during active simulated pronation-supination motion. It was hypothesized that ulnar loads would be increased in pronation and radial loads in supination. It was also hypothesized that radial lengthening will increase the load magnitudes and proportion of total forearm bone load transmitted through the distal radius and decrease that through the distal ulna and radial shortening will decrease radial loads and increase ulnar loads throughout forearm pronation. The experimental devices evaluated in Chapter 2 were employed to measure *in vitro* axial loads through the distal radius and ulna continuously throughout active forearm pronation for radial lengths from -4mm to +3mm in 1mm increments. The devices were implanted in the distal radius and ulna of eight cadaveric specimens again using the bone bridge technique and bone cement for rigid fixation. The wrist was maintained in neutral flexion-extension and radioulnar deviation while the forearm rotated from -35° of supination to 35° of pronation.

This biomechanical study supports the hypothesis that radial length change will affect loads through the distal radius and ulna during active forearm pronation. This study rejects the hypothesis that ulnar loads increase with pronation. Axial loads through the distal radius increased with radial lengthening and decreased with radial shortening, and loads through the distal ulna decreased with radial lengthening and increased with radial shortening. Radial shortening was proven to have a greater effect than radial lengthening on the magnitude of loads through both the distal radius and ulna in forearm supination. Radial lengthening had a greater effect on distal radius loads in forearm pronation. It is speculated the change in loads through the distal radius and ulna with respect to change in radial length may be due to the flexor-extensor tendon loads applied to maintain neutral wrist position throughout forearm pronation. To our knowledge this study is the first of its kind to examine the effect of radial length changes on distal forearm loading during active forearm rotation. This study provides novel information about distal forearm biomechanics and has implications to improve the diagnosis and treatment of

common traumatic wrist injuries and degenerative diseases that affect radial length such as distal radial fractures and Kienbock's disease.

5.2 Strengths and Limitations

The biomechanical studies presented in this thesis have many strengths. This work provides new insight to the axial distal forearm bone loads produced for a variety of motions that occur during the activities of daily living. The study presented in Chapter 4 provides a novel contribution to the literature on the effect of radial length changes on forearm bone loads during active forearm rotation. The sample sizes used were relatively small, however still large enough to allow for a repeated measure ANOVA for statistical analysis. Highly accurate optical tracking was utilized and allowed for the real-time measurement of joint angles throughout wrist and forearm motion. A previously established, repeatable active wrist motion simulator was used to perform all biomechanical testing. The experimental devices used to collect axial loads through the distal radius and ulna were evaluated to ensure their reliability for use in the additional biomechanical studies. These included uniaxial loads cells located along the anatomical axis of the radius and ulna, negating the requirement to accommodate eccentric loads. Both the magnitude of load and the proportion of total forearm bone load were reported separately, providing two distinct insights and contributions to biomechanical literature on distal forearm loading. Almost all soft tissues structures, excluding the distal interosseous membrane, were maintained in order to most accurately represent *in vivo* conditions. All incisions were closed throughout testing to maintain tissue hydration and retain the viscoelastic behaviours of *in vivo* soft tissues. Lastly, flexion-extension motion was simulated from 50° of wrist extension to 50° of flexion which is an increased range of motion previously reported for active wrist motion studies.

Like all *in vitro* cadaveric biomechanical studies, the studies presented in this thesis have limitations. Mechanical tendon loads were applied to generate wrist and forearm motion. The applied loads were an estimation of *in vivo* loads generated during simple movement scenarios and may not fully represent the complex *in vivo* soft tissue loading. The pronator quadratus was not loaded to assist with forearm pronation. Although this muscle assists in DRUJ stability throughout forearm rotation, activation proved difficult to integrate into the existing active motion simulator system. Distal forearm bone loads were collected strictly along the long axis of the radius and ulna. However, physiologic

loading at the wrist occurs globally in the wrist and forearm joints. Therefore, the loads reported in this study are most representative of radio- and ulnocarpal loading and further examination would be necessary to determine loading at other aspects of the wrist such as the distal radioulnar joint. The cadaveric upper extremities were mounted on the simulator in a vertical position which is uncommon during tasks of daily living. Forearm bone loading may differ in a horizontal gravity loaded position. Lastly, the range of pronation-supination motion was 70°, roughly half of the physically available range of motion, 120-165°. This means that changes in loading reported for active forearm rotation may not be entirely indicative of loading *in vivo*.

5.3 Current and Future Directions

The current studies presented in Chapters 2, 3 and 4 have successfully met the initial objectives presented at the start of this thesis. The results provide a better understanding of healthy forearm biomechanics during active wrist and forearm motion as well as an advanced understanding of the effect of radial length changes on distal radius and ulna loads during active PSM. Even with these contributions, there still exists opportunity to expand on this work and further examine forearm bone loading under normal and pathological conditions.

Measuring multidirectional loads through the distal radius and ulna will provide an improved understanding of and joint reaction forces in the wrist and distal forearm. Forces in the medial-lateral direction are of particular interest as they provide information about loading at the DRUJ. The DRUJ is often disrupted with changes in radial and ulnar variance. Therefore, it is important to examine the effect of radius length changes on DRUJ loading.

The residual effects of wrist fractures and degenerative diseases, such as Keinbock's disease, cause more than solely length change of the distal radius. Instead, radial length changes are often accompanied with more complex angulations and translations of the distal radius and compromised soft tissue integrity, such as the TFC tears. Simulated multiplanar distal radial deformities and soft tissue sectioning will provide an advanced understanding of the changes in distal forearm biomechanics associated with traumatic injuries and degenerative diseases, such as distal radius fractures and Kienbock's disease.

Different gravity loaded forearm positions should also be examined. While the vertical forearm position allows for ease of testing, it is not indicative of tasks of daily living. The simulator used in the studies presented has the capability of two additional gravity loaded forearm positions. Distal forearm bone load magnitudes and load sharing may be altered in a horizontal gravity loaded position. Therefore, loads through the distal radius and ulna should be examined in a horizontal position and compared to the results in the vertical loading position presented in this thesis.

5.4 Significance

Existing *in vitro* studies on the effect of active joint motion on distal forearm bone load magnitudes and sharing are limited. While static studies have examined the effect of radial length changes on distal forearm loading, there remains a void of literature on the combined effect of radial length changes and pronation-supination motion. The research completed in this thesis provides a more comprehensive understanding of wrist and distal forearm biomechanics in both normal and pathological states.

An improved understanding of healthy and pathological distal forearm loading will lead to better diagnosis and treatment of altered forearm bone lengths. Distal forearm loading throughout wrist and forearm motion provides valuable information about which wrist positions cause increased and decreased loading through the distal radius and ulna. These findings can then be used to optimize rehabilitation protocols in order to either decrease bone loads to decrease pain or increase bone loading to strengthen them after traumatic injuries and surgical intervention. The results of our studies suggest that to decrease loads in the distal ulna, radial deviation, wrist flexion and supination are recommended. To decrease loading through the distal radius, ulnar deviation and neutral forearm rotation are recommended. Additionally, our results provide a novel insight to the changes in distal radius and ulna loading throughout the dart throw motion. While dart throw motion is proposed as a more physiologic form of wrist flexion-extension motion, the loads through the distal forearm suggest that dart throw motion is more similar to radioulnar deviation than flexion-extension motion.

The results of the presented studies also have implications for surgical interventions prescribed at the presentation of altered radial bone length, such as radial osteotomies for the treatment of Kienbock's disease. Our results suggest that more than 2mm of radial shortening significantly decreases loads through the distal radius and increases loads through the distal ulna. Radial shortening of 2mm or greater also caused a significant increase in loads between neutral forearm rotation and the greater amounts of pronation, a phenomenon not present at native radial length. Therefore, radial shortening beyond 2mm should be approached with caution as it may cause unfavorable changes in distal forearm biomechanics.

In conclusion, this work improves the understanding of forearm bone loading and will assist clinicians in the development of rehabilitation techniques, surgical protocols and implant designs.

Appendices

Appendix A – Glossary of Terms

Active Motion	Muscle forces to move a joint, force applied directly to the muscle group of interest.
Anterior	Directed to the front; opposite of posterior.
Articular Surface	Connection made between two bones within the body.
Axial load	Load transmitted through the central long axis of the bone.
Biomechanics	The study of the control and effects of forces that are produced or applied to biological organisms.
Dart Throw	Multiplanar motion consisting of combined wrist extension-radial deviation and wrist flexion-ulnar deviation.
Deviation	Moving away from the midline of the body.
Degree of Freedom	The number of independent measurements or motions.
Distal	Located away from the origin or line of attachment.
Dorsal	Directed to the back; synonymous with posterior, opposite to volar
Dynamic loading	Variable amount of applied force exerted to produce motion
Extension	Motion moving two segments of the body apart.
Fixation	The act of holding, suturing, or fastening an extremity in a fixed position.
Flexion	Motion bringing two segments of the body closer together.
Inferior	Located below, or directed downwards.
In vitro	Latin; an experiment or process conducted outside of a living organism.
In vivo	Latin; an experiment or process conducted within a living organism.
Lateral	Directed away from the midline of the body.

Ligament	Fibrous connective tissue that connects bone to bone; supports and strengthens joints.
Medial	Directed towards the midline of the body.
Posterior	Directed to the back, opposite anterior.
Proximal	Located towards the origin or line of attachment.
Pronation	At the forearm, hand and upper limb turned inwards.
Servomotor	An electronic actuator that allows for precise force outputs
Static Loading	Constant amount of force applied, generating no motion
Superior	Located above, or directed upwards.
Supination	At the forearm, hand and upper limb turned outwards.
Volar	Directed to the front; synonymous with anterior, opposite to dorsal

Appendix B – Implant Design Measurements

Table B.1: *The widths of the distal radius and ulna in males and females at 20% and 25% of total forearm bone length based of a cadaveric specimen population.*

Bone	**Radius**				**Ulna**			
Gender	**Male**		**Female**		**Male**		**Female**	
Percentage of Total Bone Length from the Distal Terminus	**20%**	**25%**	**20%**	**25%**	**20%**	**25%**	**20%**	**25%**
1	12.2	8.9	10.6	9.0	7.8	7.3	5.4	4.9
2	13.2	11.9	9.5	8.4	6.4	7.1	5.6	4.9
3	16.7	11.7	10.9	9.7	8.5	6.5	7.2	7.2
4	13.8	10.2	10.5	8.7	7.9	7.7	5.0	4.7
5	13.6	12.6	13.2	12.5	8.4	8.6	7.6	7.9
6	17.8	15.6	13.3	11.0	14.9	11.9	8.0	7.8
7	11.5	10.7	14.5	12.3	7.6	7.7	6.9	7.2
8	16.4	14.2	12.2	9.8	9.5	9.2	8.5	8.2
9	19.1	16.1	10.2	7.4	13.7	13.7	6.6	6.8
10	18.4	14.7	12.7	10.8	9.1	8.8	5.9	6.1
11	10.9	9.5	7.7	6.3	6.8	6.7	7.4	6.7
12	18.7	14.0	13.3	10.7	12.9	13.1	6.6	6.7
13	16.9	13.6	11.9	9.2	9.6	11.0	7.9	6.9
14	14.2	11.0	14.5	12.3	9.6	9.4	6.9	7.2
15	17.7	14.6	12.6	11.4	8.7	9.3	10.8	9.8
16	20.1	17.1	10.4	6.4	10.8	10.3	10.1	9.4
17	10.2	8.0	7.9	8.7	7.1	6.9	11.8	8.4
18	14.6	14.5	12.9	10.4	8.2	8.6	7.9	9.0
Average	**15.3**	**12.7**	**11.6**	**9.7**	**9.3**	**9.1**	**7.6**	**7.2**

Appendix C – Load Cell Calibration Curves

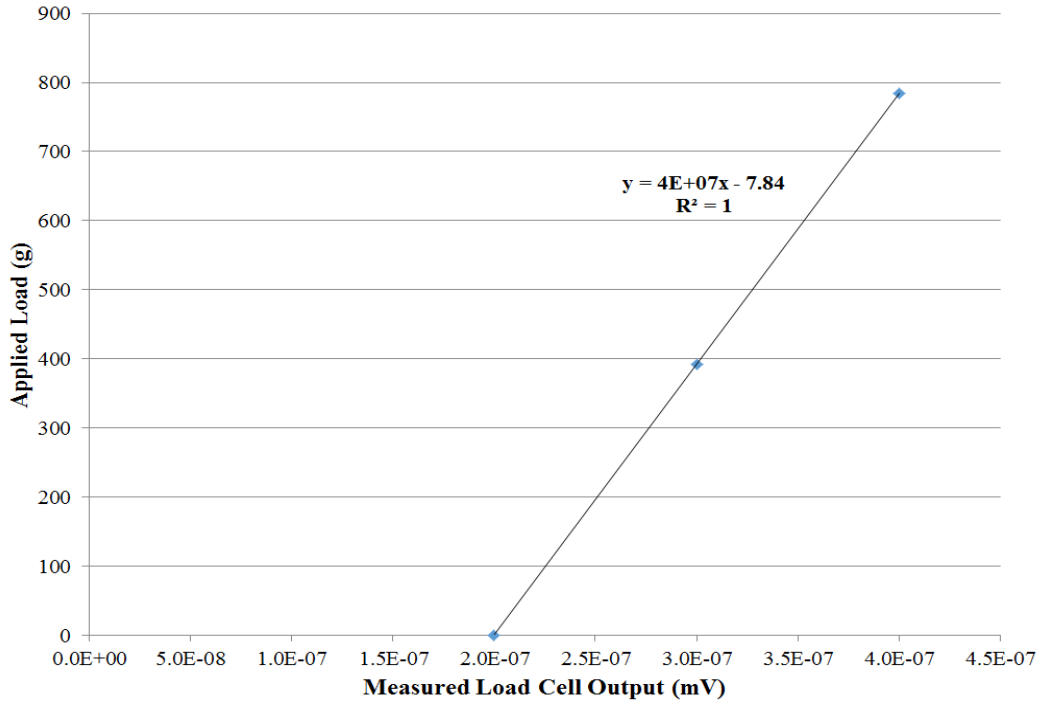

Figure C.1: Radial Load Cell Calibration Results. *The measured output of the radial load cell (mV) with a known applied load (g).*

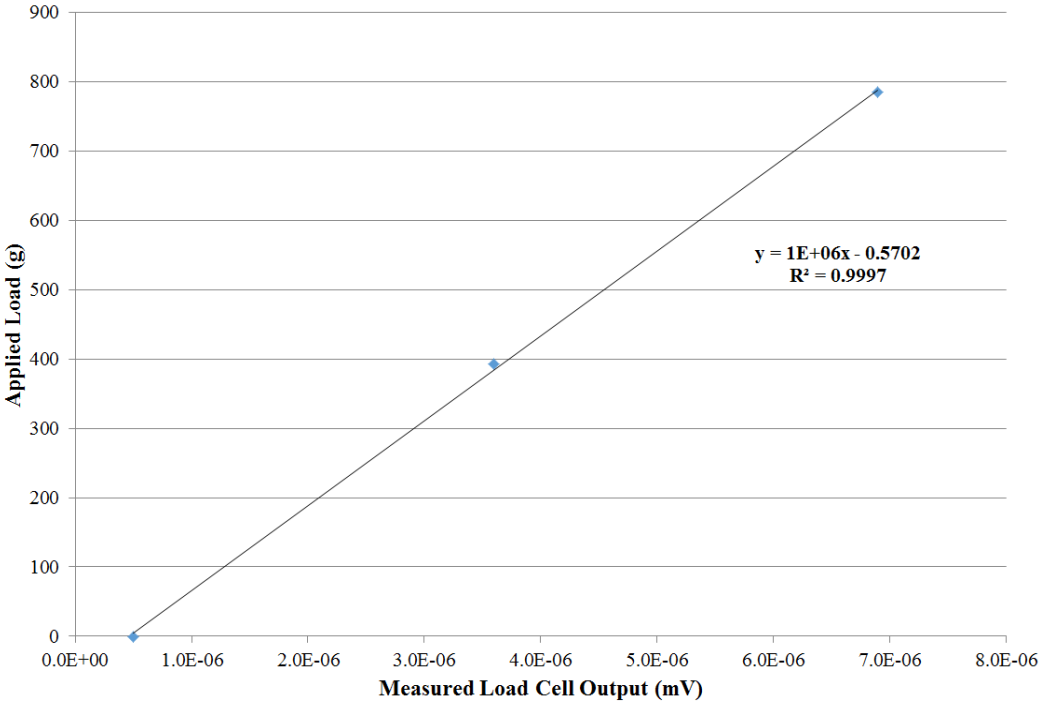

Figure C.2: Ulnar Load Cell Calibration Results. *The measured output of the ulnar load cell (mV) with a known applied load (g).*

Appendix D – Engineering Design Drawings

Overview

This section includes detailed engineering drawings for the individual components designed and evaluated in Chapter 2 and used for experimental use in Chapters 3 and 4. A detailed explanation of the design and use of the individual components can be found in Chapter 2.

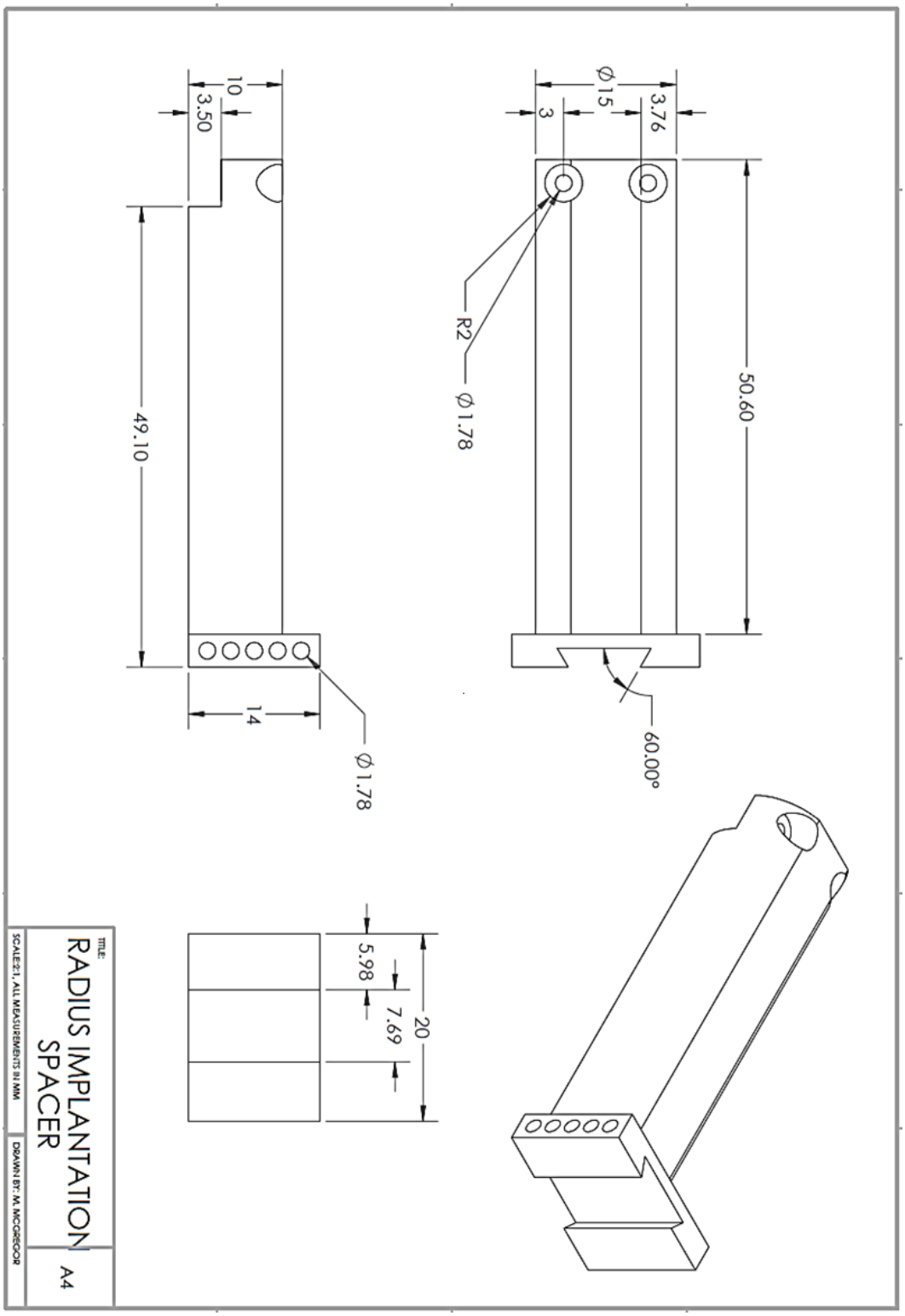

Figure D.1: Radial Implantation Spacer. *The radial implantation spacer is used to replace the modular radius device during implantation to protect the radial load cell from being damaged.*

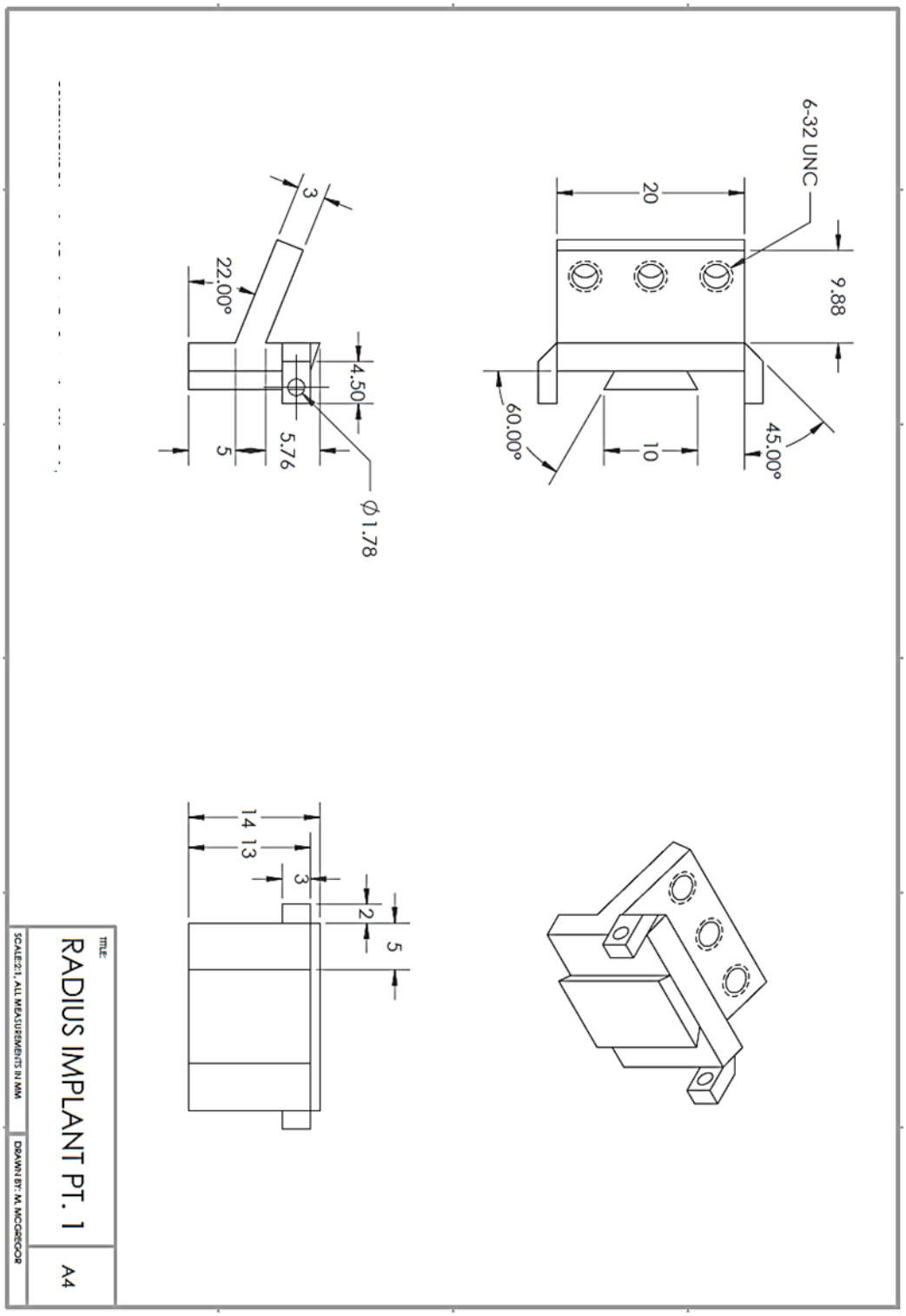

Figure D.2: Radius Implant Pt. 1. *The most distal component of the radius device is the distal radius plate which acts to fix the device distally with three bone screws and bone cement. The distal radius plate connects to the remainder of the radius device through a dovetail union and medial and lateral fixation screws.*

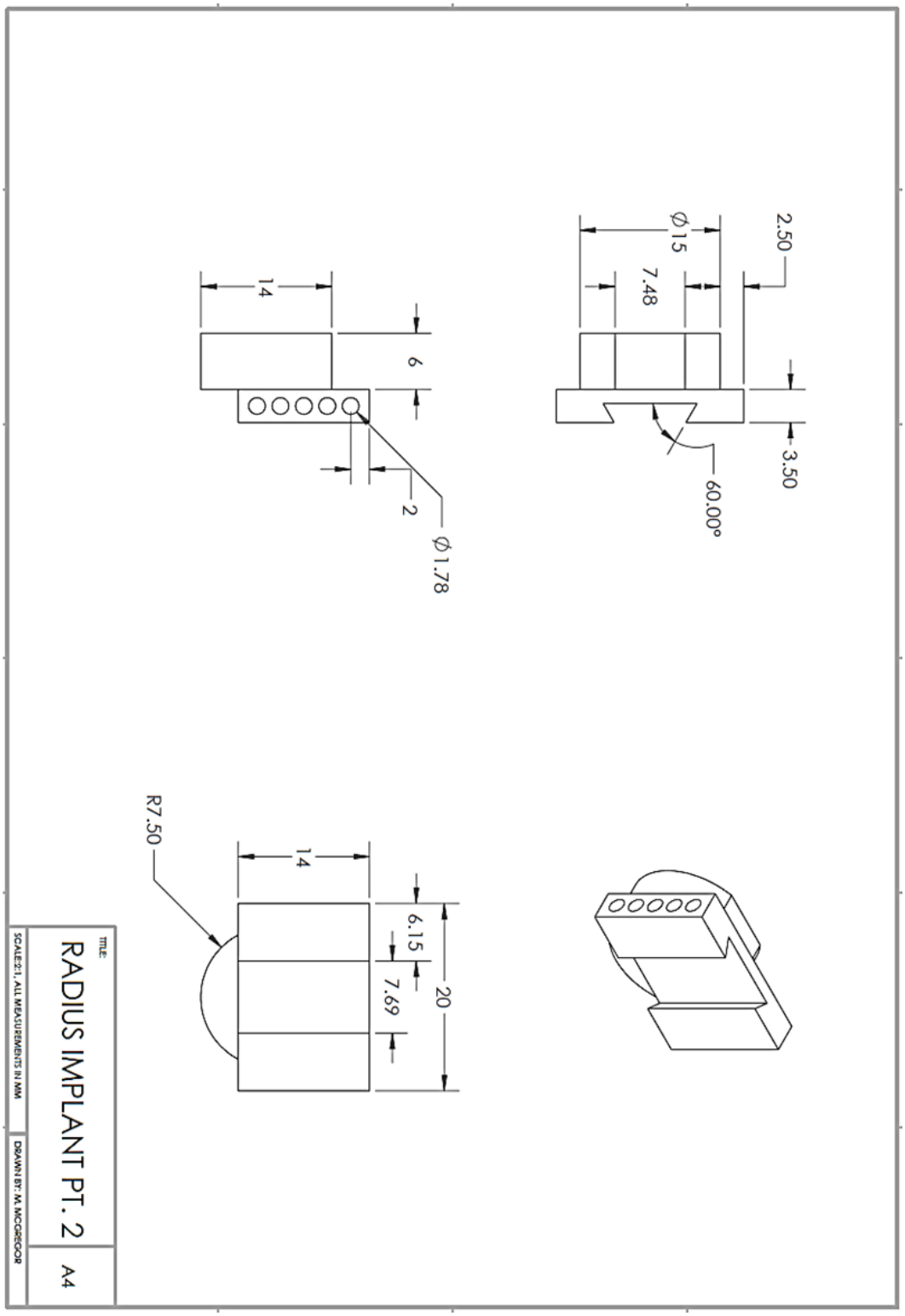

Figure D.3: Radius Implant Pt. 2. *The second part of the distal radius device mates with the distal radius plate through a dovetail union and two perpendicular fixation screws. Its proximal face mates with the distal post of the radial load cell.*

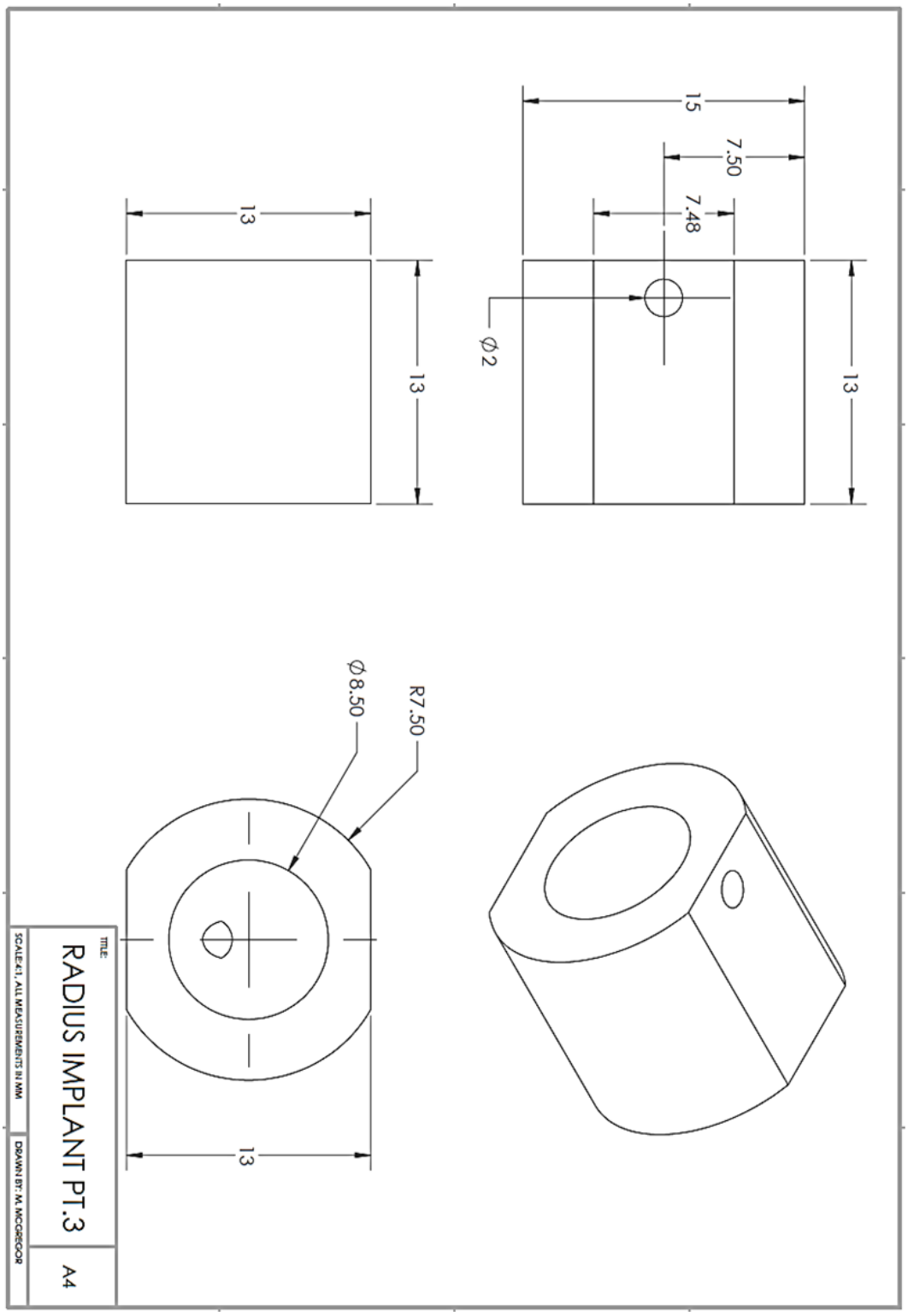

Figure D.4: Radius Implant Pt. 3. *The distal surface of the third part of the radius implant mates with the proximal post of the radial load cell. The proximal surface of part three connects to the right hand threaded aspect of radius implant part seven.*

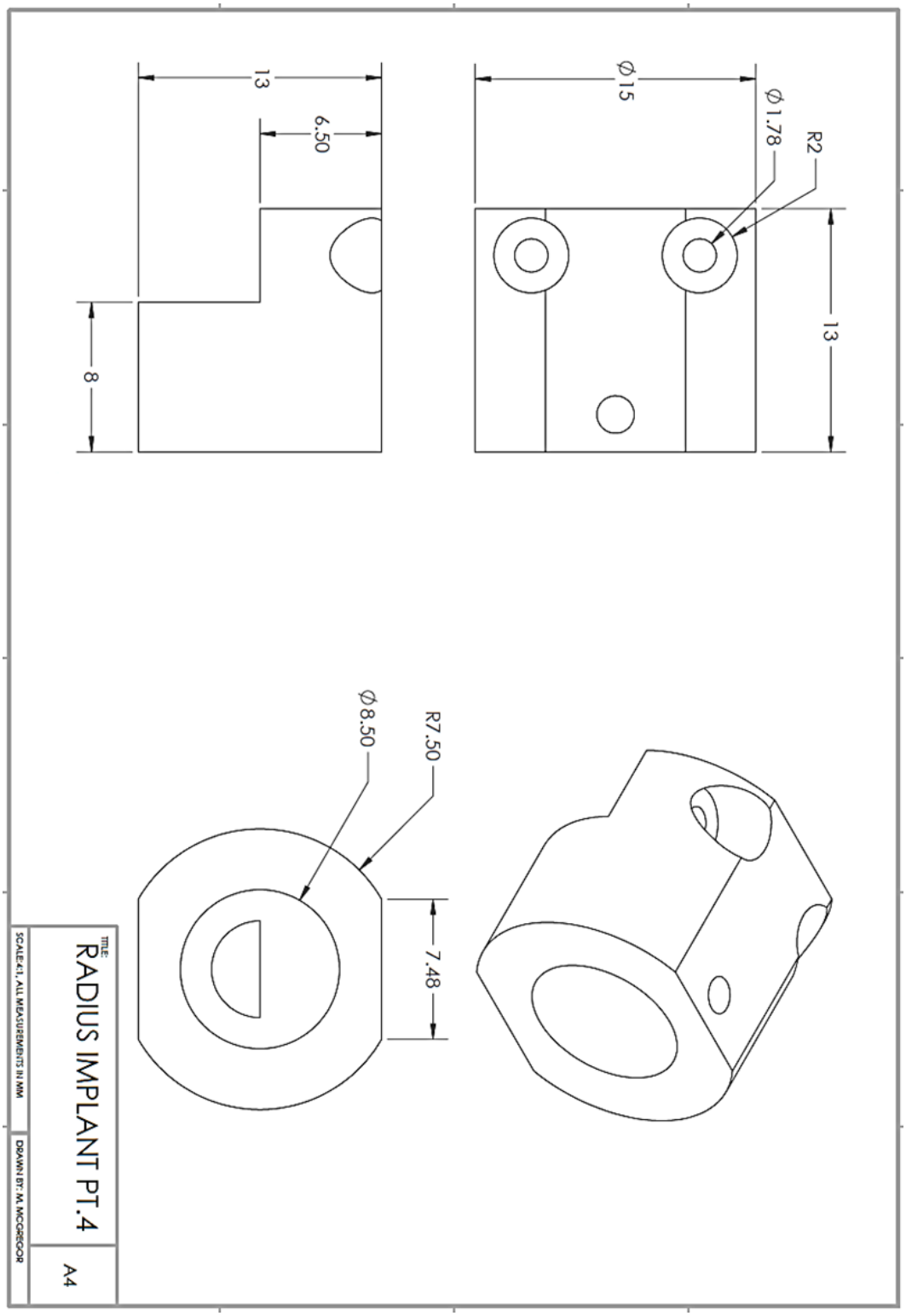

Figure D.5: Radius Implant Pt. 4. *The distal surface of the third part of the radius implant mates with the left hand threaded aspect of radius implant part seven. The proximal aspect is fixed to the proximal intramedullary stem with two perpendicular screws.*

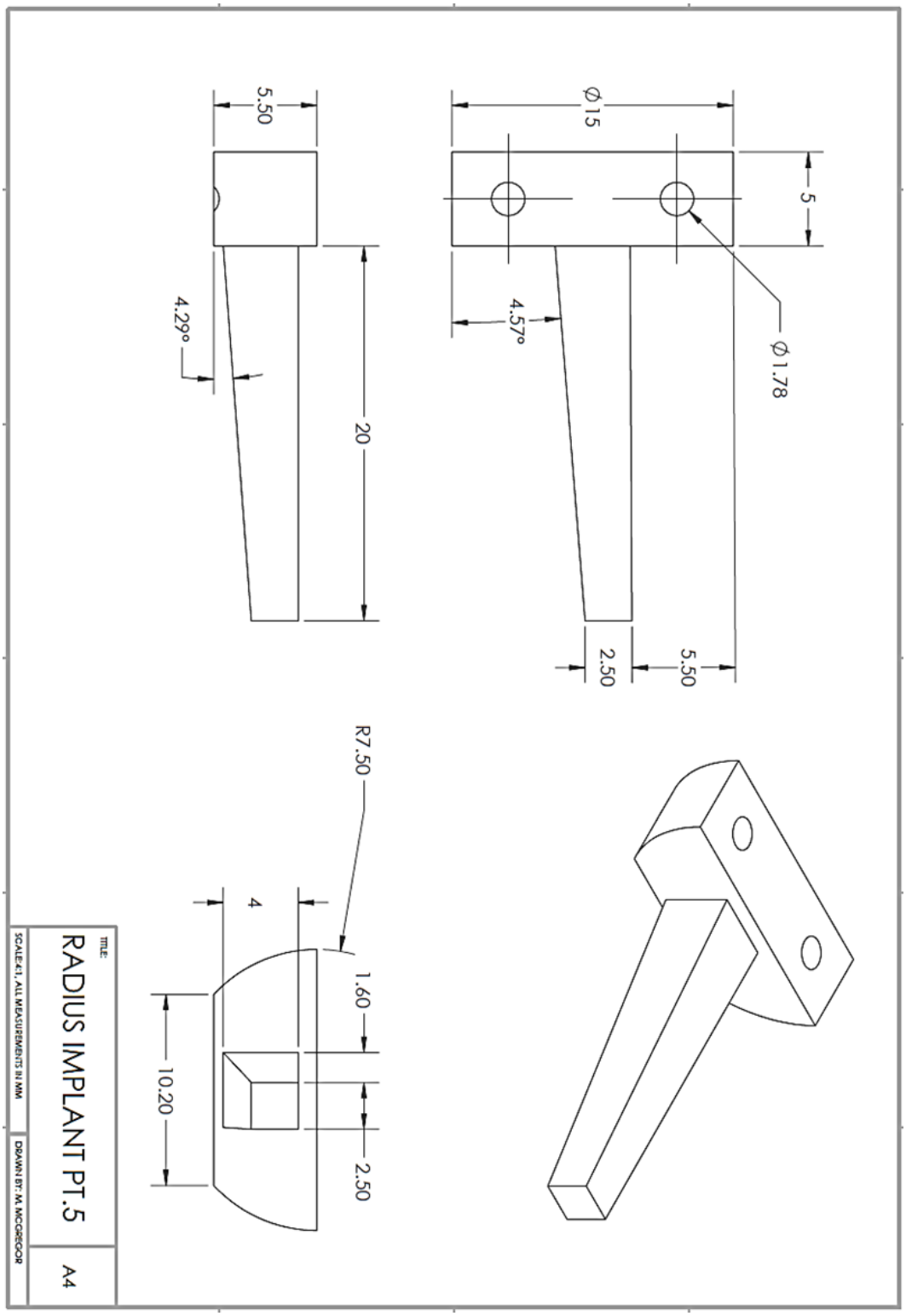

Figure D.6: Radius Implant Pt. 5. *The distal aspect of the proximal intramedullary stem is fixed to remainder of the radius device with two perpendicular screws. The proximal intramedullary stem acts to fix the radius implant proximally through the use of friction fit and bone cement.*

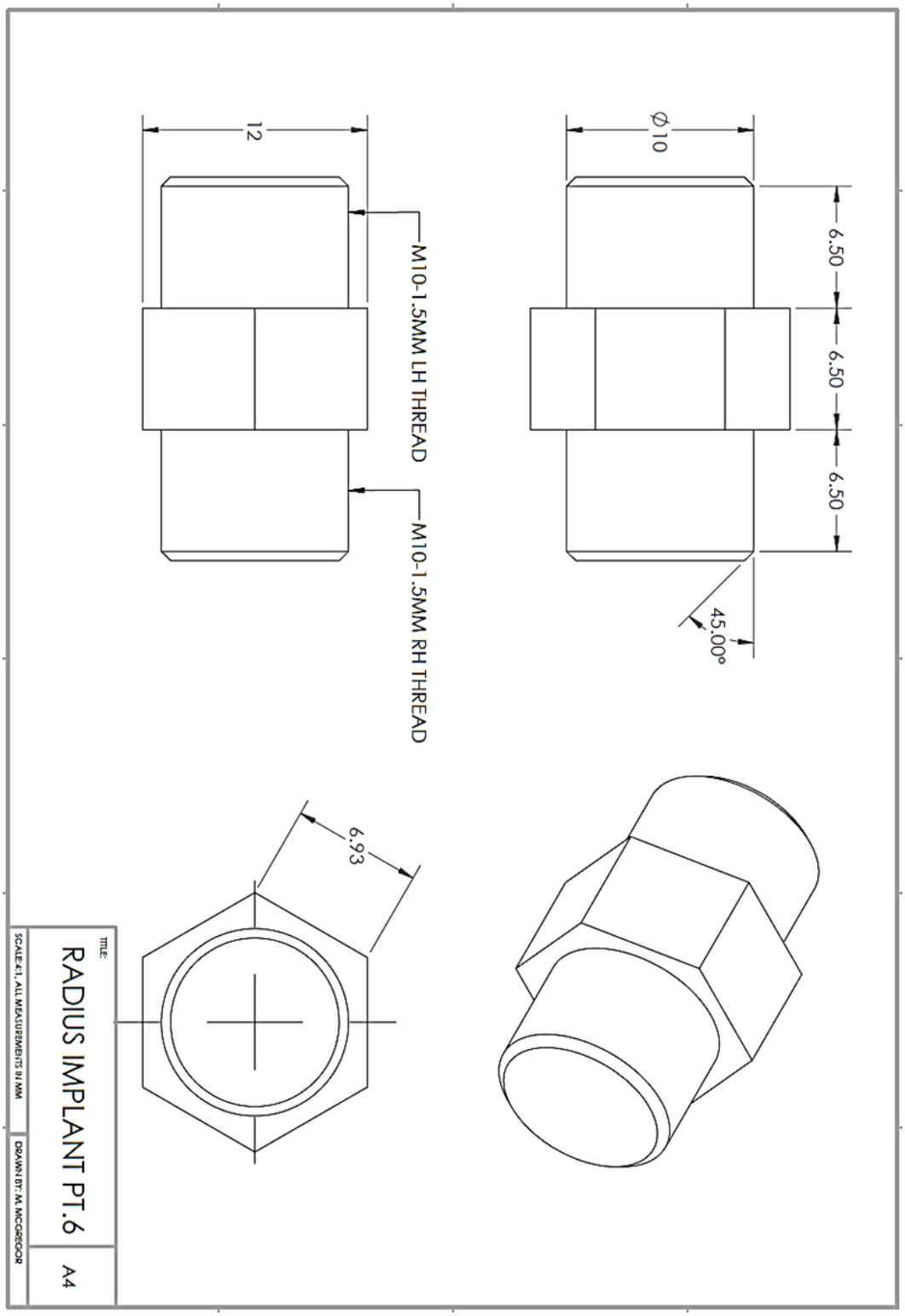

Figure D.7: Radius Implant Pt. 6. *The hexagonal nut with reversely threaded aspects acts to achieve incremental bone length changes through rotation. The distal and proximal aspects thread into the proximal surface of part three and distal surface of part four respectively.*

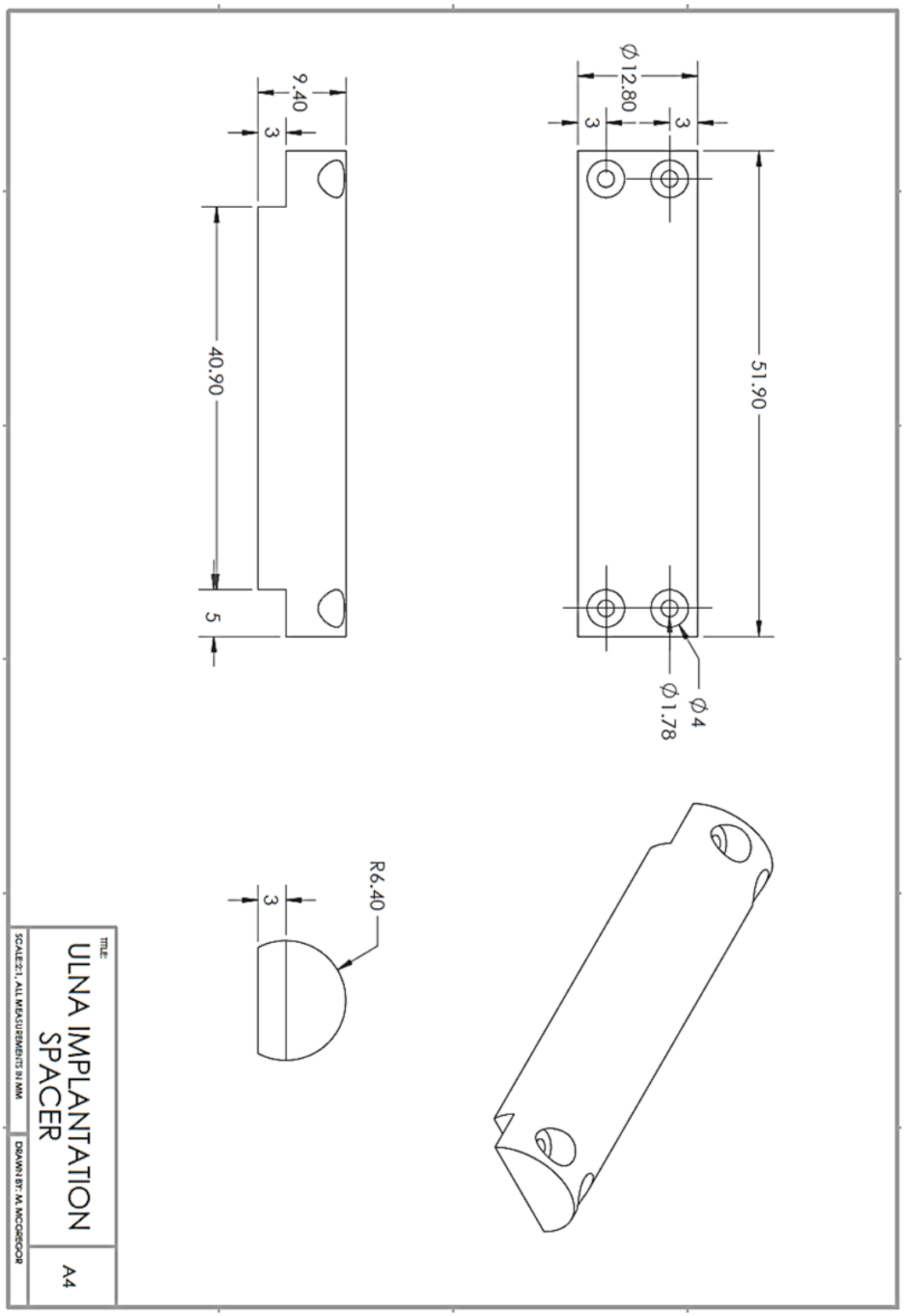

Figure D.8: Ulnar Implantation Spacer. *The ulnar implantation spacer is used to replace the modular ulna device during implantation to protect the ulnar load cell from being damaged.*

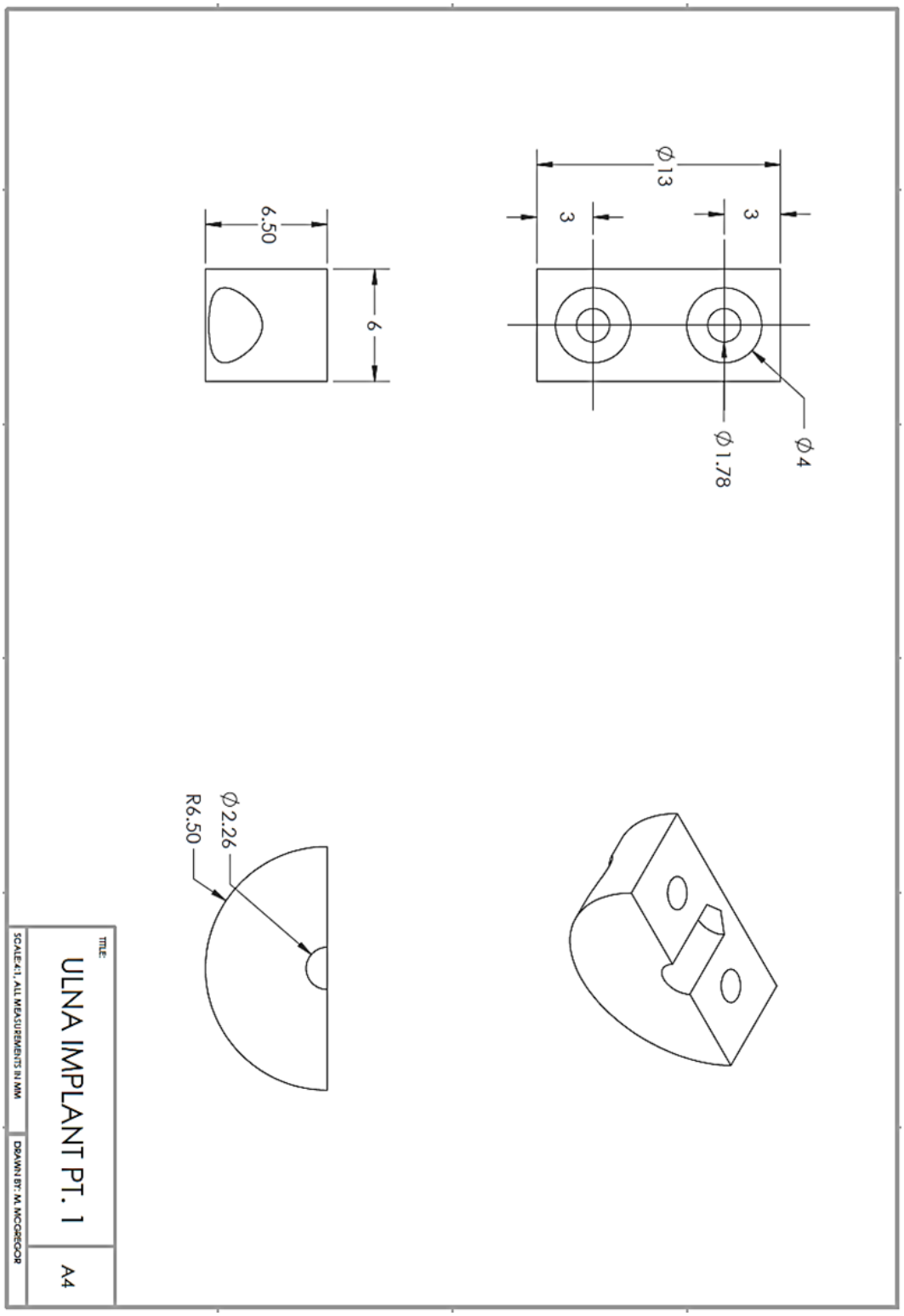

Figure D.9: Ulnar Implant Pt. 1. *The first part of the ulna implant mates to the distal post of the ulnar load cell. The ulnar load cell is held in place with two perpendicular screws which provide compression between it and the distal intramedullary stem.*

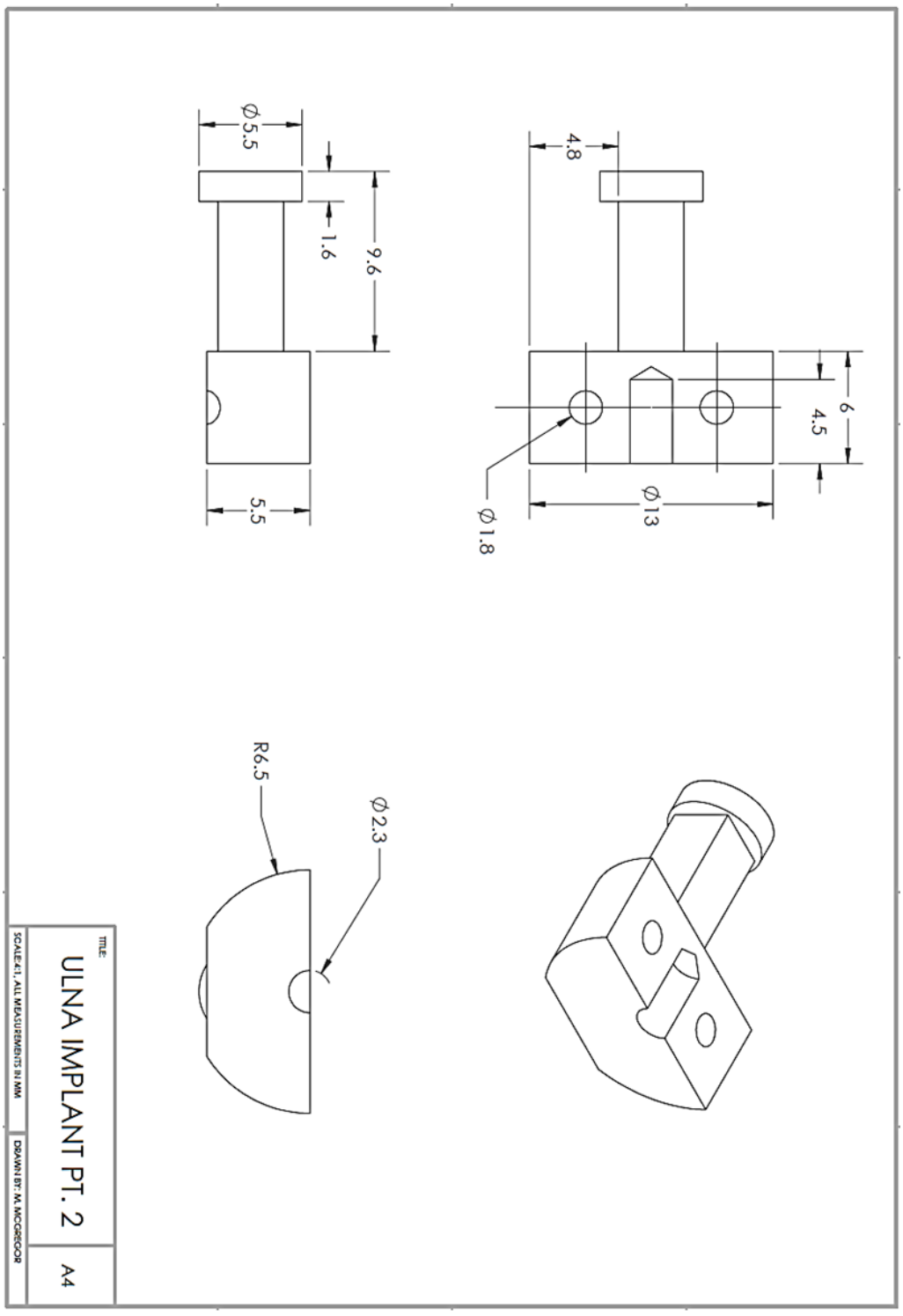

Figure D.10: Ulnar Implant Pt. 2. *The distal intramedullary stem provides distal fixation of the ulna device through friction fit and bone cement. The proximal aspect of the distal intramedullary stem is fixed to the distal post of the ulnar load cell with two perpendicular screws and compression from ulnar implant part one.*

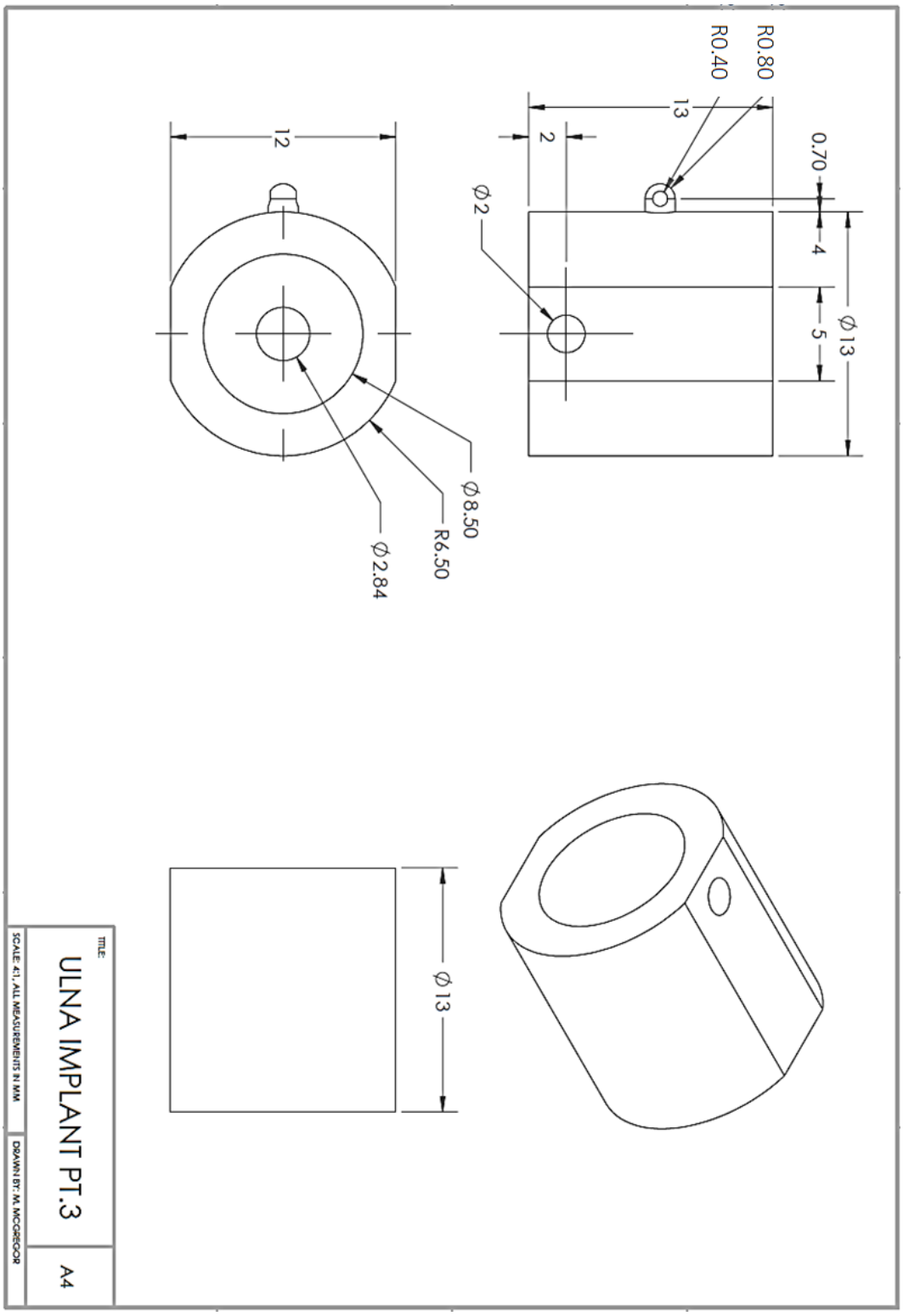

Figure D.11: Ulnar Implant Pt. 3. *The distal surface of the third part of the ulna implant mates with the proximal post of the ulnar load cell. The proximal surface of part three connects to the right hand threaded aspect of ulna implant part seven.*

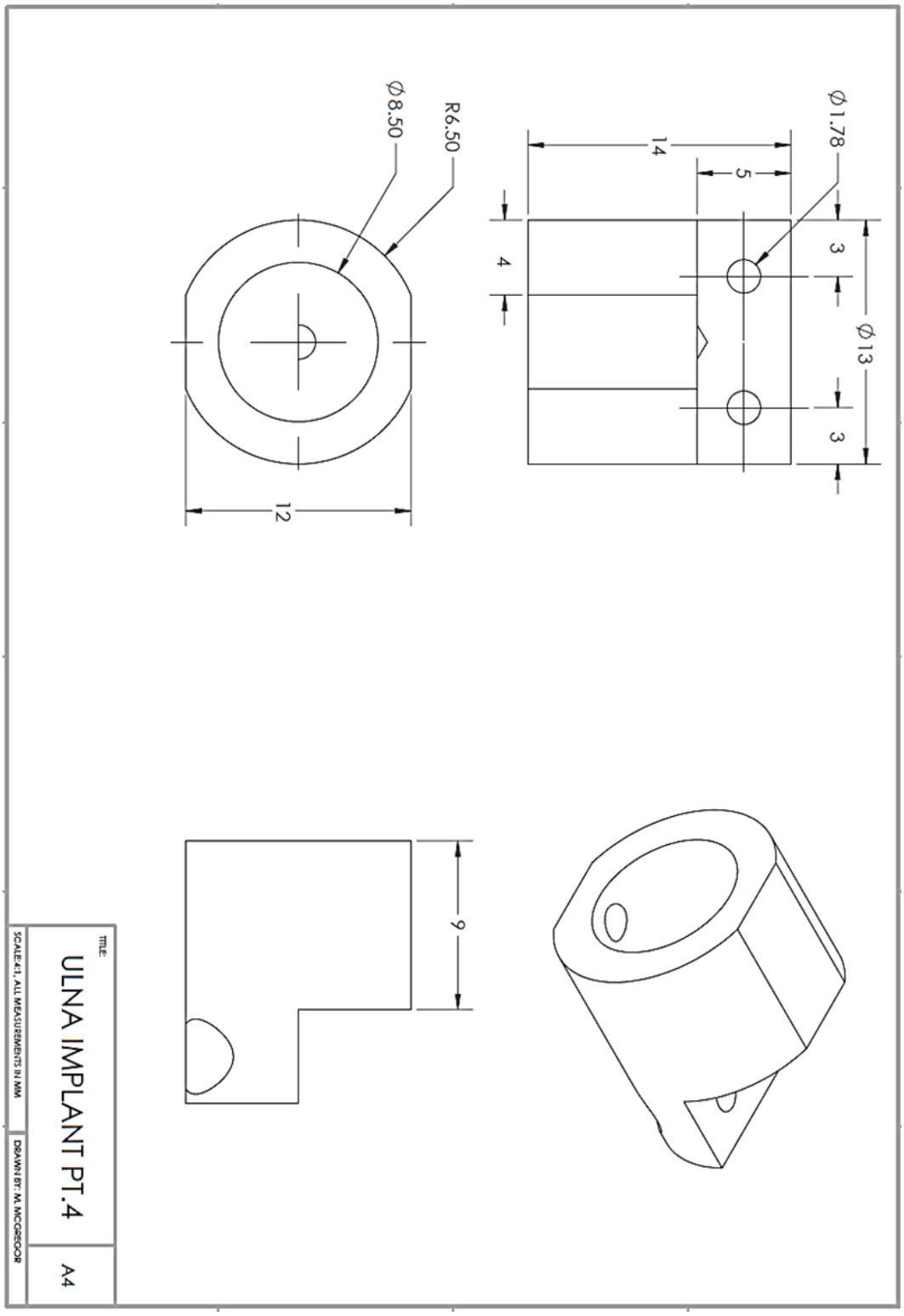

Figure D.12: Ulnar Implant Pt. 4. *The distal surface of the fourth part of the ulna implant mates with the left hand threaded aspect of ulna implant part seven. The proximal aspect is fixed to the proximal intramedullary stem with two perpendicular screws.*

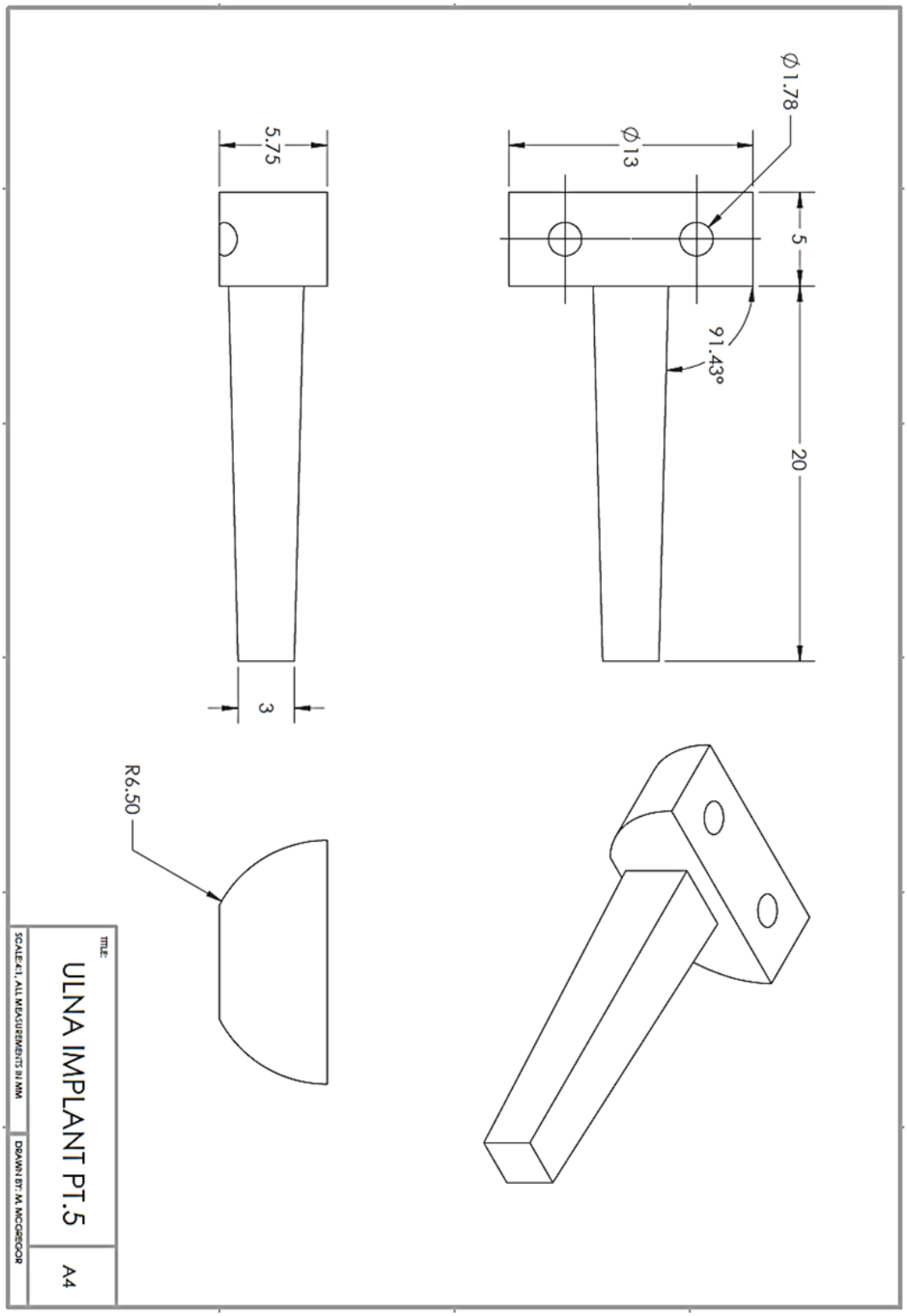

Figure D.13: Ulnar Implant Pt. 5. *The distal aspect of the proximal intramedullary stem is fixed to remainder of the ulna device with two perpendicular screws. The proximal intramedullary stem acts to fix the ulna implant proximally through friction fit and bone cement.*

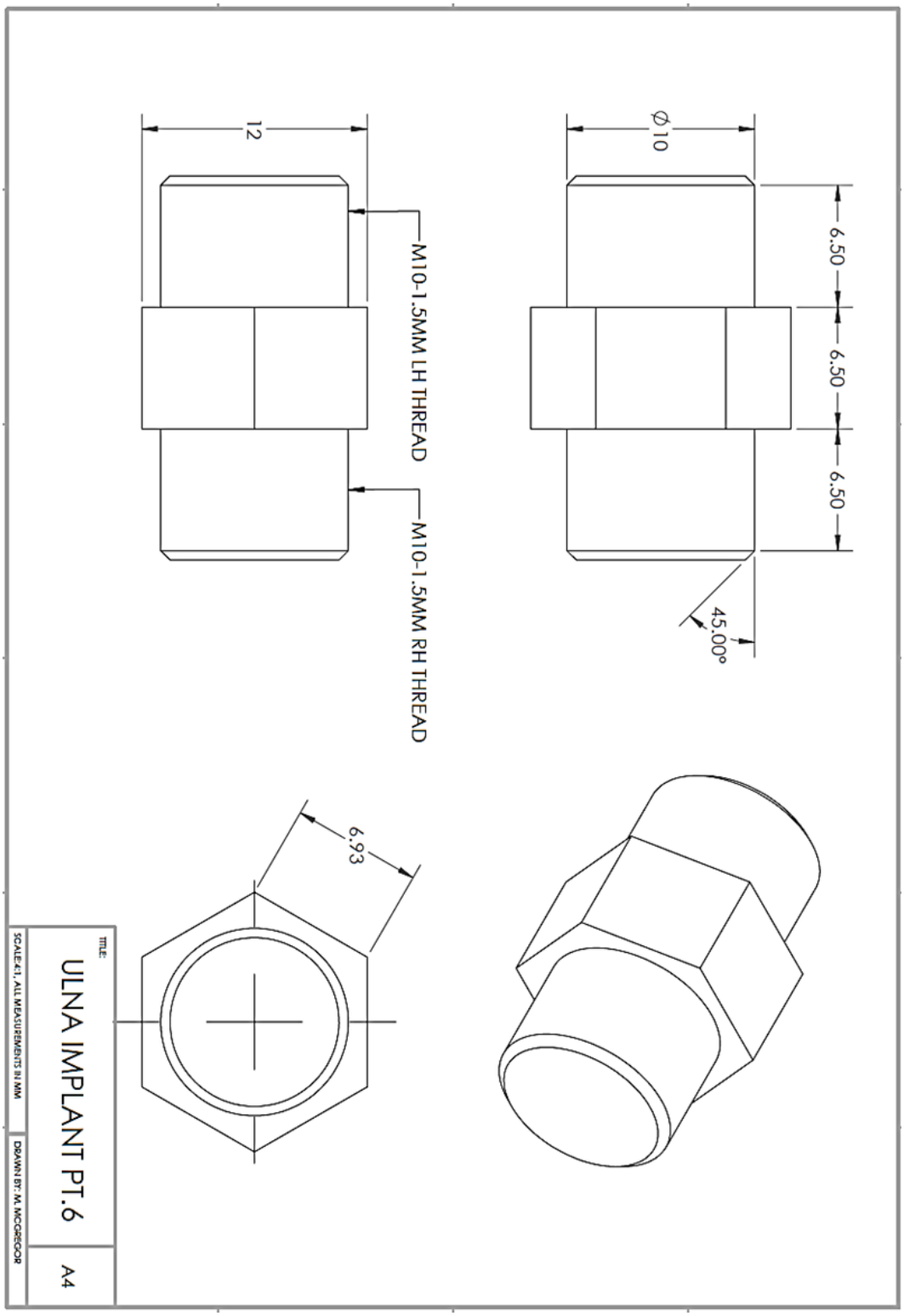

Figure D.7: Radius Implant Pt. 6. *The hexagonal nut with reversely threaded aspects acts to achieve incremental bone length changes through rotation. The distal and proximal aspects thread into the proximal surface of part three and distal surface of part four, respectively.*

Martine McGregor

EDUCATION

Master of Engineering Science [MESc], Biomedical Engineering **2015- 2017**
Western University, London, ON
Advisor(s): Dr. James Johnson, Dr. Graham King

Bachelor of Engineering [BEng], Biomedical Engineering **2011 – 2015**
University of Guelph, Guelph, ON

- Graduated with distinction (>80% cumulative average)
- Dean's Honor List

RESEARCH FUNDING & SCHOLARSHIPS

Lawson Internal Research Fund	**2015**
Western Graduate Research Scholarship	**2015**
Maximum Entrance Scholarship, University of Guelph ($3000)	**2011**
Conexus Math and Science Award, Crocus Plains Secondary School ($2000)	**2011**

HONORS & AWARDS

Dean's Honor List, University of Guelph	**2011-2015**
Class Valedictorian, Crocus Plains Secondary School	**2011**

ACADEMIC & INSTITUTIONAL AFFILIATIONS

Western University	London, ON
Lawson Research Institute	London, ON
St. Joseph's Hospital	London, ON
Faculty of Engineering, Western University	London, ON
Schulich School of Medicine & Dentistry, Western University	London, ON
School of Engineering, University of Guelph	Guelph, ON
Ontario Veterinary College, University of Guelph	Guelph, ON

SOFTWARE & HARDWARE LITERACY

- Practiced with use of MatLAB, Solidworks, AutoCAD, Microsoft Office, LabVIEW, Mimics Materialise, SPSS, field surveying equipment and radio transmitting technologies
- Experienced in data collection and processing using AMTI force plate, Vicon and OptiTrack motion capture systems, wireless and tethered EMG electrodes, goniometer, OMTS with load cell, and Instron Material Testing machinery

RESEARCH EXPIRIENCE

Graduate Research Assistant in Hand & Upper Limb Biomechanics **2015-2017**
Roth McFarlane Hand & Upper Limb Clinic, Faculty of Engineering, Western University, London ON
Advisor(s): Dr. James Johnson, Dr. Graeme King

- Designed, rapid prototyped, and machined two instrumented stainless steel implants
- Performed *in vitro* cadaveric biomechanical study
- Employed existing active motion simulator to collect bone loads and wrist kinematics
- Examined the effects of joint position and radial length on distal forearm loads

Clinical Studies Research Assistant **2015**

Department of Clinical Studies Ontario Veterinary College, School of Engineering, University of Guelph, Guelph, ON
Advisor(s): Dr. John Runciman, Dr. Luis Arroyo

- Worked collaboratively between Biomedical Engineering and the OVC Clinical Studies
- Collected *in vivo* pulse wave velocity measurements from the pulmonary artery of horses
- Examined new and existing analysis techniques to determine which provides the most statistically reliably pulse wave velocity values
- Published findings in the Artery Research journal

Engineering Biomechanics Laboratory Student **2014**
School of Engineering, University of Guelph, Guelph ON

- Designed research experiment to analyze moments produced in the knee during lateral movement with and without a prophylactic ankle brace
- Collected data using piezoelectric force plate and Vicon motion capture and analyzed / processed data using MatLAB

Undergraduate Field Research Assistant **2013**
Brandon University, Brandon, MB

- Worked collaboratively with the geology department to answer the research question: why are the skinks only found in this select region of Western Canada.
- Captured and radio tracked the endangered prairie skink in Spruce Woods Provincial Park
- Carefully followed data collection protocol and ensured ethical treatment of all living things in the field according to the Canadian Council on Animal Care guidelines

TEACHING EXPERIENCE

Introductory Engineering and Design Innovation Studios Teaching Assistant **2015-2017**
Western University, London, ON

Instructed and supervised weekly two hour tutorial sessions for a class of 50 first year engineering students; marked presentations, final design reports and weekly assignments; provided academic and emotional guidance

Workshop Facilitator and Physics and Math instructor **2016**
Ms. Infinity Ontario, Guelph, ON

Gave four individual presentations on basic physics and math concepts to 125 female students in grades 9-12; organized and facilitated a group work period aimed at applying basic physics concepts to construct and present a Rube Goldberg machine

Introduction to Biomedical Engineering Guest Lecturer **2015**
Western University, London, ON

Gave an independent presentation on current research being conducted in the Biomedical Engineering department at Western University titled: The Development of an Experimental Apparatus for Examining Load Sharing in the Distal Forearm

Mathletics Instructor – Grand River Chapter **2015**
Professional Engineers of Ontario, Cambridge, ON

Instructed and facilitated a mathematics competition on basic mathematic concepts for 100+ children, grades 5-8; ensured academic integrity of all competition participants

PUBLICATIONS

1. Silva, G., Guest, B., Gomez, D.E., **McGregor, M.**, Viel, L., O'Sullivan, ML., Runciman, J., Arroyo, L.G. Development of a technique for determination of pulmonary artery pulse wave velocity in horses. *J Appl Physiol.* 2017; 122(5), 1088-1094.
2. Runciman, J., **McGregor, M.,** Silva, G., Montheith, G., Viel, L., Arroyo, L. A new statistical phase offset techniques for the calculation of *in vivo* pulse wave velocity. *Artery Research.* 2016; 13, 17-27.
3. Silva, G., Guest, B., Gomez, D.E., **McGregor, M.**, Runciman, J., Arroyo, L.G. Development of a technique for determination of pulmonary artery pulse wave velocity in horses. *Artery ' 15. 2015. Status: Presented in Krakow, Poland October 2015*

PRESENTATIONS

The Effect of Sex and Transverse Bone Region on Cortical and Trabecular Bone Mineral Density at the Distal Radius **2017**
Poster Presentation at the 2017 Annual Meeting of the Canadian Orthopaedic Association/ Canadian Orthopaedic Research Society, Ottawa, ON

The Effect of Sex and Transverse Bone Region on Cortical and Trabecular Bone Mineral Density at the Distal Radius **2017**
Poster Presentation at the 2017 Annual Meeting of the Orthopaedic Research Society, San Diego, CA

Camp 17 Iron Ring Ceremony – Student Representative **2015**
University of Guelph, Guelph, ON

Graduating Class Valedictorian **2011**
Crocus Plains Regional Secondary School, Brandon, MB

RELAVENT PROJECT WORK

An age-matched in-vitro assessment of the effects of sex and transverse bone region on cortical and trabecular bone mineral density at the distal radius **2016**
Western University, London, ON

- Employed Mimics Materialise Software to examine bone mineral density (BMD)
- Compared cortical and trabecular BMD between sexes and on the basis of transverse distance from the distal radius terminus
- Completed a primary article draft for scientific journal submission

VisuTrack: Smart Cane with Line Tracking Capabilities **2015**
University of Guelph, Guelph, ON

- Designed and prototyped a smart mobility assist with line tracking capabilities
- Obtained ethics approval and completed a clinical study to prove function of mobility assist
- Developed an in depth design report outlining design objective, constraints, methods, production cost and clinical study results
- Presented final design to a panel of judges comprised of industry and academic professionals in a formal poster presentation

Terrain-in-Motion Rehabilitation Device **2014**
University of Guelph, Guelph, ON

- Designed a retrofitted treadmill obstacle device for gait rehabilitation at St. Joseph's Health Care Centre, Guelph, ON
- Communicated with clinicians and patients to optimize device design
- Presented final design to St. Joseph's director and clinicians in a formal poster presentation

Environmental Monitoring Device with Bluetooth Android Application **2014**
University of Guelph, Guelph, ON

- Designed and constructed electrical circuitry and mechanical components of a bio-instrument used to monitor, display and wirelessly transmit various environmental parameters
- Programmed Arduino microcontroller to provide sensor readings through LED and LCD display
- Developed basic Android Bluetooth application using Java

PROFESSIONAL EXPERIENCE

HULC Laboratory Cadaveric Inventory Manager **2015 –2016**
Hand of Upper Limb Centre, St. Joseph's Hospital, London, Ontario

Sales Associate and Outdoor Guide **2012 - 2014**
Stream and Wood, Brandon, Manitoba

Engineering Department Land Surveyor and General Laborer **2011 - 2012**
City of Brandon, Brandon, Manitoba

LEADERSHIP & INTERPERSONAL SKILLS

Biomedical Student Representative **2016 –2017**
BME Program Operations Committee, Western University, London, ON

Represented the BME graduate students of Western University at monthly meetings; proposed and designed a survey for the student body aimed at collecting data to improve academic, social and bureaucratic aspects of the BME graduate program at Western University.

Ontario Network of Women in Engineering (ONWiE) Student Ambassador **2015-2017**
Ontario Network of Women in Engineering, Waterloo University, Waterloo, ON

Provided mentorship to female high school and undergraduate students with interest in Biomedical Engineering through official ONWiE website.

Biomechanical Student Representative **2015**
BME Standing Pedagogy Committee, Western University, London, ON

Evaluated and report on how well BME is providing a depth and breadth of multidisciplinary education.

Professional Development Conference Promotions and Advertising Officer **2014 –2015**
University of Guelph Engineering Society, Guelph ON

Organized and facilitated a conference aimed at improving undergraduate engineering student's networking and job searching skills; performed all advertising and promotional tasks to ensure attendance and student participation.

Biomedical and Biological Year Representative **2014 – 2015**
University of Guelph Engineering Society, Guelph ON

Attended weekly meetings and presented important announcements to peers on various communication platforms; organized, promoted and facilitated the society's public events.

Orientation Week Volunteer and Campus Ambassador **2012 –2015**
University of Guelph Engineering Society and University of Guelph, School of Engineering, Guelph ON

Facilitated group tours of engineering building and biomedical / biological laboratories.

CERTIFICATIONS & TRAINING

Comprehensive WHMIS Certification	2017
Biosafety Training	2015
Worker Health & Safety Training	2015
Safe Campus Community Training	2015
Laboratory Safety – Hazardous Waste Training	2015
Accessibility in Teaching (AODA) Certification	2015